ENHANCING OLIGODENDROCYTE FORMATION VIA INHIBITION OF THE CHOLESTEROL BIOSYNTHESIS PATHWAY

by

ZITA MARIA LUPE HÜBLER

Submitted in partial fulfillment of the requirements for the degree of

Doctor of Philosophy

Genetics and Genome Sciences

CASE WESTERN RESERVE UNIVERSITY

August, 2020

CASE WESTERN RESERVE UNIVERSITY

SCHOOL OF GRADUATE STUDIES

We hereby approve the thesis/dissertation of

Zita Maria Lupe Hübler

candidate for the degree of **Doctor of Philosophy***.

Committee Chair

Paul Tesar

Committee Member

Mukesh Jain

Committee Member

Anthony Wynshaw-Boris

Committee Member

Ann Harris

Committee Member

Drew Adams

Date of Defense

4/30/2020

*We also certify that written approval has been

obtained for any proprietary material contained therein.

For my family, especially my father: Dr. Alfred Hübler.

Contents

List of Tables

List of Figures

Acknowledgements

While it would be impossible to recognize everyone who has contributed to my life path or to the work herein, I would like to take this section to highlight a select few that have left a lasting impression on me. I would like to thank:

- My advisor, Dr. Drew Adams, for giving me countless opportunities to learn and grow. His rigorous testing of my scientific knowledge and ideas challenged me to explore beyond my comfort zone. While his flexibility to adapt to circumstances outside the lab, provided me with a strong sense of stability. He has set the bar extremely high for all future mentors.
- My family for standing by me and reminding me that, regardless of the outcome, they will always be proud of me.
- My friends for keeping me sane, and when necessary, reminding me that a little insanity can be quite fun.
- My co-workers and collaborators for lively conversations, insights, and contributions to this work.

- My thesis committee, Dr. Paul Tesar, Dr. Anthony Wynshaw-Boris, Dr. Mukesh Jain, Dr. Ann Harris, Dr. Goutham Narla, and other unofficial mentors, to whom I turned to for guidance both in my personal and professional life.
- The CWRU MSTP for enabling me to pursue my dream of being a physician-scientist.
- The Department of Genetics and Genome Sciences, and all those in it, for welcoming me and giving me their unyielding support.

Enhancing Oligodendrocyte Formation via Inhibition of the Cholesterol Biosynthesis Pathway.

Abstract

by

ZITA MARIA LUPE HÜBLER

Loss of myelin-producing oligodendrocytes in the central nervous system (CNS) underlies several neurological diseases, including multiple sclerosis. Demyelinating disorders lead to cognitive and motor deficits, yet there are no FDA-approved remyelinating therapeutics. In the CNS, oligodendrocyte progenitor cells (OPCs) give rise to oligodendrocytes, which are capable of regenerating myelin. To discover novel therapies for demyelinating disorders, we performed *in vitro* chemical-genetic screens in OPCs looking for small molecules that enhance oligodendrocyte formation and remyelination. We found that the vast majority of pro-myelinating small molecules identified function, not through their canonical targets, but instead converge upon enzymes in the cholesterol biosynthesis pathway: CYP51, sterol-14-reductase, or EBP. Genetic experiments show that depletion of CYP51 or EBP enhances oligodendrocyte formation indepen-

dent of small molecule treatment. Likewise, evaluation of *in vivo* validated remyelinating compounds, identified by other labs, confirmed that inhibition of CYP51, sterol-14-reductase, and EBP is a dominant mechanism shared by dozens of small molecules that enhance oligodendrocyte formation. The accumulation of the 8,9-unsaturated sterol substrates of CYP51, sterol-14- reductase, and EBP is a critical mechanistic node of these pro-myelinating compounds. Multiple molecules that enhance 8,9-unsaturated sterol intermediate levels can regenerate functional myelin *in vivo* and a human cortical spheroid model. Evaluation of 8,9-unsaturated sterol structural variants revealed that 24,25-epoxycholesterol also promotes oligodendrocyte formation, despite lacking an 8,9-unsaturation. 24,25-epoxycholesterol accumulates upon partial inhibition of LSS in the cholesterol biosynthesis pathway through the epoxycholesterol shunt. Therefore, our work establishes the epoxycholesterol shunt and 24,25- epoxycholesterol as another sterol signaling axis regulating OPC differentiation and validates LSS as a druggable target for promoting oligodendrocyte formation. Overall, our findings establish a novel paradigm in which the cholesterol biosynthesis pathway can be leveraged to enhance the formation of new oligodendrocytes by inhibiting the enzymes LSS, CYP51, sterol-14-

reductase, or EBP. We outline a unifying sterol-based mechanism of action for most known small molecule enhancers of oligodendrocyte formation. Ultimately, our work demonstrates that modulating the sterol landscape in OPCs can enhance the formation of oligodendrocytes and points to new therapeutic targets, potent inhibitors for these targets, and metabolite-based biomarkers to accelerate the development of optimal remyelinating therapeutics.

1

Introduction

The human brain is often attributed with distinguishing humans from other animals as it allows us to reason on a higher level. Despite granting us with a cognitive advantage, we, as humans, are ironically ignorant about the inner workings of the very organ that gives us the ability to think. In consequence, we are similarly ill-equipped to treat patients that are burdened with neurocognitive disease. To accelerate the development of novel therapeutics, in spite of our incomplete understanding of neurology, high-throughput phenotypic screening has been successfully employed to identify novel small molecules for the treatment of diverse neurological symptoms and disorders. (2) Phenotypic screening is agnostic to known signaling mechanisms, and instead classifies small molecules based on their effects in a cell model of interest. (118) Nevertheless, one substantial drawback to phenotypic screening is that the mechanism by which the small molecules work is often con-

voluted, making it challenging to optimize them for therapeutic translation. (118) In consequence, there is a distinct lack of medications in use clinically for neurological disorders with a fully elucidated mechanism of action. Without a known mechanism, medical-chemistry endeavors to optimize these small molecules are fraught with off-target effects and complicated structure-function-relationship associations. The primary goal of this work is to identify the mechanism of action of small molecule therapies to facilitate the generation of safer and more potent medications. Specifically, this work focuses on small molecule therapies that aim to treat neurological disorders afflicting one cell-type in the central nervous system (CNS), the oligodendrocyte. The therapies pursued herein, aim to replenish the destroyed oligodendrocytes to increase both quantity and quality of life in patients.

Broadly, brain cells can be divided into two classes: neurons and glial cells. Each cell type plays a role in maintaining brain homeostasis, and to understand this, it can help to think of the brain as an electrical circuit. The conducting wires in the circuit represent the neurons; they carry electrical signals from one part of the brain to another along their axons. The oligodendrocyte is a glial cell that is represented by the insulation of the conducting wires. Oligodendrocytes wrap the axons of neurons with their lipid-rich membrane, called myelin, which allows for rapid signal conduction between neurons and promotes neuronal survival. (8, 22, 86) Myelin forms concentric rings around neuronal axons to prevent charge dissipation to the

extracellular space. (8, 22) To facilitate long-distance signal propagation, at pre-defined intervals, there are gaps in the myelin, called Nodes of Ranvier, which allow for regeneration of action potentials through ion exchange. (86) These structural features of myelin are essential for normal signaling within the brain circuit, and their loss is sufficient to cause neurological impairment. (11)

One crucial difference between an electrical circuit and a living brain, though, is that the brain can remodel and adapt when the system is disrupted. For example, if myelin is lost or damaged, such as in demyelinating disorders, the brain can generate new insulation to protect the bare axons: either by encouraging existing oligodendrocytes to expand their myelin sheaths or through the generation of new oligodendrocytes. (73, 147, 164) As mature oligodendrocytes are post-mitotic, oligodendrocyte precursor cells (OPCs) are thought to be the principal source of new oligodendrocytes at all life stages. (17, 112, 131) OPCs arise during development from neural stems before migrating throughout the brain in sequential waves, differentiating into oligodendrocytes, and myelinating neuronal axons throughout the brain. (141) In adult mammals, OPCs maintain their ability to migrate, proliferate, and differentiate, enabling dynamic control of myelination throughout life.

Despite the remarkable ability of the brain to adapt to demyelination, in the face of chronic disease, these systems can fail and leave patients with

symptoms of a broken brain circuit. (32, 33, 79, 139) In patients, repeated episodes of oligodendrocyte and myelin loss leads to slowed neuronal conduction velocity, misfiring between neurons, and neuronal death. (46) The most prevalent demyelinating disease, Multiple Sclerosis (MS), is caused by autoimmune-mediated destruction of oligodendrocytes, leading to cognitive, motor, and psychological deficits. (10, 64, 103) Currently approved immunomodulatory therapies for MS fail to compensate for lost myelin, and therefore as a patient's disease progresses, their symptoms persist.

To treat the persistent and increasing symptoms of MS patients, therapies that promote remyelination in the face of demyelinating insults are clinically sought after. Interestingly, in MS, despite widespread oligodendrocyte loss, OPCs are spared from destruction, providing us with a therapeutic opportunity. (17, 112) If we can encourage the preserved OPCs to generate new oligodendrocytes, we may be able to remyelinated the lesioned area and reduce symptoms of MS patients. Based on this therapeutic hypothesis, high-throughput phenotypic screens found dozens of small molecules that promote OPCs to form oligodendrocyte *in vitro* and enhance remyelination *in vivo*. (17, 60, 107, 122, 130) However, the hits from these screens were diverse in annotation and did not align with known oligodendrocyte biology, making the exact mechanism of action unclear. Therefore, the primary goal of this work is to identify the mechanism of action for small molecules that promote oligodendrocyte formation from OPCs, especially those found via

high-throughput unbiased phenotypic screening.

1.1 Oligodendrocyte progenitor cells as a target for remyelinating therapeutics

In demyelinating disorders, loss of myelin and oligodendrocytes in the central nervous system leads to cognitive, motor, and psychological deficits. Disorders in which patients are intrinsically deficient in myelin, hypomyelinating disorders, have many of these same symptoms. One approach to remedy the lack of myelin is to promote the formation of new oligodendrocytes from OPCs. Even in adults, OPCs are capable of differentiating into oligodendrocytes and remyelinating bare axons, allowing for functional recovery. (17) Therefore, one goal of remyelinating therapeutics is to target existing OPCs for the treatment of myelin deficits in demyelinating and hypomyelinating disorders. To discover *in vivo* remyelinating compounds, a number of cellular models have been employed for high-throughput screening.

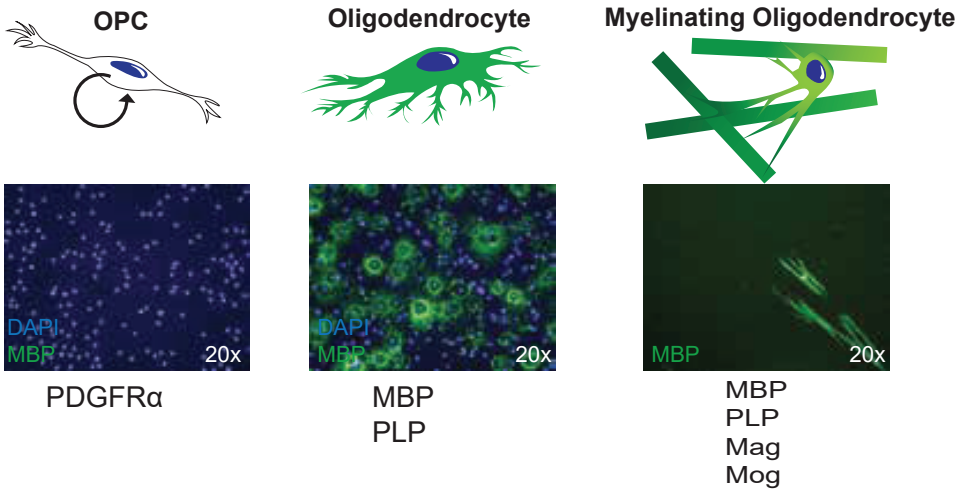

Figure 1.1: Stages of *in vitro* differentiation - Schematic showing OPC differentiation and myelination with specific markers that indicate each stage.

1.1.1 Modeling remyelination for high-throughput screening

There are three main classes of *in vivo* myelination models: developmental myelination models, global remyelination models, and focal remyelination models. However, animal models are resource- and time- intensive; therefore, they are not ideal for drug discovery (table 1.1). Fortunately, due to recent advances, *in vitro* assays represent a convenient way to recapitulate the remyelination process in a high-throughput manner. Different *in vitro* remyelination and OPC differentiation assays vary based on the following parameters: the cells used, the substrate the cells are plated on, and the readout used.

***In vivo* myelination (Weeks)**	***In vitro* myelination (Days-Week)**	**OPC Differentiation (Days)**
developmental myelination	micropillar wrapping	tissue culture plates
global demyelination	microfiber wrapping	
focal demyelination	cortical slice culture	
	neuronal co-culture	

Table 1.1: OPC/Oligodendrocyte models

1.1.1.1 OPC cellular models

An essential component of these *in vitro* assays is the cells used to model oligodendrocyte formation. The most direct way to obtain OPCs is to isolate them from rodent brains using immunopanning, an approach that uses antibodies to separate OPCs from other cells. (44, 110) While screens have

been executed using primary OPCs, these protocols do not easily lend itself to the scale required for small molecule drug screening and necessitate repeated animal sacrificing for experiments. (38, 88, 108) There are three main types of scalable OPC models used for drug screening: immortalized cells, OPCs generated through directed differentiation of OPC precursor cell types, and OPCs generated from reprogramming of non-precursor cell types.

Immortalized OPC lines can improve scalability and readily available; these advantages made them an obvious choice for early OPC drugs screens. (130) However, these cells failed to recapitulate all the expected features of OPCs, such as the heavily arborized morphology seen with *ex vivo* OPCs. (110, 130) Therefore, further models of OPCs have been explored.

Initial studies proved that the generation of glial progenitor cells from mouse embryonic stem cells was possible and scalable. (13, 21) More recently, a model of OPCs derived from epiblast cells has been shown to recapitulate the biology seen in primary *ex vivo* OPCs, be scalable(85, 120), and was used in a number of drug screens. (43, 122) Nevertheless, because isolation of mouse embryonic and epiblast precursor cells from mouse brains is non-trivial, there are challenges associated with reproducibility between labs.

The third class of *in vitro* derived OPCs used for screening, employ lentiviral expression of transcription factors to reprogram cells that are not OPC progenitors, such as fibroblasts. The fibroblasts can either be di-

rectly reprogrammed to OPCs or indirectly through an intermediate induced pluripotent stem cell stage. These approaches are also scalable, however there are some concerns that the lentivirus alters the genetic composition of the cells, which could alter the cellular behavior. (85, 121)

Despite the apparent shortcomings of the various cellular OPC models, small molecule drug screening hits have had high concordance regardless of the model used. The hits from these screens have also successfully translated to compounds which promote remyelination in animals, suggesting the OPC models are reasonably able to recapitulate *in vivo* biology. (17) (table 1.2)

1.1.1.2 *In vitro* assay format

To study the myelination process *in vitro*, OPCs can grow on a number of surfaces that provide substrates for oligodendrocyte maturation or wrapping of myelin. (6) (figure 1.1) Slice culture and co-culture are difficult to scale-up to the level necessary for high-throughput screening. However, micropillar wrapping and microfiber wrapping are both suitable for screening purposes and have lead to the discovery of small molecules that have advanced to clinical trials for remyelination. Unfortunately, use of the micropillar and microfiber assay for screening is limited by the availability of these plates.

By contrast, hundreds of thousands of small-molecules have been screened using the simplest and most popular model for oligodendrocyte formation

screening, two-dimensional tissue culture plastic. Several of these compounds have gone on to validate in the more complicated *in vivo* assays, demonstrating the utility of this simple assay and its relevance to more complex biology. (table 1.2)

1.1.1.3 Quantification of differentiation

While the previously describe approaches generate relatively pure populations of OPCs, when placed in differentiation media, OPCs can differentiate into either oligodendrocytes or astrocytes *in vitro*, leading to a heterogeneous cellular population at the termination of the differentiation assay. Therefore most assays use high-content imaging and fluorescence-based read-outs to stain for each cell type and more accurately quantify myelination and oligodendrocyte formation. Further, antibodies or reporter constructs highlight specific stages in the differentiation process, most commonly, myelin basic protein (MBP), proteolipid protein (PLP), or O4 designate mature oligodendrocytes. (table 1.1, figure 1.1) To analyze the extent of oligodendrocyte formation present in two-dimensional culture researchers have used: the staining intensity of the whole well, the percentage of cells which stain positively for a specific marker, or Scholl analysis to determine the morphology of the cells. (130) Three-dimensional culture systems of myelination, such as the microfiber assays, are quantified by the extent of microfiber tracking or the total amount of staining per well. However, most fre-

quently, a combination of these metrics allows for higher-dimensional analysis of OPC differentiation and oligodendrocyte myelination.

1.1.2 Pro-myelinating small molecules

Using the tools described above, hundreds of small molecules have been discovered which are capable of enhancing OPC differentiation *in vitro*. (130) Several of these have been validated to enhance remyelination *in vivo*. (table 1.2) And a further subset have been advanced to clinical trials. (17)

Interestingly, these drugs are strikingly diverse in annotated mechanism and do not align with known oligodendrocyte biology. Within classes, not all drugs of the same class enhanced oligodendrocyte formation. While some of the targets validated with genetic approaches, several studies noted confusing results of the genetic validation. (60) Of the small-molecules that enhance oligodendrocyte formation, miconazole and olesoxime are the only ones without a proposed target in OPCs.(table 1.2) Importantly, while it was not known how miconazole leads to enhanced oligodendrocyte formation, miconazole is known to inhibit the mammalian cholesterol biosynthesis pathway, which may provide an insight into it's mechanism in OPCs. (17)

Compound	Proposed Targets	Reference	Expressed?	Screen?
Miconazole	unknown	(122)		Y
Clemastine	M1 receptor	(17, 107)	-	Y
Benztropine	M1/M3 receptor	(17, 38)	-	Y
Tamoxifen	ER modulator	(60)	-	Y
Diarylpropionitrile	ER β	(17, 35)	-	N
G1	GPR30	(69)	+	N
Liothyronine	THRA/THRB	(25, 41)	+	N
9-cis retinoic acid	RXR agonist	(71)	+	N
MENT	Androgen receptor	(74)	-	N
TO901317, 25-OH	LXR	(105)	+	N
Olesoxime	unknown	(97)		N
XAV939	Tankyrase inhibitor	(47)	+	N
Quetiapine	GPCRs (not selective)	(17, 170)		Y

Table 1.2: *In vivo* validated remyelinating small molecules Expression level is defined as being greater than 5 Fragments Per Kilobase of exon per Million reads (FPKM) in primary mouse OPCs. (171) The screen column indicates if a compound was identified based on screening. 7alpha-methyl-19-nortestosterone(MENT)

1.2 Cholesterol Biosynthesis Pathway

Given that miconazole was known to inhibit the cholesterol biosynthesis pathway in mammalian cells, we decided to focus on this pathway as a possible target for miconazole in OPCs. Cholesterol is an essential membrane component that is ubiquitous to all metazoans. (146) Cholesterol synthesis begins with acetyl coenzyme A, uses 23 enzymatic steps, and is located in three distinct cellular compartments: the mitochondria, the peroxisome, and the endoplasmic reticulum. (102) The first branch point in the cholesterol biosynthesis pathway is at farnesyl pyrophosphate, which is the precursor for several non-steroidal metabolites such as farnesyl, dolichol, heme A, and ubiquinone. (1, 146) Monoepoxysqualene represents another branch point; it is a precursor for both 24,25-epoxycholesterol and cholesterol. (146) Fi-

nally, 7-DHC can be converted to vitamin D and specific oxysterols in some tissues. (82, 116) (figure 1.3) In addition to its role as a cell membrane component, cholesterol itself is a precursor for other metabolites such as steroid hormones, bile acids, cholesterol esters, and oxysterols. (116, 146) Our work specifically focused on the post-squalene cholesterol biosynthesis pathway and the epoxycholesterol shunt, which are described in more detail below.

1.2.1 Post-squalene Cholesterol Biosynthesis Pathway

The post-squalene portion of the cholesterol biosynthesis pathway has two limbs, the Bloch and the Kandutch-Russell, which use the same enzymes, starting material, and form the same product. (figure 1.3) The only distinction between these two pathways is the presence of a double bond at the 24,25 position among all Bloch pathway intermediates. (1) Both pathways begin with 2,3-oxidosqualene being cyclized by lanosterol synthase (LSS) to form lanosterol, the first sterol (for the precise mechanism, please see (156)). In the Bloch pathway, CYP51 demethylates C-14 using oxygen and NADPH as cofactors, leaving a double bond at the $\triangle$14,15 position to generate FF-MAS. (1) Next, sterol-14 reductase reduces the newly generated $\triangle$14,15 double bond and makes T-MAS with NADPH as a cofactor. (93) T-MAS then undergoes sequential demethylation at the C4 position via the C4-demethylation complex (C4DMC) consisting of SC4MOL, NSDHL, and

HSD17B7 using oxygen, NADPH, and NAD as cofactors to form zymosterol. (133) After this demethylation, zymosterol is isomerized to dehydrolathosterol by EBP, which migrates the $\triangle$8,9 double bond to the $\triangle$7,8 position. (1) SC5D oxidizes dehydrolathosterol at the $\triangle$5,6 position leading to the formation of 7-dehydrodesmosterol. (1) DHCR7 then reduces the $\triangle$7,8 double bond to generate desmosterol, which is reduced at $\triangle$24,25 by DHCR24 to generate cholesterol. In the Kandutch-Russell pathway, DHCR24 acts upon lanosterol to generate dihydrolanosterol. (1) Dihydrolanosterol is then metabolized by the same enzymes leading to intermediates that lack the $\triangle$24,25 unsaturation: dihydro-FFMAS, dihydro-TMAS, zymostenol, lathosterol, 7-dehydrocholesterol, and finally, cholesterol. (1)

However, most tissues do not strictly follow either the Bloch or the Kandutch-Russell pathway; instead, DHCR24 can reduce the double bond of any metabolites in the Bloch pathway. (1, 116) Therefore, depending on the relative expression and kinetics of the different enzymes in the pathway, the point of cross-over varies, and some cells may use both pathways. (116) Further, in the context of pathway inhibition, novel metabolites that are not in either the Bloch or Kandutch-Russell pathways can accumulate; this happens with sterol-14 reductase inhibition and DHCR7 inhibition. (See fig. 1.4) With sterol-14 reductase inhibition, the C4-demethylation complex converts FF-MAS and dihydro-FFMAS to 14- dehydrozymosterol and 14- dehydrozymostenol. (145) Similarly, with DHCR7 inhibition, EBP metabolizes 7-DHC

and 7-DHD to 8,9-DHC and 8,9-DHD by shifting the double bond at $\triangle$7,8 back to the $\triangle$8,9 position. (7, 82) These non-canonical metabolites highlight that some enzymatic reactions in the cholesterol biosynthesis pathway are capable of working in reverse if the pathway is sufficiently perturbed.

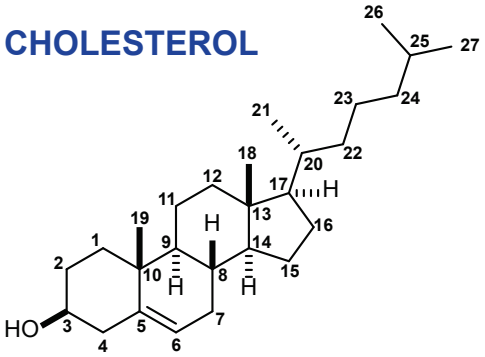

Figure 1.2: Cholesterol with numbered carbons - This numbering convention is used when discussing all metabolites in the pathway.

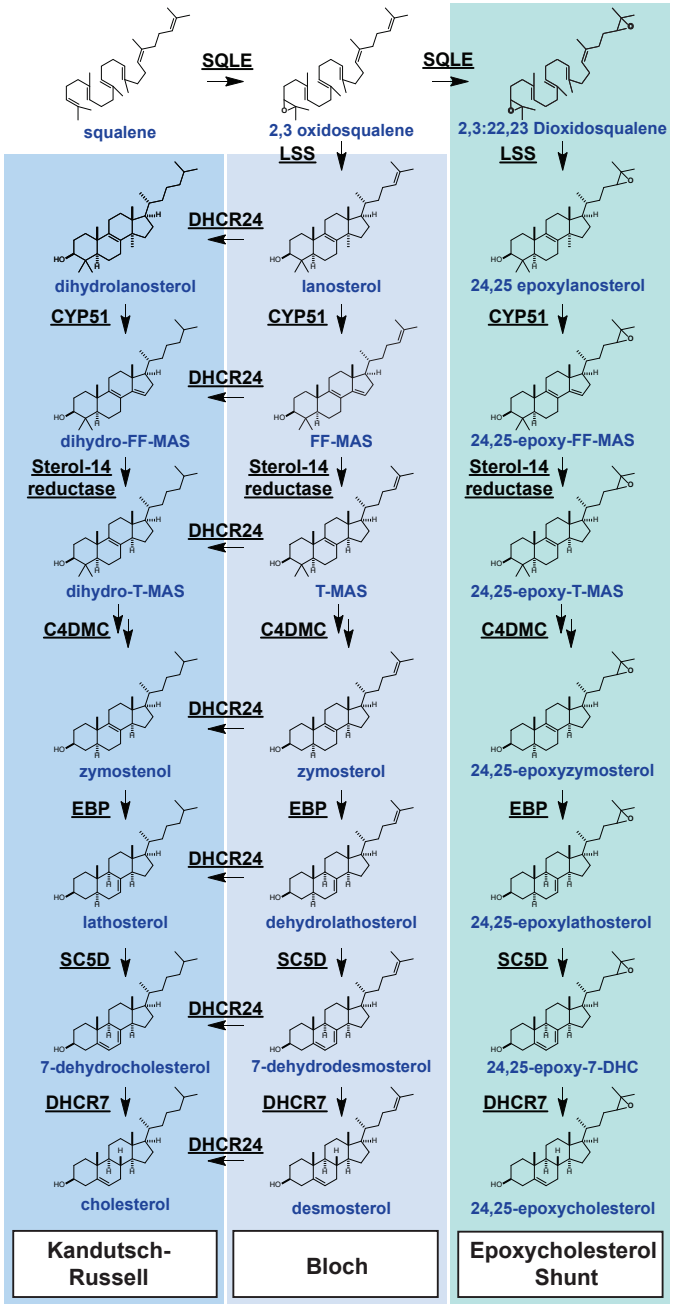

Figure 1.3: Post-squalene cholesterol biosynthesis pathway - Enzymes are underlined while metabolites are labelled in blue.

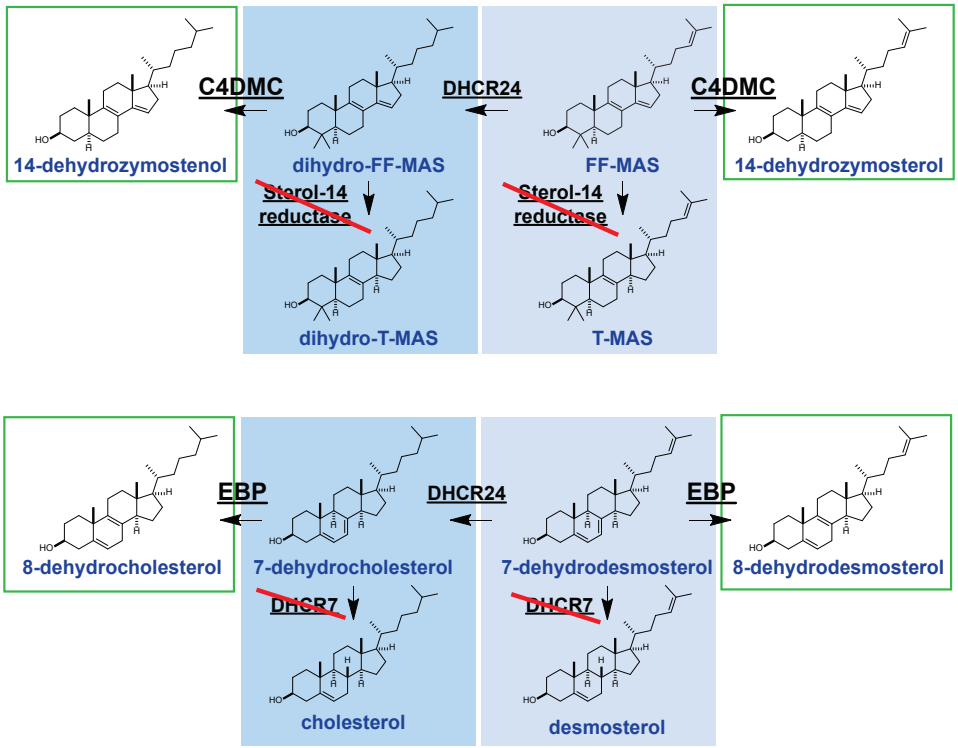

Figure 1.4: Non-canonical metabolites: 14-DHZ, 8,9-DHC, 8,9-DHD - Diagram demonstrating alternative metabolism of sterols upon inhibition of sterol-14 reductase or DHCR7.

1.2.2 Epoxycholesterol Shunt

In 1982 it was first described that squalene could give rise to a unique bioactive metabolite, 24,25-epoxycholesterol, via the epoxycholesterol shunt. (126) Since then, 24,25 epoxycholesterol has been found to play a role in a variety of signaling contexts and is an important signaling molecule in its own right. (119) The epoxycholesterol pathway branches off of the classic cholesterol biosynthesis pathway between 2,3 oxidosqualene and lanosterol. (figure 1.3) 2,3 oxidosqualene can be cyclized by LSS, committing it to the cholesterol biosynthesis pathway, or epoxidized again to make dioxidosqualene, committing it to the epoxycholesterol biosynthesis pathway. (126) The two pathways use identical enzymes and arise from a common substrate. Ergo, the synthesis of cholesterol and epoxycholesterol happens in parallel. (161) What fraction of squalene becomes epoxycholesterol versus cholesterol varies in different tissues and can be modulated with genetic and pharmacological tools. (140, 161, 168) Typically levels of 24,25 epoxycholesterol tend to be between 0.1-1$\%$ of the total cholesterol depending on the cell type and context. (18) Interestingly, LSS prefers to cyclize dioxidosqualene over oxidosqualene. (16) Therefore partial inhibition of LSS leads to the preferential formation of epoxycholesterol over cholesterol. (140, 161) Conversely, overexpression of LSS leads to decreased levels of 24,25 epoxycholesterol, and preferential formation of cholesterol. (161) In short, the epoxycholes-

terol shunt is a branch off the post-squalene cholesterol biosynthesis pathway whose use can be modulated by titrating the enzymatic activity of LSS.

1.3 Sterols in Oligodendrocytes

1.3.1 Origin of Cholesterol used by Oligodendrocytes

Myelin contains 80% of all brain cholesterol and represents the largest cholesterol pool in adult mice. (39, 142) The brain is one of the most cholesterol dense organs, and it relies entirely on locally synthesis as cholesterol can not cross the blood-brain barrier. (142) All major cell types in the brain express the enzymes required for cholesterol biosynthesis and actively generate cholesterol: neurons, astrocytes, OPCs, oligodendrocytes, and microglia. (53, 77, 127, 135) Within the brain, the various cell types share a cholesterol pool with ample transport between cell types. (26, 142) Oligodendrocytes can generate cholesterol during development, in addition to receiving cholesterol synthesized by astrocytes or other cell types. (26, 143)

1.3.2 Inhibition of Cholesterol Biosynthesis in Oligodendrocytes

Overall, the consensus in the field is that blocking the pre-squalene cholesterol biosynthesis pathway is likely detrimental to oligodendrocytes and OPC

differentiation. This observation is supported by studies *in vitro* and *in vivo*.

In *in vitro* rodent OPC culture, using simvastatin to block 3-hydroxy-3- methylglutaryl-CoA (HMG-CoA) globally leads to impaired oligodendrocyte process formation, less mature oligodendrocytes, and increased cell death. (148) Interestingly, co-treatment with simvastatin and geranylgeranyl pyrophosphate (a metabolite downstream of farnesyl pyrophosphate) was able to rescue some of these deficits associated with simvastatin treatment; suggesting that not all the effects seen with simvastatin are due to cholesterol depletion. (148) In a different study, treating with lovastatin leads to decreased expression of PLP and MBP in myelin sheaths. (98) Also, the treatment of oligodendrocytes with a squalene synthase inhibitor leads to decreased arborization and decreased staining of PLP at the cell surface. (98, 148)

In vivo zebrafish models show that mutating or inhibiting HMGCR leads to decreased OPC migration and decreased myelin gene expression. (101) Inhibition of protein prenylation leads to OPC migration deficits, whereas depleted cholesterol levels lead to decreased myelin gene expression. (101) LSS inhibitors decrease PLP and MBP expression, which was rescued with cholesterol supplementation. Further, in the presence of LSS inhibitors, mature oligodendrocytes failed to ensheath neuronal axons. (101)

In *in vivo* mouse models, conditional knockout of squalene synthase (fdft1) in the oligodendrocyte lineage leads to delayed myelination, ataxia,

tremor, and premature death. (143) However, mice that survived to adulthood with this mutation live an average life span, and their phenotype improved. (143) This result supports the notion that other cell types in the brain can compensate for inhibition of the cholesterol biosynthesis pathway in OPCs. (142)

The challenge in interpreting many of these studies is that the experiments performed lead to decreases in metabolites other than cholesterol, such as 24,25 epoxycholesterol, which may be contributing to the phenotypes observed. Despite trying to quantify the effects on non-steroidal products of the cholesterol biosynthesis pathway, these experiments failed to address the effects on the post-squalene cholesterol biosynthesis intermediates.

1.3.3 Screens for inhibitors of cholesterol formation

Screening for small molecule inhibitors of the cholesterol biosynthesis pathway in brain cells has focused on finding treatments for genetic disorders, tor example, for Smith-Lemli-Opitz syndrome (SLOS). In SLOS, DHCR7 is mutated leading to an accumulation of 7-DHC, a toxic metabolite in the post-squalene cholesterol biosynthesis pathway that is known to kill neuronal cells. LC-MS based high-throughput screening of several libraries in neuronal cells found compounds that prevent the accumulation of 7-DHC. (81, 82) These screens delineated several cholesterol synthesis inhibiting

compounds from diverse categories including estrogen receptor modulators (including tamoxifen), antipsychotics, muscarinic receptor antagonists (including clemastine), and antifungals (such as azole antifungals). (28, 81, 82, 153)

1.4 Summary

In vitro screens using various OPC models have highlighted dozens of compounds that promote oligodendrocyte formation *in vitro*, *in vitro* myelination, and myelination *in vivo*. However, the mechanism by which these compounds promote oligodendrocyte formation is less clear. Most of these drugs are thought to function through their canonical targets despite these targets not being expressed in OPCs. (table 1.2) Interestingly, miconazole is known to inhibit the cholesterol biosynthesis pathway in mammalian cells and robustly enhance remyelination in a large number of models. (122) Screens using neuronal cells highlighted compounds that inhibit the post-squalene portion of the cholesterol biosynthesis pathway. The cholesterol biosynthesis inhibition hits overlap with hits in pro-myelinating screens. This observation suggests that the inhibition cholesterol biosynthesis pathway may be involved in the mechanism of pro-myelinating compounds. However, previous work suggests that blocking cholesterol formation is likely to be detrimental for myelin production. Therefore the hypothesis that blocking choles-

terol biosynthesis may promote oligodendrocyte formation is a bit counter-intuitive. How can these two discordant observations both be true?

2

Accumulation of 8,9-unsaturated sterols drives oligodendrocyte formation and remyelination

2.1 Introduction

Regeneration of myelin is mediated by oligodendrocyte progenitor cells—an abundant stem cell population in the central nervous system (CNS) and the principal source of new myelinating oligodendrocytes. Loss of myelin-producing oligodendrocytes in the CNS underlies a number of neurological diseases, including multiple sclerosis and diverse genetic diseases (45, 50, 59). High-throughput chemical screening approaches have been used to identify small molecules that stimulate the formation of oligodendrocytes

from oligodendrocyte progenitor cells and functionally enhance remyelination *in vivo* (38, 60, 71, 88, 106, 108, 122). Here we show that a wide range of these pro-myelinating small molecules function not through their canonical targets but by directly inhibiting CYP51, TM7SF2, or EBP, a narrow range of enzymes within the cholesterol biosynthesis pathway. Subsequent accumulation of the 8,9-unsaturated sterol substrates of these enzymes is a key mechanistic node that promotes oligodendrocyte formation, as 8,9-unsaturated sterols are effective when supplied to oligodendrocyte progenitor cells in purified form whereas analogous sterols that lack this structural feature have no effect. Collectively, our results define a unifying sterol-based mechanism of action for most known small-molecule enhancers of oligodendrocyte formation and highlight specific targets to propel the development of optimal remyelinating therapeutics. [1]

2.2 Results

2.2.1 Imidazole antifungals inhibit CYP51 to promote oligodendrocyte formation

Imidazole antifungal drugs are a structurally diverse class of small molecules that robustly stimulate the generation of new mouse and human oligodendrocytes and enhance remyelination in mouse models of disease(122). Im-

[1] This work is published. (72)

idazole antifungals mediate their effects in yeast by inhibiting CYP51, an essential enzyme for sterol biosynthesis in both fungal and mammalian cells (for a detailed cholesterol biosynthesis diagram, see fig.2.5). Across a panel of nine azole-containing molecules, the ability to inhibit CYP51 *in vitro* and in oligodendrocyte progenitor cells (OPCs) predicted enhanced formation of myelin basic protein-positive (MBP+) oligodendrocytes from mouse epiblast stem cell-derived OPCs (See fig. 2.1a-d, 2.6a–c). To measure inhibition of CYP51 in OPCs, we used gas chromatography and mass spectrometry (GC–MS) to quantify the increase in levels of lanosterol (the substrate of CYP51) and decrease in cholesterol (56, 57, 81) (See fig. 2.1b, 2.62c–e). In cells treated with ketoconazole, the dose–response curve for accumulation of lanosterol closely resembled the dose–response curve for enhanced oligodendrocyte formation (See fig. 2.1c, 2.6b, f, g). Notably, we confirmed all effects of small molecules on oligodendrocyte formation and sterol levels using a second, independently isolated batch of OPCs, and key results were also validated using mouse primary OPCs (See fig. 2.6b–i; see Methods). In addition, the effects of azole molecules were confirmed using an orthogonal image quantification approach, a second oligodendrocyte marker, and liquid chromatography with mass spectrometry (LC–MS) to detect cellular sterols (See fig. 2.6j–l).

We next used RNA interference and metabolite supplementation to independently confirm the role of CYP51 in oligodendrocyte formation. Cell-

permeable small interfering RNA (siRNA) reagents depleted CYP51 transcript levels in OPCs by 80% (114), led to substantial accumulation of lanosterol, and enhanced formation of MBP+ oligodendrocytes (See fig. 2.1e, f, 2.6m–o). In addition, we treated OPCs directly with purified lanosterol and observed enhanced formation of MBP+ oligodendrocytes in a dose-responsive fashion (See fig. 2.1g, h, 2.6p, q). These findings support the idea that CYP51 is the functional target of imidazole antifungals in OPCs and suggest that accumulation of sterol intermediates may play a direct role in enhancing oligodendrocyte formation.

2.2.2 Inhibtion of CYP51, TM7SF2, or EBP promotes oligodendrocyte formation

As inhibition of CYP51 was sufficient to induce the formation of oligodendrocytes, we used a chemical genetics approach to test whether modulation of other steps in cholesterol biosynthesis had a similar effect (See fig. 2.2a, 2.5). We used GC–MS-based sterol profiling in OPCs to confirm that a panel of eight small molecules selectively inhibited their known enzyme targets within the cholesterol biosynthesis pathway (See fig. 2.7a–d; see Source Data for abundance of all quantified metabolites in all GC–MS-based sterol profiling experiments). Only molecules targeting CYP51 (ketoconazole), TM7SF2 (amorolfine(75)), and EBP (TASIN-1(169)) enhanced

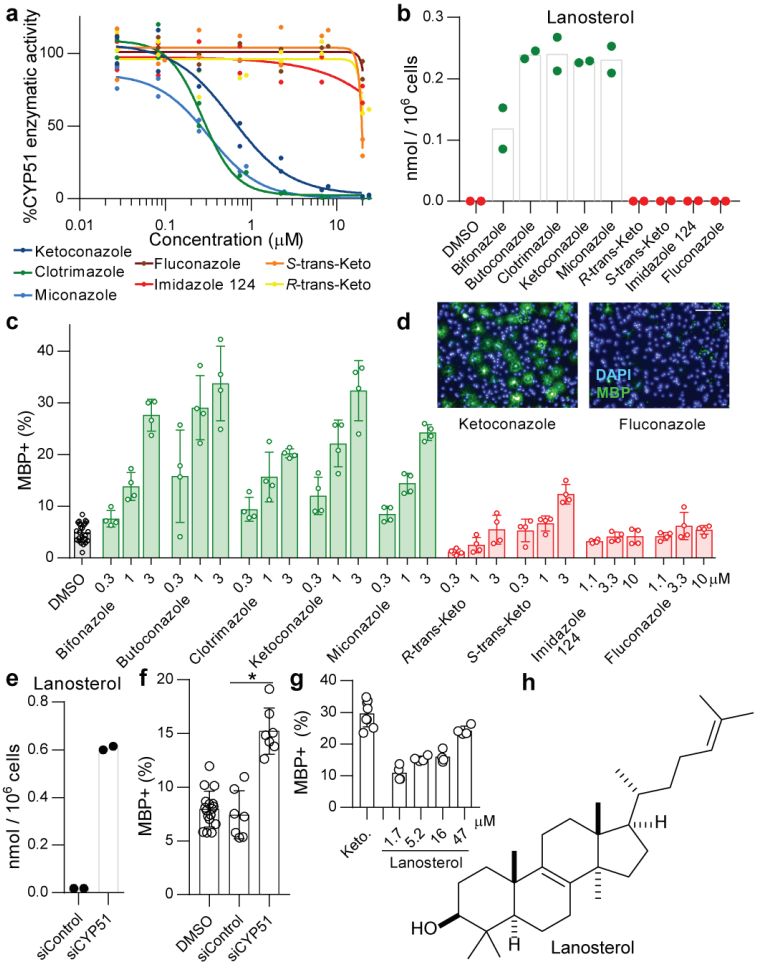

Figure 2.1: Imidazoles inhibit CYP51 to enhance oligodendrocyte formation - a, Rat CYP51 enzymatic activity following treatment with azoles. n = 2 independent enzymatic assays. b, GC–MS-based quantification of lanosterol levels in OPCs treated with the indicated azoles at 2.5 μM. n = 2 wells per condition. c, f, g, Percentage of MBP+ oligodendrocytes generated from OPCs following treatment with azoles (c), cell-permeable siRNA reagents (f), or lanosterol (g). n $\geq$ 4 wells per condition; for exact well counts in all figures, see Methods section 'Statistics and reproducibility'. In f, *P = 0.0005, two-tailed Student's t-test. d, Representative images of OPCs treated with the indicated azoles. Nuclei are labelled with DAPI (blue) and oligodendrocytes are indicated by immunostaining for MBP (green). Scale bar, 100 μm. e, GC–MS-based quantification of lanosterol levels in OPCs treated with the indicated reagents. n = 2 wells per condition. h, Structure of lanosterol. All bar graphs indicate mean $\pm$ s.d. Results in c, d, g are representative of three independent experiments; those in b, e, f are representative of two independent experiments using OPC-5 cells; for validation in an independent derivation of OPCs, see Extended Data 2. Keto, ketoconazole.

formation of MBP+ oligodendrocytes, whereas inhibitors of the five other pathway enzymes were ineffective (See fig. 2.2b, 2.7e–h). Treatments had little effect on cell number (See fig. 2.7e). Concentrations of amorolfine and TASIN-1 that enhanced oligodendrocyte formation also led to accumulation of 14-dehydrozymostenol and zymostenol, respectively (See fig. 2.7i, j). Moreover, distinct structural classes of inhibitors of CYP51, TM7SF2 and EBP comparably enhanced oligodendrocyte formation, including at picomolar doses(See fig. 2.8a–h)(37).

We also used CRISPR–Cas9 targeting to evaluate the effects of genetic suppression of EBP. OPCs expressing Cas9 and guide RNA targeting EBP demonstrated reduced EBP transcript levels, robust accumulation of the expected intermediate zymostenol, and enhanced formation of oligodendrocytes under differentiation-permissive conditions (See fig. 2.2c, d, 2.8k). Two independent guide RNA sequences produced similar results (See fig. 2.8i–l). In total, this genetic and chemical genetic analysis suggests that inhibition of the cholesterol biosynthesis pathway within a limited window of enzymes between CYP51 and EBP is sufficient to enhance the formation of oligodendrocytes.

2.2.3 8,9-unsaturated sterols are sufficient to promote oligodendrocyte formation

The efficacy of these small molecules and genetic perturbations was not mediated by a simple reduction in sterol levels, as treatment with statin drugs or methyl -cyclodextrin depleted cholesterol levels comparably without enhancing oligodendrocyte formation (See fig. 2.2b, 2.7a, b, 2.9a, b). Because treatment of OPCs with the CYP51 substrate lanosterol enhanced oligodendrocyte formation, we examined the effects of other purified sterols. Treatment of OPCs with 8,9-unsaturated sterols, including 14-dehydrozymostenol (which accumulates following TM7SF2 inhibition) and zymostenol (which accumulates following EBP inhibition), enhanced the formation of MBP+ oligodendrocytes. By contrast, sterols lacking 8,9-unsaturation, including cholesterol itself(144), were ineffective (See fig. 2.2e, h, 2.9c). A total of nine natural and unnatural 8,9-unsaturated sterols enhanced oligodendrocyte formation from OPCs, with 2,2-dimethyl-zymosterol the most potent among those evaluated to date (See fig. 2.2f, 2.9d–l, o). Conversely, treating OPCs with Ro 48-8071, which inhibits lanosterol synthase and thereby prevents the accumulation of 8,9-unsaturated sterols, abrogated the enhanced oligodendrocyte formation induced by the CYP51 inhibitor ketoconazole (See fig. 2.9m, n, p). In addition, analogues of either zymostenol or 8-dehydrocholesterol that lacked 8,9-unsaturation were inactive, demonstrating that 8,9-unsaturation

is a crucial structural feature for activity in OPCs (See fig. 2.2g, 2.9k, l). Finally, co-treating OPCs with ketoconazole and MAS-412 provided no further benefit over ketoconazole alone, confirming that these molecules act through a redundant mechanism (See fig. 2.9q, r). Together these findings indicate that the accumulation of 8,9-unsaturated sterols in OPCs is a central mechanism for enhancing oligodendrocyte formation, whether these sterols arise from small-molecule inhibition of cholesterol biosynthesis enzymes or are supplied to OPCs in purified form.

2.2.4 SREBP is not the mechanism for 8,9-unsaturated sterols

Most of the 8,9-unsaturated sterols that are shown here to enhance oligodendrocyte formation have previously been shown to function as signalling lipids in oocytes by inducing the resumption of meiosis(24, 62). While the direct cellular targets of 8,9-unsaturated 'meiosis-activating sterols' remain poorly understood, there is evidence nuclear hormone receptors (NHRs) may play a role(24). We evaluated 2,2-dimethylzymosterol and the pathway inhibitors ketoconazole and TASIN-1 in cell-based reporter assays for 20 NHRs, but no molecule showed significant activity in any assay (See fig. 2.9s–u). Additional experiments discounted a role for SREBP2, which transcriptionally regulates cholesterol homeostasis, suggesting that these sterols act by mechanisms beyond NHRs or SREBP2 (See fig. 2.9v). Together, these studies suggest a novel role for the meiosis-activating sterols

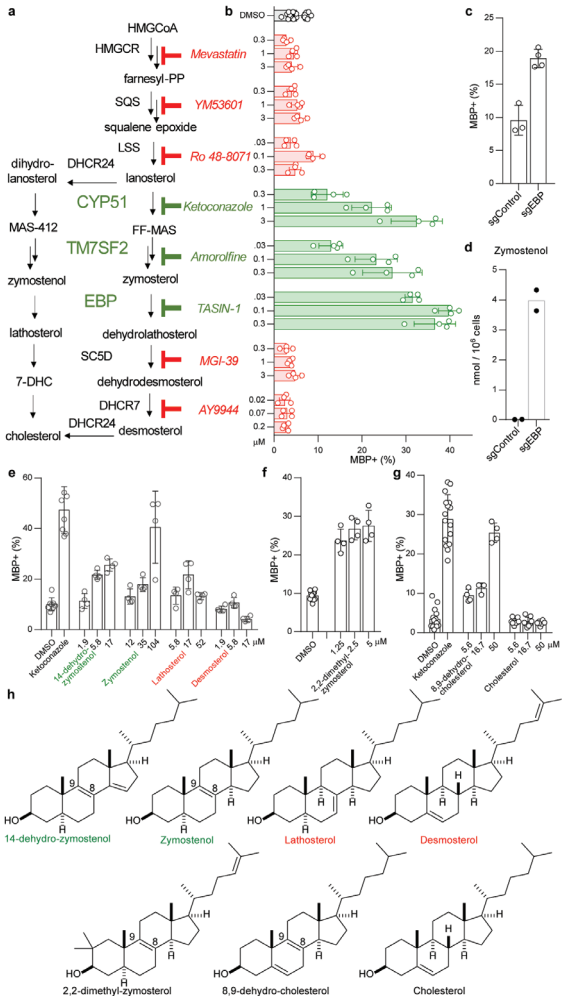

Figure 2.2: Small-molecule inhibition of CYP51, TM7SF2, or EBP enhances oligodendrocyte formation via accumulation of 8,9-unsaturated sterols. - a, Abbreviated cholesterol biosynthesis pathway. For greater detail, see 2.5. FF-MAS, follicular fluid-meiosis-activating sterol. b, Percentage of MBP+ oligodendrocytes generated from OPCs treated with the indicated pathway inhibitors. n $\geq$ 4 wells per condition. c, Percentage of MBP+ oligodendrocytes generated from OPCs expressing Cas9 and guide RNA targeting EBP. n $\geq$ 3 wells per condition. d, Functional validation of Cas9-based targeting of EBP using GC–MS-based quantification of zymostenol levels. n = 2 wells per condition. e–g, Percentage of MBP+ oligodendrocytes generated from OPCs with the indicated purified sterols. n $\geq$ 4 wells per condition. h, Structures of various sterols. All bar graphs indicate mean $\pm$ s.d. See Methods section 'Statistics and reproducibility' for exact well counts. Experiments in b–g are representative of two or more independent experiments using OPC-5 cells; for validation in an independent derivation of OPCs, see Extended Data Figs. 3–5.

in promoting oligodendrocyte formation.

2.2.5 Most pro-differentiation screening hits inhibit CYP51, TM7SF2, or EBP

In parallel, we executed a screen of over 3,000 bioactive small molecules and approved drugs at a uniform dose of 2 μM (See fig. 2.10a). In addition to molecules previously annotated as enhancing OPC differentiation(38, 60, 106), we also identified many confirmed hits whose known targets did not cluster into easily discernible categories (See table 2.1). Among the top ten novel enhancers of oligodendrocyte formation, four molecules had previously been shown to inhibit TM7SF2 or EBP in CNS-derived cells(28, 81). In fact, GC–MS-based sterol profiling revealed that all ten top hits led to accumulation of 8,9-unsaturated sterols at the screening dose, whereas randomly selected library members had no effect on sterol levels or oligodendrocyte formation. (See fig. 2.3a, 2.10b–f).

Given the frequency of cholesterol pathway modulators within our top screening hits, we assessed whether any previously reported enhancers of remyelination identified by drug screening might also induce accumulation of sterol intermediates. At concentrations that promoted oligodendrocyte formation, benztropine, clemastine, tamoxifen, and U50488 induced accumulation of zymostenol and zymosterol and decreased basal sterol levels, in-

Table 2.1: Enhancers of oligodendrocyte formation identified by screening of a 3,000-molecule bioactives library

Name	Total Cells	% Oligos	MW	DMSO% oligos_ Mean	DMSO% oligos_StdDev	cell viability (% relative to DMSO)	fold-change in % MBP+ oligodendrocytes
Isoconazole nitrate	584	53.25	479.14	7.95	3.66	106.98	**6.70**
EPZ005687	610	50.00	539.67	8.47	2.61	91.36	**5.90**
Clotrimazole	666	27.93	344.85	4.75	2.75	122.50	**5.88**
Ketoconazole	847	52.77	531.44	9.33	3.87	121.51	**5.65**
Butoconazole nitrate	809	46.85	474.79	8.92	2.63	122.03	**5.25**
Sertaconazole nitrate	777	39.38	500.78	7.52	1.87	134.49	**5.23**
Pyrimethamine	604	43.87	248.71	8.92	2.63	91.11	**4.92**
Ifenprodil Tartrate	693	41.41	475.53	8.47	2.61	103.79	**4.89**
Varenicline tartrate	783	22.86	361.36	4.75	2.75	144.02	**4.81**
Raloxifene HCl	777	35.01	510.04	7.29	3.37	114.37	**4.80**
Hydroxyzine 2HCl	896	40.63	447.83	8.47	2.61	134.19	**4.80**
Ziprasidone HCl	1003	34.10	449.40	7.29	3.37	147.64	**4.68**
Bifonazole	820	40.98	310.39	8.92	2.63	123.69	**4.59**
SB408124	704	39.63	356.37	8.92	2.63	106.19	**4.44**
Sulconazole Nitrate	700	37.57	460.76	8.47	2.61	104.84	**4.44**
Pentamidine isethionate	758	41.29	592.69	9.33	3.87	108.75	**4.42**
Clemastine fumarate	449	20.49	459.97	4.75	2.75	82.59	**4.31**
Raltegravir (MK-0518)	768	38.02	444.42	8.92	2.63	115.85	**4.26**
Fenticonazole Nitrate	687	35.66	518.41	8.92	2.63	103.63	**4.00**
Mubritinib (TAK 165)	779	31.45	468.47	7.95	3.66	142.71	**3.95**
Pramoxine HCl	755	32.98	329.86	8.47	2.61	113.08	**3.89**
TMB-8 hydrochloride	758	18.47	432.00	4.75	2.75	139.42	**3.89**
(±)-Vesamicol hydrochloride	821	34.23	295.86	8.84	3.16	112.02	**3.87**
Clotrimazole	748	34.36	344.84	8.92	2.63	112.83	**3.85**
Fulvestrant	758	18.21	606.79	4.75	2.75	139.42	**3.83**
Raloxifene hydrochloride	924	33.33	510.06	8.84	3.16	126.07	**3.77**
Praziquantel	728	33.24	312.41	8.92	2.63	109.81	**3.72**
Ziprasidone hydrochloride monohydrate	851	32.78	467.42	8.84	3.16	116.11	**3.71**
LY2784544	480	28.75	469.94	7.95	3.66	87.93	**3.62**
Ifenprodil tartrate	739	33.69	801.00	9.33	3.87	106.02	**3.61**
L-745,870 hydrochloride	647	32.61	363.29	9.33	3.87	92.82	**3.49**
Hexahydro-sila-difenidol hydrochloride, p-fluoro analog	654	26.76	386.03	7.68	3.55	95.08	**3.49**

KEY

Imidazole antifungal
Enhances oligodendrocyte formation and causes sterol intermediate accumulation
False positive (did not confirm as enhancing oligodendrocyte formation)
not retested

dicative that they inhibited EBP in OPCs (See fig. 2.3b, 2.10g–l). Tamoxifen has been shown to inhibit the enzymatic activity of EBP directly(63, 81, 117), and we confirmed that benztropine, clemastine, tamoxifen, U50488, and several high-throughput screening (HTS) hits all inhibited EBP directly in a biochemical assay22 (See fig. 2.3c). By contrast, liothyronine and bexarotene showed minimal effects on sterol levels in OPCs (See fig. 2.3b, 2.10g), consistent with their known functions as modulators of transcription factor function and confirming that many, but not all, treatments that enhance oligodendrocyte formation cause accumulation of 8,9-unsaturated sterols.

2.2.6 Inhibition of EBP correlates with enhanced oligodendrocyte formation for known remyelinating compounds

While each of these bioactive small molecules has a previously annotated 'canonical' target, extensive structure–activity relationship data show that the ability to inhibit EBP, rather than the canonical target, predicts enhanced oligodendrocyte formation. For example, we validated a panel of six muscarinic receptor antagonists that all showed near-complete inhibition of the M1, M3, and M5 muscarinic receptor subtypes at the HTS dose of 2 μM (See fig. 2.10m, p). Among these molecules, only clemastine and benztropine inhibited EBP in OPCs, and only clemastine and benztropine enhanced oligodendrocyte formation (See fig. 2.10j, k, m–r). Likewise, among selective

oestrogen receptor modulators (SERMs), toremifene and ospemifene are structurally near-identical and show comparable cellular anti-oestrogen activity. However, only toremifene inhibited EBP in OPCs, and only toremifene enhanced oligodendrocyte formation (See fig. 2.11a–g). Conversely, while 4-hydroxy-tamoxifen, as expected, showed 100-fold enhanced cellular anti-oestrogen activity relative to tamoxifen, both molecules have comparable potency for inhibition of EBP and comparable potency for enhancing oligodendrocyte formation (See fig. 2.11h–j). Finally, the leading novel hit from our HTS, EPZ005687, was annotated as an inhibitor of the histone methyltransferase EZH2. However, analysis of three additional structurally related EZH2 inhibitors revealed that only EPZ005687 inhibited EBP and enhanced oligodendrocyte formation (See fig. 2.11k–r). Across various antimuscarinic agents, SERMs, and EZH2 inhibitors, the ability to inhibit EBP, rather than each molecule's canonical activity, predicted enhanced oligodendrocyte formation.

2.2.7 8,9-unsaturated sterols are additive with liothyronine with respect to pro-differentiation effects

We next tested the potential for combinations of small molecules to show additive or non-additive effects. Combining the thyroid hormone agonist liothyronine with a range of treatments that both modulated sterols and induced

differentiation of OPCs produced additive effects on oligodendrocyte formation, indicating that these molecules are likely to function by mechanisms other than thyroid hormone receptor signalling to enhance oligodendrocyte generation (See fig. 2.12a, b). By contrast, combinations of ketoconazole at a maximally effective dose with benztropine, clemastine, tamoxifen, or U50488 did not enhance differentiation above levels seen for ketoconazole alone (See fig. 2.12c–e), consistent with these molecules sharing 8,9-unsaturated sterol accumulation as a common mechanism for induction of oligodendrocyte formation.

2.2.8 8,9-unsaturated sterols promote *in vitro* myelination

Because our *in vitro* OPC assays modelled only the initial differentiation event into oligodendrocytes, we next tested whether sterol pathway modulation also enhanced subsequent oligodendrocyte maturation and myelination *in vitro* and *in vivo*. First, we cultured OPCs on electrospun microfibres to assess the effects of sterol pathway modulators on the ability of oligodendrocytes to track and wrap along axon-like substrates(9, 91). Ketoconazole (CYP51), amorolfine (TM7SF2), and TASIN-1 (EBP) all robustly enhanced tracking along and wrapping around microfibres by MBP+ oligodendrocytes. By contrast, inhibition of other enzymes up- or downstream in the pathway had little effect on oligodendrocyte maturation and ensheathment of microfibres (See fig. 2.12f–k).

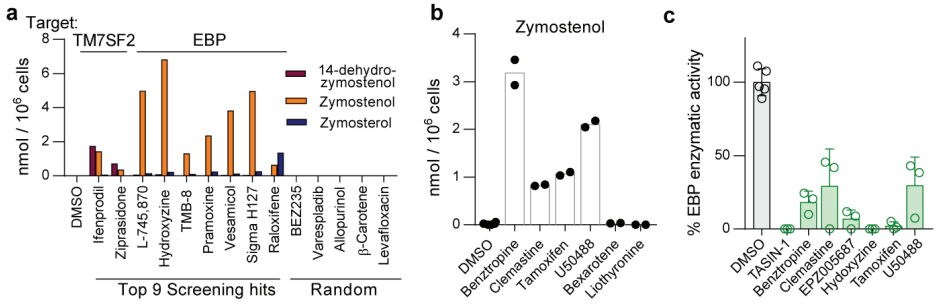

Figure 2.3: Inhibition of TM7SF2 and EBP is a unifying mechanism for many small-molecule enhancers of oligodendrocyte formation - a, Quantification of sterol levels in OPCs treated with the indicated molecules at 2 μM (one well per condition; for validation in a second derivation of OPCs, see Extended Data Fig. 6). b, Quantification of sterol levels in OPCs treated with the indicated previously reported enhancers of oligodendrocyte formation (n = 2 wells per condition except DMSO, n = 6). Representative of two independent experiments; for concentrations, see Extended Data Fig. 6g. c, Quantification of EBP enzymatic activity in a biochemical assay. All treatments 10 μM. n = 3 independent enzymatic assays, except DMSO, n = 5. Bars indicate mean; error bars indicate s.d. Sigma H127, p-fluorohexahydro-sila-difenidol.

2.2.9 8,9-unsaturated sterols promote *in vivo* myelination

The imidazole antifungal miconazole, which targets CYP51, penetrates the mouse blood–brain barrier and enhances remyelination in mouse models of demyelination(122). Here we evaluated brain-penetrant molecules with affinity for TM7SF2 (ifenprodil) and EBP (tamoxifen) using a well-established mouse model in which injection of lysolecithin is used to create focal lesions of demyelination in the dorsal column white matter of the adult spinal cord(111). In vehicle-treated mice, profiles of sparsely distributed remyelinating axons characterized by thin myelin sheaths were detected mainly at the periphery of the lesion, while ultrastructural analyses revealed unmyelinated axons or axons with a single wrap of myelin (See fig. 2.4a, b).

By contrast, after eight days of treatment with ifenprodil or tamoxifen, remyelination was widespread throughout the lesion (See fig. 2.4a, b, 2.13a), consistent with a recent report regarding tamoxifen(60). Critically, we used GCMS-based sterol profiling of brain tissue from mice treated with miconazole, ifenprodil, and tamoxifen to demonstrate that these therapeutic dosing regimens all led to substantial accumulation of 8,9-unsaturated sterols within the mouse brain, indicating that CYP51, TM7SF2, and EBP, respectively, were inhibited (See fig. 2.4c). Collectively, these data show that small-molecule inhibitors of CYP51, TM7SF2, and EBP can engage their sterol pathway targets and enhance remyelination in mice.

2.2.10 8,9-unsaturated sterols promote oligodendrocyte formation in human models

Finally, the oligodendrocyte-enhancing and sterol-modulating activities of leading pathway inhibitors extend to human cells and tissue. Various small molecules caused accumulation of the expected 8,9-unsaturated sterol intermediates both in a human glioma cell line and in human pluripotent stem cell-derived cortical spheroids(96), confirming that these molecules similarly engage the sterol synthesis pathway in mouse and human cells and CNS tissue (See fig. 2.13b, c). Critically, miconazole and ifenprodil also substantially enhanced the generation human oligodendrocytes in a 3D human

pluripotent stem cell-derived cortical spheroid model, indicating conservation of function across species(See fig. 2.4d, e).

2.3 Discussion

We have defined a dominant mechanism shared by many small-molecule enhancers of remyelination: elevation of levels of 8,9-unsaturated sterol intermediates by inhibition of a narrow range of cholesterol biosynthesis enzymes between CYP51 and EBP. We have identified 27 small molecules that both enhance oligodendrocyte formation and increase levels of 8,9-unsaturated sterol intermediates(28, 63, 81). Mechanistically, several lines of evidence support a central signalling role for 8,9-unsaturated sterols in the observed enhanced oligodendrocyte formation, including the ability of nine independent 8,9-unsaturated sterols to enhance the formation of oligodendrocytes when supplied to OPCs(See fig. 2.14).

Myelin is cholesterol-enriched, and past work has established that genetic or pharmacological treatments that inhibit early enzymes in cholesterol biosynthesis lead to hypomyelination *in vivo*(80, 115, 143). Our work supports these observations, as inhibition of HMGCoA reductase or squalene synthase had neutral-to-negative effects on oligodendrocyte formation in our assays (See fig. 2.2b, 2.7). These enzymes catalyse steps before the synthesis of the first sterol intermediate, so their inhibition prevents the syn-

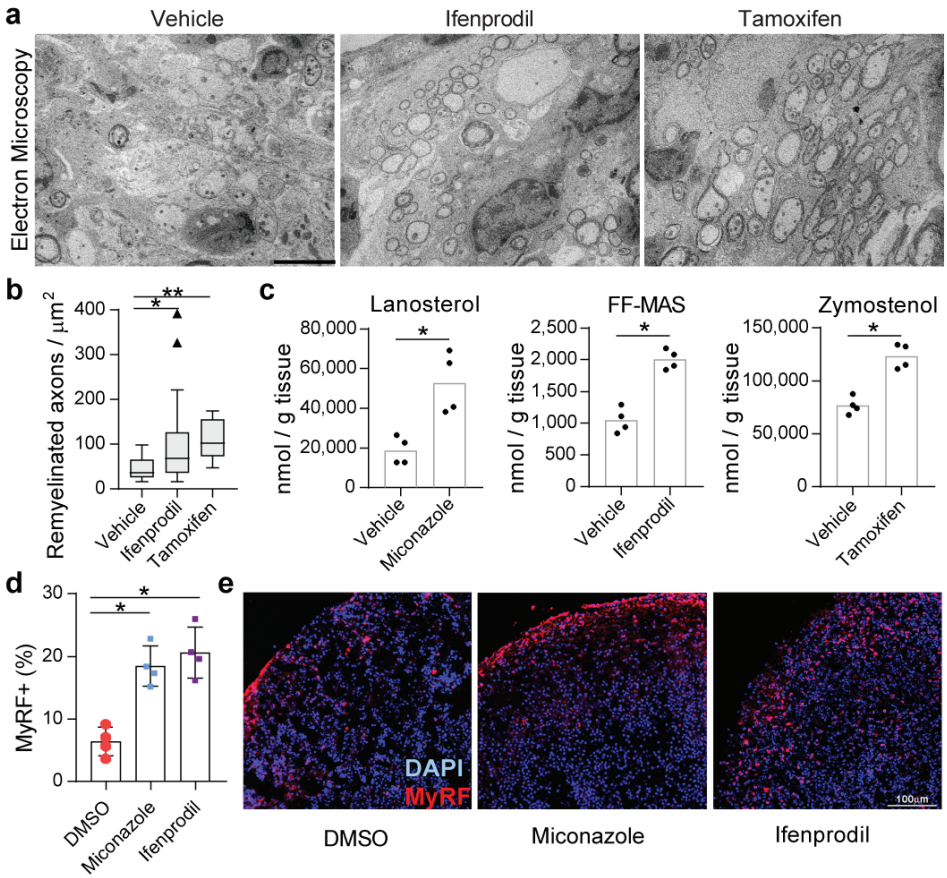

Figure 2.4: Accumulation of 8,9-unsaturated sterols enhances remyelination *in vivo* and in human brain spheroids. - a, Representative electron microscopy images of LPC-lesioned dorsal spinal cord from mice treated with ifenprodil or tamoxifen. Scale bar, 5 μm. b, Tukey plot showing quantification of remyelinated axons in LPC-lesioned spinal cord from mice in a. n = 6 animals per group except vehicle, n = 4. **P = 0.0004, *P = 0.048, two-tailed Mann–Whitney test. Boxes indicate the interquartile range, horizontal lines represent the median, and whiskers represent the smaller of 1.5 times the interquartile range and the minimum–maximum range. c, Quantification of brain sterol levels in mice treated with miconazole, ifenprodil, or tamoxifen. n = 4 animals per group. P = 0.0007 for miconazole, P = 0.0003 for ifenprodil, P = 0.0006 for tamoxifen; two-tailed Student's t-test. d, Quantification of myelin regulatory factor (MYRF)+ oligodendrocytes within human myelinating cortical spheroids following treatment with miconazole (2 μM) or ifenprodil (2 μM). n = 4 spheroids per treatment condition. P = 0.0009 for miconazole, P = 0.0009 for ifenprodil; two-tailed Student's t-test. e, Representative images of spheroids. DAPI+ nuclei (blue) and MYRF+ oligodendrocytes (red) are labelled. Scale bar, 100 μm. In c, d, bar graphs indicate mean and error bars indicate s.d.

thesis of all cellular sterols. Our findings establish an alternate paradigm in which the cholesterol biosynthesis pathway can be leveraged to enhance the formation of new oligodendrocytes by targeting later steps whose inhibition does not cause net depletion of cellular sterols. Instead, acute inhibition of CYP51, TM7SF2, or EBP during OPC differentiation induces a 'sterol shift' in which a minority of cellular cholesterol is diverted to 8,9-unsaturated sterol intermediates that signal to enhance oligodendrocyte formation. Notably, we and others have independently shown that multiple molecules now annotated by us as enhancing 8,9-unsaturated sterol intermediate levels can regenerate functional myelin *in vivo*, as evidenced by reversal of paralysis in mice with MS-like disease(38, 106, 122). Ultimately, our work demonstrates that modulating the sterol landscape in OPCs can enhance the formation of oligodendrocytes and points to new therapeutic targets, potent inhibitors for these targets, and metabolite-based biomarkers to accelerate the development of optimal remyelinating therapeutics.

2.4 Methods

Statistics and reproducibility No statistical methods were used to predetermine sample size. Data were expressed as mean $\pm$ s.d. and P values were calculated using an unpaired two-tailed Student's t-test for pairwise comparison of variables with a 95$\%$ confidence interval and n$-$2 degrees of

freedom, where n is the total number of samples, in all figures except 2.4b. In 2.4b, P values were calculated using an unpaired two-tailed Mann–Whitney test with 95% confidence interval and the data plotted as a Tukey box and whisker plot. Boxes indicate the interquartile range, and the horizontal line represents the median. Biological replicates: 2.1c, n=4 wells per condition, except DMSO, n=24; 2.1f, n=17 wells for DMSO, n=7 for siControl and siCYP51; 2.1g, n=8 wells for DMSO and n=4 for lanosterol; 2.2b, n=4 wells per condition, except DMSO, n=24; 2.2c, n=3 wells for sgControl and n=4 for sgEBP; 2.2e–g, n=4 wells per condition, except n=8 for DMSO and n=7 for ketoconazole in 2.2e, n=12 for DMSO in 2.2f, n=16 for DMSO and ketoconazole, n=8 for cholesterol in 2.2g. Independent experiments: 2.2b, f are representative of three and 2.2c, e, g of two independent experiments using OPC-5 cells; for validation in an independent derivation of OPCs, see 2.72.82.9.

Small molecules The identity and purity of small molecules were authenticated by LC–MS before use. The following compounds were purchased from Sigma-Aldrich as solids: ketoconazole, miconazole, clotrimazole, fluconazole, fulvestrant, ifenprodil, benztropine, bexarotene, tamoxifen, 4-hydroxytamoxifen, medroxyprogesterone acetate, ospemifene, GSK343, trans-U50488, methyl-β-cyclodextrin, 5α-cholestan-3β-ol, and cholesterol. The following compounds were purchased from Cayman Chemicals as solids: liothyronine, clemastine, AY9944, YM53601 and Ro-48-8071. The follow-

ing compounds were obtained from Janssen Pharmaceuticals as solids: 2-methyl-ketoconazole, R-trans-ketoconazole, and S-trans-ketoconazole. Mevastatin was purchased as a solid from Selleck Chemicals. The following compounds were purchased from Selleck Chemicals as 10 mM DMSO solutions: bifonazole, butoconazole, amorolfine, toremifene, EPZ005687, EPZ6438, UNC1999, hydroxyzine, ziprasidone, p-fluorohexahydro-sila-difenidol (abbreviated in figures as Sigma H127), vesamicol, raloxifene, L-745870, TMB-8, pramoxine, varespladib, tanshinone-I, levofloxacin, nateglinide, abiraterone, allopurinol, detomidine, rivastigmine, β-carotene, BEZ-235, scopolamine, and homatropine. Pirenzepine and telenzepine were purchased from Sigma-Aldrich as 10 mM DMSO solutions. Cholesterol biosynthetic intermediates were purchased from Avanti Polar Lipids as solids: lanosterol, zymosterol, zymostenol, lathosterol, desmosterol, 7-dehydrodesmosterol, FF-MAS (4,4-dimethyl-5α-cholesta-8,14,24-trien-3β-ol), 8,9-dehydrocholesterol, and 2,2-dimethylzymosterol (2,2-dimethyl-5α-cholesta-8,24-dien-3β-ol). 14- dehydrozymostenol (5α-cholesta-8,14-dien-3β-ol), MAS-412 (4,4-dimethyl- 5α-cholesta-8,14-dien-3β-ol), and MAS-414 (4,4-dimethyl-5α-cholesta-8-en-3β-ol) were provided by F.B. Imidazole 124(58), TASIN-1(169), TASIN-449(37), and MGI39 were synthesized as reported. T-MAS (4,4-dimethyl-5α-cholesta-8,24-dien-3β-ol) from HPLC purification of yeast extracts was provided by J.J. and W.K.W.

Mouse OPC preparation To rigorously assess the effects of small-molecule

and genetic treatments on OPCs, all treatments were assayed in two batches of epiblast stem cell-derived OPCs, and key results were confirmed using mouse primary OPCs. OPCs were generated from two separate EpiSC lines, EpiSC5 (giving rise to OPC-5 OPCs) and 129O1 (giving rise to OPC-1 OPCs). Unless otherwise noted, results in OPC-5 cells are presented in 2.1 2.2, 2.3, 2.4. while results in OPC-1 are presented in 2.5, 2.6, 2.7, 2.8, 2.9, 2.10, 2.11, 2.12, 2.13, 2.14.

EpiSC-derived OPCs were obtained using *in vitro* differentiation protocols and culture conditions described previously(120). To ensure uniformity throughout all *in vitro* screening experiments, EpiSC-derived OPCs were sorted to purity by fluorescence activated cell sorting at passage five with conjugated CD 140a-APC (eBioscience, 17-1401; 1:80) and NG2-AF488 (Millipore, AB5320A4; 1:100) antibodies. Sorted batches of OPCs were expanded and frozen down in aliquots. OPCs were thawed into growth conditions for one passage before use in further assays. Cultures were regularly tested and shown to be mycoplasma free.

To obtain mouse primary OPCs, whole brain was removed from postnatal day 2 pups anaesthetized on ice. Brains were placed in cold DMEM/F12, and the cortices were isolated and the meninges were removed. The cortices were manually chopped and processed with the Tumour Dissociation Kit (Miltenyi) and incubated at 37℃ for 10 min. The cell suspension was filtered through a 70μm filter and centrifuged at 200g for 4 min at room tem-

perature. The cells were washed in DMEM/F12, re-centrifuged and plated in poly-Ornithine and Laminin-treated flasks containing DMEM/F12 supplemented with N2 Max, B27 (ThermoFisher), 20ng/ml FGF, and 20ng/ml PDGF. OPCs were passaged once before treatment. Media was changed every 48 h.

***In vitro* phenotypic screening of OPCs** EpiSC-derived OPCs were grown and expanded in poly-ornithine (PO) and laminin-coated flasks with growth medium (DMEM/F12 supplemented with N2-MAX (R&D Systems), B-27 (ThermoFisher), GlutaMax (Gibco), FGF2 (10μg/ml, R&D systems, 233-FB-025) and PDGF-AA (10μg/ml, R&D systems, 233-AA-050) before harvesting for plating. The cells were seeded onto poly-D-lysine 96-well CellCarrier or CellCarrierUltra plates (PerkinElmer) coated with laminin (Sigma, L2020; 15μg/ml) using multi-channel pipet. For the experiment, 800,000 cells/ml stock in differentiation medium (DMEM/F12 supplemented with N2-MAX and B-27) was prepared and stored on ice for 2 h. Then, 40,000 cells were seeded per well in differentiation medium and allowed to attach for 30 min before addition of drug. For dose–response testing of all molecules except sterols, a 1,000$\times$ compound stock in dimethyl sulfoxide (DMSO) was added to assay plates with 0.1μl solid pin multi-blot replicators (V & P Scientific; VP 409), resulting in a final primary screening concentration of 1$\times$. Sterols were added to cells as an ethanol solution (0.2% final ethanol concentration). Positive control wells (ketoconazole, 2.5μM) and DMSO vehicle

controls were included in each assay plate. Cells were incubated under standard conditions (37℃, 5% CO2) for 3 days and fixed with 4% paraformaldehyde (PFA) in phosphate buffered saline (PBS) for 20 min. Fixed plates were washed with PBS (200μl per well) twice, permeabilized with 0.1% Triton X-100 and blocked with 10% donkey serum (v/v) in PBS for 40 min. Then, cells were labelled with antibodies recognizing MBP (Abcam, ab7349; 1:200) or PLP1 (1:1,000, clone AA3, generously provided by B. Trapp, Cleveland Clinic) for 16 h at 4℃ followed by detection with Alexa Fluor conjugated secondary antibodies (1:500) for 45 min. Nuclei were visualized by DAPI staining (Sigma; 1μg/ml). During washing steps, PBS was added using a multi-channel pipet and aspiration was performed using Biotek EL406 washer dispenser (Biotek) equipped with a 96-well aspiration manifold.

High-content imaging and analysis Plates were imaged on the Operetta High Content Imaging and Analysis system (PerkinElmer) and a set of 6 fields captured from each well resulting in an average of 1,200 cells being scored per well. Analysis (PerkinElmer Harmony and Columbus software) began by identifying intact nuclei stained by DAPI; that is, those traced nuclei that were larger than 300μm2 in surface area. Each traced nucleus region was then expanded by 50% and cross-referenced with the mature MBP stain to identify oligodendrocyte nuclei, and from this the percentage of oligodendrocytes was calculated. In some experiments, PLP1 staining was performed instead of MBP, or the total process length of MBP+ oligodendro-

cytes was calculated as previously described4.

OPCs differentiation and sterol profiling after cyclodextrin treatment EpiSCs derived OPCs harvested from culture flasks were resuspended in 10 ml of differentiation medium to a final cell density of 500,000 cells/ml. To this, cell-culture grade water or methyl-β-cyclodextrin (1 mM) was added and incubated at 37℃. After 30 min the cells were washed twice with differentiation medium (5 ml), and split into two portions for differentiation and sterol profiling. The 1,000,000 cells per condition were directly processed as described in GC–MS-based sterol profiling to measure the endogenous sterol levels. For differentiation, the cells were resuspended in differentiation medium to a final cell density of 800,000 cells/ml and plated in a PDL/laminin coated 96-well CellCarrierUltra plate. After 72 h, the cells were fixed, stained, imaged and quantified as described above.

High-throughput screening of 3,000 bioactive small molecules EpiSC-derived OPCs were grown and expanded in poly-ornithine and laminin-coated flasks before harvesting for plating. Cells were dispensed in differentiation medium supplemented with Noggin (R&D Systems; 100 ng/ml), Neurotrophin 3 (R&D Systems; 10 ng/ml), cAMP (Sigma; 50μM), and IGF-1 (R&D Systems; 100 ng/ml)) using a Biotek EL406 Microplate Washer Dispenser (Biotek) equipped with 5μl dispense cassette (Biotek), into poly-D-lysine/laminin (Sigma, L2020; 4μg/ml)-coated sterile, 384-well, CellCarrier ultra plates (PerkinElmer), to a final density of 12,500 cells per well and al-

lowed to attach for 45 min before addition of drug. A 3 mM stock of bioactive compound library in dimethylsulphoxide (DMSO) were prepared in an Abgene storage 384-well plate (ThermoFisher Scientific; AB1055). These were added to assay plates using a 50 nl solid pin tool attached to a Janus automated workstation (Perkin Elmer), resulting in a final screening concentration of 2μM. Cells were incubated at 37℃ for 1 h and then T3 (Sigma; 40 ng/ml) was added to all wells except negative controls, to which FGF (20 ng/ml) was added instead. Negative controls and T3-alone were included in each assay plate. After incubation at 37℃ for 72 h, cells were fixed, washed and stained similarly to the 96-well OPC assay protocol, although all the washing steps were performed using a Biotek EL406 Microplate Washer Dispenser (Biotek) equipped with a 96-well aspiration manifold. Cells were stained with DAPI (Sigma; 1μg/ml) and MBP antibody (Abcam, ab7349; 1:100). Plates were imaged on the Operetta High Content Imaging and Analysis system (PerkinElmer) and a set of 4 fields captured from each well resulting in an average of 700 cells being scored per well. Analysis was performed as in High-Content Imaging and Analysis, above. All plates for the primary screen were processed and analysed simultaneously to minimize variability. Molecules causing more than 20$\%$ reduction in nuclear count relative to DMSO control wells were removed from consideration, and hits were called on the basis of largest fold-increase in percentage of MBP+ oligodendrocytes relative to DMSO controls within the same plate. When selecting the leading hits for

further experiments, molecules obtained in previous screens were omitted, including imidazole antifungals and clemastine.

GC–MS-based sterol profiling EpiSC-derived OPCs were plated at 0.5 million cells per ml in PDL- and laminin-coated six or twelve well plate with differentiation media. After 24 h, cells were dissociated with Accutase, rinsed with saline, and cell pellets were frozen. For sterol analyses, cells were lysed in methanol (Sigma-Aldrich) with agitation for 30 min and cell debris removed by centrifugation at 10,000 rpm for 15 min. Cholesterol-d7 standard (25,26,26,26,27,27,27-2H7-cholesterol, Cambridge Isotope Laboratories) was added before drying under nitrogen stream and derivatization with 55μl of bis(trimethylsilyl)trifluoroacetamide/trimethylchlorosilane to form trimethylsilyl derivatives. Following derivatization at 60℃ for 20 min, 1μl was analysed by GC–MS using an Agilent 5973 Network Mass Selective Detector equipped with a 6890 gas chromatograph system and a HP-5MS capillary column (60 m $\times$ 0.25 mm $\times$ 0.25μm). Samples were injected in splitless mode and analysed using electron impact ionization. Ion fragment peaks were integrated to calculate sterol abundance, and quantitation was relative to cholesterol-d7. The following m/z ion fragments were used to quantitate each metabolite: cholesterol-d7 (465), FF-Mas (482), cholesterol (368), zymostenol (458), zymosterol (456), desmosterol (456, 343), 7-dehydrocholesterol (456, 325), lanosterol (393), lathosterol (458), 14-dehydrozymostenol (456). Calibration curves were generated by injecting

varying concentrations of sterol standards and maintaining a fixed amount of cholesterol-d7. The human glioma cell line GBM528 was a gift of Jeremy Rich (Cleveland Clinic). These cells were validated as unique by STR profiling. (113)

LC–MS-based sterol profiling Sterols were extracted after treatment of OPC-5 OPCs with ketoconazole as described in GC–MS-based sterol profiling above. Picolinate derivatization, chromatographic separation, and mass spectrometric detection were performed as reported previously(70). Peaks from selective reaction monitoring were integrated to calculate sterol abundance, and quantitation was relative to cholesterol-d7.

Human cortical spheroids Human cortical spheroids were generated as described previously with modifications to enable the inclusion and differentiation of OPCs27. In brief, spheroids were treated with miconazole or ifenprodil (2μM) from days 62-72 and assayed on day 93 for MyRF+ oligodendrocytes (rabbit anti-MyRF antibody was generously provided by M. Wegner and used at 1:1,000).

CYP51 enzymatic assay CYP51 enzymatic activity was measured using a reported method with slight modifications(154): rat CYP51 (Cypex, Inc.) was used as enzyme; reaction volume was 500μl; reaction time was 30 min; lanosterol concentration was 50μM; and reactions were quenched with 500μl isopropanol. Finally, 15μl of each reaction/isopropanol mixture was injected onto a SCIEX Triple Quad 6500 LC-MS/MS system using an APCI

ion source in positive ion mode with a Shimadzu UFLC-20AD HPLC and a Phenomenex Kinetix C18XB 50 $\times$ 2.1 $\times$ 2.6 column at 40℃.

EBP enzymatic assay EBP enzymatic activity was measured using a reported method with slight modifications22: active EBP was obtained from mouse microsomes, inhibitors were added, zymostenol was added at a final concentration of 25 μM in a final reaction volume of 500μl, and the reaction incubated at 37℃ for 2 h. Sterols were extracted using 3 $\times$ 1 ml hexanes, cholesterol-d7 was added to enable quantitation, and the pooled organics were dried (Na2SO4) and evaporated under nitrogen gas. Samples were then silylated and analysed using GC/MS as described above.

siRNA treatments Cell-permeable siRNAs were obtained as pools of 4 individual siRNAs targeting mouse CYP51, or a non-targeting control (Accell siRNAs, Dharmacon. Pooled CYP51 siRNA sequence: GUCUGUUUUGA-GAUUAGU; CGACUAUGCUUCGUUUAUA; CGCUGCUCUUCAAUAGUAA; CUAUUAAGUUAUUGUGAAC. Non-targeting control siRNA: UGGUUUACAU-GUCGACUAA). For differentiation analysis, cells were plated in a 96-well plate (as detailed above) and treated with 1μM pooled siRNA suspended in RNase free water diluted in differentiation media (as detailed above). For sterol analysis cells were plated in a six-well plate at 300,000 cells per well in standard differentiation media supplemented with PDGF (R&D Systems, 20 ng/ml), neurotrophin 3 (R&D Systems; 10 ng/ml), cAMP (Sigma; 50μM), IGF-1 (R&D Systems; 100 ng/ml), noggin (R&D Systems; 100 ng/ml). At 24

h, 1μM siRNA was added to the media. Cells were grown for three more days in siRNA containing media, with growth factor supplementation every 48h, before harvesting and processing for GC–MS analysis as detailed above.

CRISPR–Cas9-mediated targeting of EBP Guide RNA sequences were obtained using the Broad Brie library and manufactured by IDT. Nucleotide sequences (sgRNA sequence: GAAACGCAATCACTACCCAT (sgEBP); GGGGCCTAATTGTGATCACG (sgEBP2)) were prepared and inserted into the LentiCRISPRv2 plasmid (Addgene, 52961) using the instructions from GeckoLibrary preparation: in brief, Fastdigest BsbmB1 (fermentas) was used for plasmid digestion, T4 PNK (NEB M0201S) for nucleotide annealing, and Quick Ligase (NEB M2200S) for sgRNA insertion. Insertion was confirmed by Sanger sequencing. Hek293T cells were transfected using Lenti-x shots as per the manufacturer's protocol (Clontech). After 24 h the media was changed to OPC media for collection of virus. 48 h later the media was collected, supplemented with FGF, PDGF, and protamine sulfate (Sigma, 8 μg/ml), and used to transduce OPCs. 24 h later the media was changed to non-virus containing media for 48 h. Cells underwent two 48 h stretches of puromycin selection (Invitrogen). After 24 h of recovery in non-selection media, cells were plated for differentiation, GC–MS, and qPCR as described above.

Focal demyelination, drug treatment and histological analysis Focal demyelination in the dorsal column of the spinal cord was induced by

the injection of 1% LPC solution. 12 week old C57BL/6 female mice were anaesthetized using isoflurane and T10 laminectomies were performed. 1 μl of 1% LPC was infused into the dorsal column at a rate of 15μl/h. At day 4, animals were randomized into treatment groups before treatment (2 animals were excluded due to surgical complications). Between days 4 and 11 post-laminectomy, animals received daily injections of either vehicle or drug intraperitoneally. Drugs were dissolved in DMSO or corn oil and then diluted with sterile saline for injections such that final doses were 2 mg/kg for tamoxifen and 10 mg/kg for ifenprodil. This experiment was done in a blinded manner: compounds were coded to ensure the researchers performing the experiments were unaware of the treatment being administered to each animal. All animals were euthanized 12 days post-laminectomy (n=4–6 per group). Mice were anaesthetized using ketamine/xylazine rodent cocktail and then euthanized by transcardial perfusion with 4% PFA, 2% glutaraldehyde, and 0.1 M sodium cacodylate. Samples were osmicated, stained en bloc with uranyl acetate and embedded in EMbed 812, an Epon-812 substitute (EMS). 1μm sections were cut and stained with toluidine blue and visualized on a light microscope (Leica DM5500B). The number of myelinated axons per unit area was counted from sections obtained from the middle of each lesion and then averaged over each treatment group. All sections within the lesion area were scored (vehicle, 10 sections; tamoxifen, 11 sections; ifenprodil, 28 sections). A Mann–Whitney statistical analysis

was performed to assess statistical significance.

Analysis of mouse brain sterol levels Ten to twelve week old male C57BL/6 mice were injected with 2mg/kg tamoxifen, 10 mg/kg ifenprodil, or 10 mg/kg miconazole dissolved in corn oil (tamoxifen) or DMSO (ifenprodil, miconazole) in sterile saline daily for three days. Mice were anaesthetized with isoflurane and perfused with phosphate buffered saline to remove blood from the brain. Brains were collected and flash frozen using liquid nitrogen. The samples were pulverized and 50-100 mg of tissue were collected for further processing. A modified Folch protocol was used for extraction of sterols(49). Briefly, samples were resuspended in a 2:1 chloroform/methanol mixture and homogenized. Cell debris was removed by centrifugation at 4,000g for 10 min. The solution was dried under air and resuspended in hexane with a cholesterol-d7 standard and dried again. Lipids were derivatized with 70μl of bis(trimethylsilyl)trifluoroacetamide; 2μl were injected and analysed by GC–MS as described above.

Oestrogen-dependent cell proliferation assay Oestrogen-dependent cell proliferation was measured as previously described with minor modifications. (132) After growth in oestrogen-free media (Phenol red-free RPMI supplemented with 10$\%$ charcoal stripped fetal bovine serum) for 5 days, cells were seeded at 2,500 cells/well into 96 well plates. The following day 3$\times$ drug containing media was added to triplicate wells and cells were allowed to grow for an additional 5 days at 37℃ in a standard 5$\%$ CO2 humid-

ified incubator. Total DNA per well was measured using an adaptation of the method of Labarca and Paigen(84). At this time media was removed, cells were washed one time with 0.25$\times$ PBS and 100μl of distilled water was added. Plates were frozen and thawed to enhance cell lysis and 200μl of 10μg/ml Hoechst 33258 (Sigma-Aldrich, St. Louis, MO.) in 2 M NaCl, 1 mM EDTA, 10 mM Tris-HCl pH 7.4 was added. After incubation at room temperature for 2 h, plates were read in a SpectraMax i3 fluorescent plate reader (Molecular Devices, Sunnyvale, CA) with excitation at 360 nm and emission at 460 nm. All values were converted to microgram DNA per well using a standard curve derived from purified salmon testes DNA. T47D cells were provided by the Translational Research Shared Resource of the Case Comprehensive Cancer Center and used without further authentication beyond the observed oestrogen-dependent cell proliferation.

Oligodendrocyte formation and imaging on electrospun microfibres

A 12-well plate containing Mimetex aligned scaffold (microfibre plate, AMS-BIO, AMS.TECL-006-1X, Electrospun poly-L-lactide Scaffold, 2μM fibre diameter cell crown inserts) was prepared as previously described24. In brief, fibre inserts were sterilized with 70$\%$ ethanol and washed with PBS before being coated with polyornithine and laminin. After laminin coating, 100,000 cells/ml of EpiSC-derived OPCs (1.5 ml/well) were plated in differentiation medium. After 24 h the media was replaced with fresh media containing small-molecule treatments. Every 48 h the media was replaced with fresh

compound containing media for a total of 14 days. Plates were fixed with 4% PFA, permeabilized with 0.1% Triton X-100, and blocked with 10% donkey serum (v/v) in PBS for 60 min. Plates were stained for MBP (Abcam, ab7349; 1:100) and DAPI staining (Sigma; 5 μg/ml). After staining, the inserts were moved into new 12-well plate and covered with 2 ml of PBS before imaging in Operetta high content Imaging and analysis system. Plates were imaged on the Operetta High Content Imaging and Analysis system (PerkinElmer) and a set of 8 fields captured from each well resulting in an average of 45,000 cells being scored per well. Analysis (PerkinElmer Harmony and Columbus software) identified intact nuclei stained by DAPI and calculated the MBP signal intensity per cell per well. Microfibre insert tracking images were taken using a Leica DMi8 with a 20$\times$ dry/NA 0.40 objective. Microfibre plate inserts were mounted using Flouromount-G (SouthernBiotech) and allowed to partially harden before coverslips were added and the insert ring was removed. Confocal images were obtained on a Leica SP8 confocal scanning microscope, with 40 $\times$ oil/NA 1.30 objective. Confocal stacks of 0.336 μm z-steps were taken at 1,024 $\times$ 1,024. Each fluorophore was excited sequentially and all contrast and brightness changes were applied consistently between images.

A separate analysis approach was performed on an independent experiment performed as above except the small-molecule treatment was limited to the first 4 days of the 14 day culture period. After staining, the fibre in-

serts were mounted on a glass slide (Fisherbrand Superfrost Plus Microscope Slides) using Fluormount-G (Southern Biotech) with a cover glass (Fisherbrand Microscope Cover Glass) and dried at RT in dark for 36 h. The mounted inserts were imaged on the Operetta High Content Imaging and Analysis system (PerkinElmer) and a set of 22 fields captured from each condition resulting in an average of 2,000 cells being scored per well. The total microfibre area was calculated using bright filed imaging and a spot-finding function (area larger than 2 pixels2). The MBP+ pixel area within the defined microfibre area was then defined and the percentage of the total microfibre area calculated.

CYP51 qPCR Cells were plated at 500,000 cells per well in a six-well plate and were grown in standard differentiation media supplemented with PDGF, neurotrophin 3, cAMP, IGF-1, and noggin for four days as described above. At 24 h, cells were treated with 1μM siRNA. Growth factors were added every 48 h. After three days of siRNA treatment, RNA was isolated with the RNeasy Mini Kit (Qiagen), and cDNA was made using High-Capacity RNA-to-cDNA Kit (Applied Biosystems). Exon spanning primers for ActinB (Thermo-Fisher, Taqman, Mm02619580_g1) and CYP51 (Thermo-Fisher, Taqman, Mm00490968_m1) were used for detection of relative RNA levels by quantitative real time PCR (Applied Biosystems, 7300 Realtime PCR system). Cycle time and outliers were calculated using Applied Biosystems' 7300 System Sequence Detection Software version 1.4.

EBP qPCR OPCs were accutased, 1 million cells per cell line were spun down and RNA was isolated with the RNeasy Mini Kit (Qiagen). DNA was removed using DNAse (Invitrogen), and cDNA was made using High-Capacity RNA-to-cDNA Kit (Applied Biosystems). Primers for exon 5 of EBP (forward primer: TGTGCGAGGAGGAAGAAGAT, reverse primer: GATAGGCCACCCCGTTTATT) and GAPDH (forward primer: AGGTCGGTGTGAACGGATTTG; reverse primer: GGGGTCGTTGATGGCAACA) were manufactured by IDT and gene expression was assessed using Power SYBR Green Master Mix (Applied Biosystems) were used for detection of relative RNA levels by quantitative real time PCR (Quantstudio 7 flex system). Cycle time and outliers were calculated using QuantStudio Software V1.3.

Muscarinic receptor antagonism assay GeneBLAzer M1-NFAT-bla CHO-K1 cells (or M3- or M5-NFAT-bla CHO-K1 cells) (ThermoFisher) were thawed into Assay Media (DMEM, 10% dialysed FBS, 25 mM HEPES pH 7.3, 0.1 mM NEAA). 10,000 cells/well were added to a 384-well TC treated assay plate and incubated 16–24 h at 37℃. 4μl of a 10x stock of antimuscarinic molecules was added to the plate and incubated 30 min. 4μl of 10x control agonist Carbachol at the pre-determined EC80 concentration was added to wells containing antimuscarinic molecules. The plate was incubated 5 h and 8μl of 1μM substrate + solution D loading solution was added to each well and the plate was incubated 2 h at room temperature before reading on a fluorescence plate reader. This cell line was validated in each run on the

basis of $z\prime > 0.5$ for carbachol versus control treatment.

SREBP qPCR Cells were plated at 1 million cells per well in a six-well plate and were grown in standard differentiation media supplemented with with DMSO, mevastatin (2.5μM), Ro 48-8071 (500 nM), ketoconazole (2.5μM), TASIN-1 (100 nM), or amorolfine (100 nM). At 24 h, RNA was isolated with the RNeasy Mini Kit (Qiagen), and cDNA was made using High-Capacity RNA-to-cDNA Kit (Applied Biosystems). Exon spanning primers ActinB (Thermo-Fisher, Taqman, Mm02619580_ g1), LSS (Thermo-Fisher, Taqman, Mm00461312_ m1), LDLR (Thermo-Fisher, Taqman, Mm01177349_ m1), and DHCR7 (Thermo-Fisher, Taqman, Mm00514571_ m1) were used for detection of relative RNA levels by quantitative real time PCR (Applied Biosystems, 7300 Realtime PCR system). Cycle time and outliers were calculated using Applied Biosystems 7300 System Sequence Detection Software version 1.4.

NR2C2 and NR2F1 luciferase assays Forty-eight hours before transfection, 100,000 Hek293T cells were plated per well in a 24 well plate. HEK293T cells were chosen because they were used previously in this assay and not validated further(15). NR2C2 (Origene, MR221079) or NR2F1 (gift from C. Schaaf) and NGFI promoter reporter plasmid (gift from C. Schaaf) were transfected using Lipofectamine 2000 (Thermo-Fisher, 11668027) as per the manufacturer's protocol. After 16 h, Hek293 cells were treated with the compounds (2,2-dimethyl-zymosterol 5μM, FF-MAS 10μM, ketocona-

zole 2.5μM, TASIN-1 100 nM, mevastatin 2.5μM, liothyronine 3μM, and all-trans retinoic acid 5μM). 32 h later cells were lysed using a firefly luciferase assay system (Promega, E1500) and readout using Synergy Neo2 High Performance plate reader.

Nuclear receptor profiling Luciferase reporter assays performed by Indigo Biosciences were used to assess interaction of 2,2-dimethylzymosterol (5μM), ketoconazole (2.5μM), and TASIN-1 (250 nM) with human ERα, GR, LXRβ, NFκB, NRF2, PGR, PPARα, PPARγ, RARα, RARγ, RXRα, RXRβ, TRα, TRβ and VDR in agonist mode and ERRα, RORα and RORγ in inverse-agonist mode. The reporter for these assays is firefly luciferase linked with either the genetic response elements (GRE) or the Gal4 upstream activation sequence (UAS). These cells also express either the native receptor or a receptor in which the native N-terminal DNA binding domain (DBD) has been replaced with that of the yeast Gal4 DBD. The specifics of each assay are shown in the table below. In brief, a suspension of reporter cells was prepared in cell recovery medium (CRM; containing 5$\%$ (RORγ) or 10$\%$ charcoal stripped FBS for others). 100μl of the reporter cell suspension was dispensed into wells of a white 96-well assay plate. Test compound, reference compounds, and the respective vehicle were diluted into INDIGO's compound screening medium (CSM; containing 5$\%$ (RORγ) or 10$\%$ charcoal stripped FBS for others). 100μl of each treatment medium was dispensed into duplicate assay wells pre-dispensed with reporter cells. Assay

plates were incubated at 37℃ for 24 h. Following the incubation period, for agonist and inverse-agonist assays, treatment media were discarded and 100μl/well of luciferase detection reagent was added. RLUs were quantified from each assay well to determine agonist or inverse-agonist activity using the following assay designs:

ERα (NR3A1); native receptor; ER GRE-luciferase

ERRα (NR3B1); Gal4 DBD hybrid receptor; Gal4 UAS-luciferase

GR (NR3C1); native receptor; GR GRE-luciferase

LXRβ (NR1H2); Gal4 DBD hybrid receptor; Gal4 UAS-luciferase

PGR (NR3C3); native receptor; PGR GRE-luciferase

PPARδ (NR1C2); Gal4 DBD hybrid receptor; Gal4 UAS-luciferase

PPARγ (NR1C3); Gal4 DBD hybrid receptor; Gal4 UAS-luciferase

RARα (NR1B1); Gal4 DBD hybrid receptor; Gal4 UAS-luciferase

RARγ (NR1B3); Gal4 DBD hybrid receptor; Gal4 UAS-luciferase

RORα (NR1F1); Gal4 DBD hybrid receptor; Gal4 UAS-luciferase

RORγ (NR1F3); Gal4 DBD hybrid receptor; Gal4 UAS-luciferase

RXRα (NR2B1); Gal4 DBD hybrid receptor; Gal4 UAS-luciferase

RXRβ (NR2B2); Gal4 DBD hybrid receptor; Gal4 UAS-luciferase

TRα (NR1A1); Gal4 DBD hybrid receptor; Gal4 UAS-luciferase

TRβ (NR1A2); Gal4 DBD hybrid receptor; Gal4 UAS-luciferase

VDR (NR1I1); Gal4 DBD hybrid receptor; Gal4 UAS-luciferase

NF-κB; native NF-κB; NF-κB GRE-luciferase

NRF2; native receptor; ARE-luciferase

2.5 Supplement

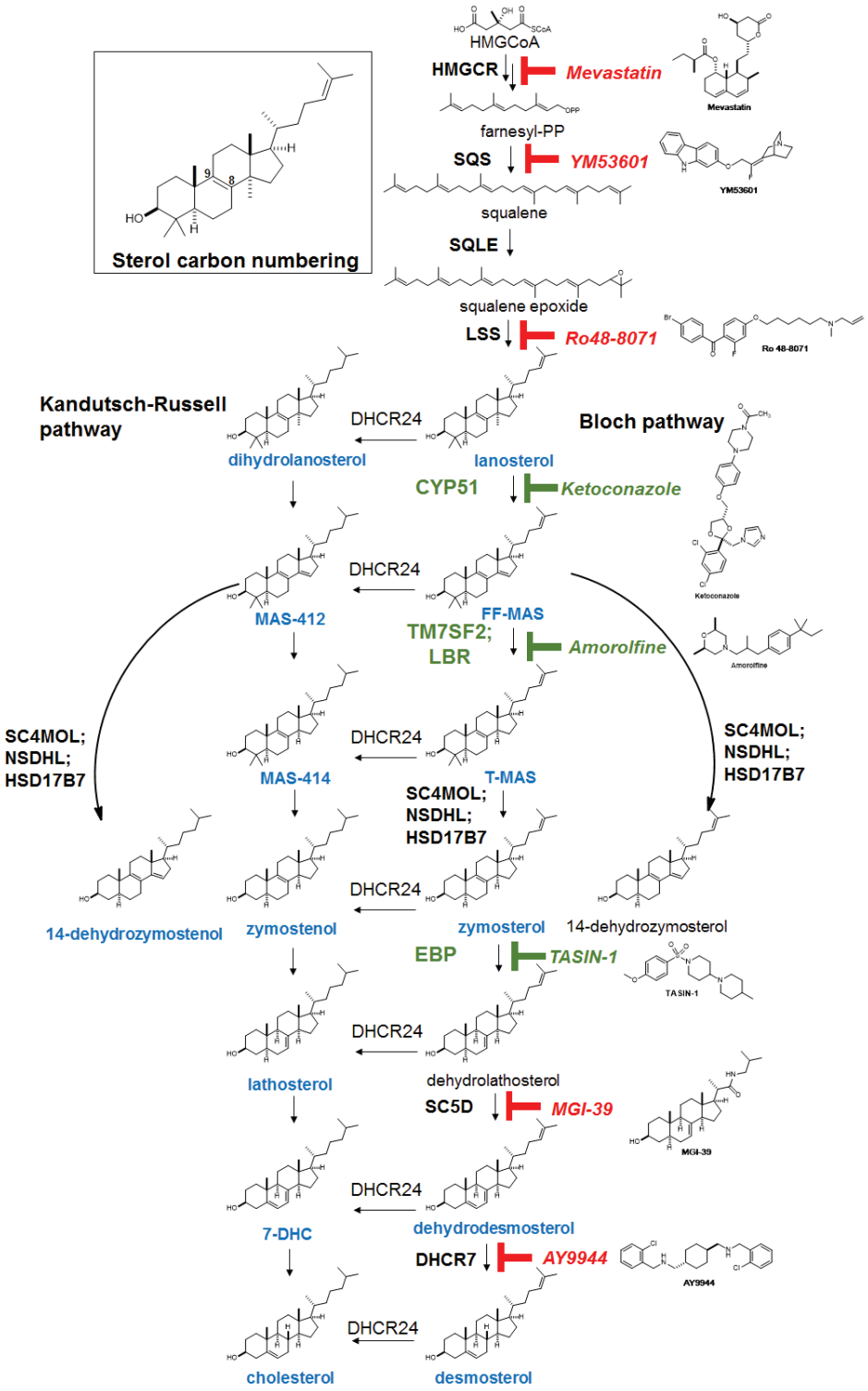

Figure 2.5: Extended Data Fig. 1 | Expanded cholesterol synthesis pathway diagram - Caption on next page

Extended Data Fig. 1 | Expanded cholesterol synthesis pathway diagram The cascade cyclization of squalene epoxide, catalysed by lanosterol synthase (LSS), provides the first sterol, lanosterol. Processing of lanosterol to cholesterol can proceed via the Kandutsch–Russell and/or Bloch pathways, which use the same enzymes and process substrates that vary only in the presence or absence of the C24 double bond. Intermediates in blue have been confirmed in our GC–MS-based sterol profiling assay using authentic standards. Sterol 14-reductase activity in mouse is shared by two genes, TM7SF2 and LBR. Consistent with past reports21, inhibition of sterol 14-reductase activity can lead to accumulation of the expected upstream intermediate (FF-MAS) or 14-dehydrozymostenol, also known as cholesta-8,14-dien-3-β-ol. Green indicates enzyme targets and small molecules whose inhibition promotes oligodendrocyte formation.

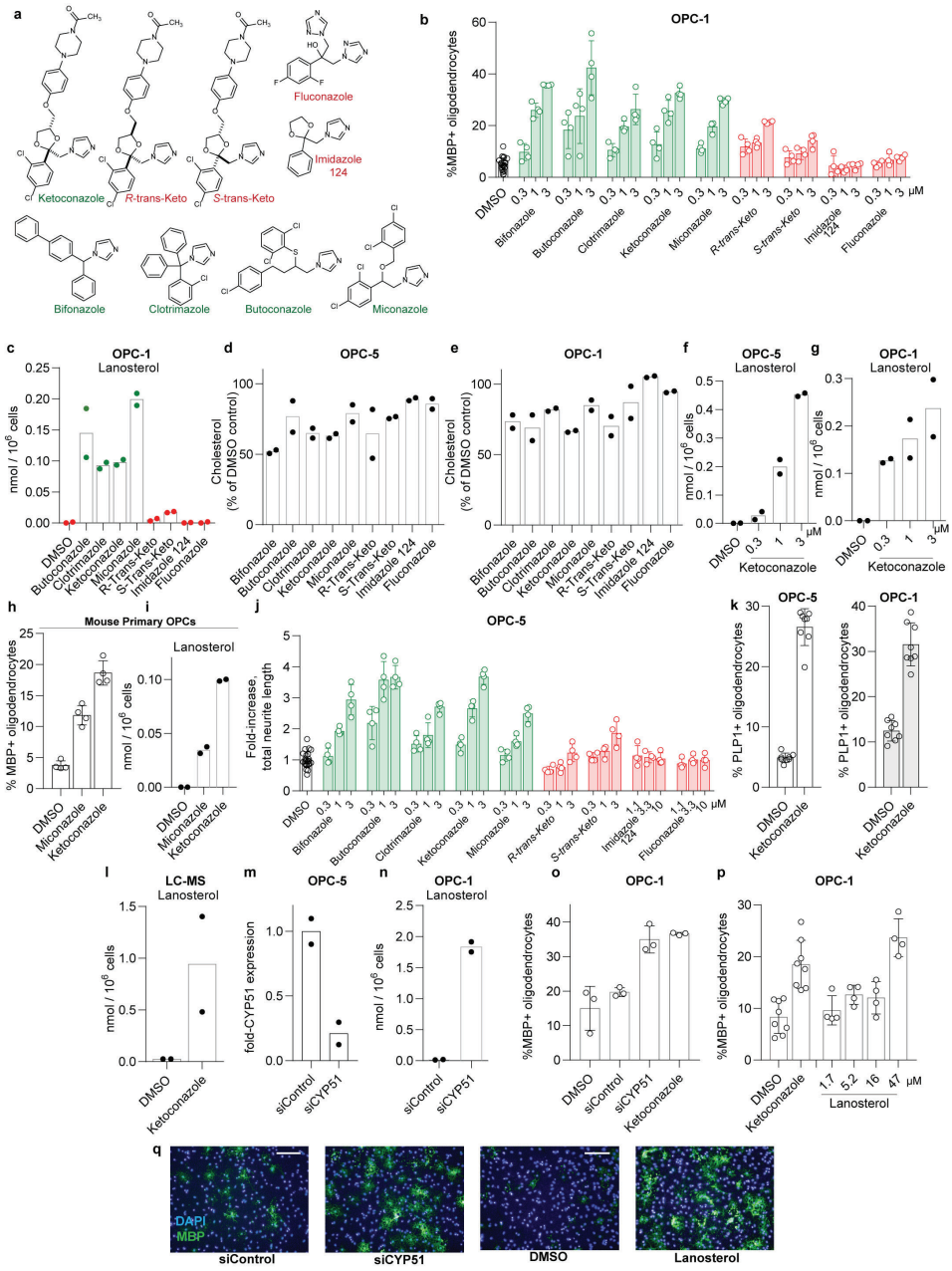

Figure 2.6: Extended Data Fig. 2 | CYP51 is the functional target by which imidazole antifungals enhance oligodendrocyte formation. - Caption on next page

Extended Data Fig. 2 | CYP51 is the functional target by which imidazole antifungals enhance oligodendrocyte formation. a, Azole molecules with varying degrees of potency for mammalian CYP51 inhibition. Throughout, green labels indicate molecules considered active, while red labels indicate inactive molecules. b, Percentage of MBP+ oligodendrocytes generated from a second, independent derivation of OPCs (OPC-1) at 72 h following treatment with the indicated concentrations of azoles. n = 4 wells per condition except DMSO (n = 24), with >1,000 cells analysed per well. c, GC–MS-based quantification of lanosterol levels in a second derivation of OPCs (OPC-1) treated for 24 h with the indicated azoles at 2.5 μM. n = 2 wells per condition. d, e, GC–MS-based quantification of cholesterol levels in OPCs (OPC-5 and OPC-1) treated for 24 h with the indicated azoles at 2.5 μM. n = 2 wells per condition. f, g, GC–MS-based quantification of lanosterol levels in OPCs (OPC-5, OPC-1) treated for 24 h with the indicated doses of ketoconazole. n = 2 wells per condition. Concentrations shown in f and g mirror those shown in b and Fig. 1c. h, Percentage of MBP+ oligodendrocytes generated from mouse primary OPCs at 72 h following treatment with the indicated imidazole antifungals at 3 μM. n = 4 wells per condition, with >1,000 cells analysed per well. i, GC–MS-based uantification of lanosterol levels in mouse primary OPCs treated for 24 h with the indicated imidazole antifungals at 3 μM. n = 2 wells per condition. j, Assessment of oligodendrocyte formation using an alternative image quantification metric, fold increase in total neurite length. Re-analysis of data shown in Fig. 1c. n = 4 wells per condition except DMSO (n = 24), with >1,000 cells analysed per well. k, Percentage of oligodendrocytes generated from OPCs at 72 h following treatment with ketoconazole (2.5 μM) as measured by PLP1 immunostaining. Left, OPC-5; right, OPC-1. n = 8 wells per condition, with >1,000 cells analysed per well. l, LC–MS-based quantification of lanosterol levels in OPC-5 cells treated for 24 h with ketoconazole at 2.5 μM. n = 2 wells per condition. m, CYP51 mRNA levels measured by RT–qPCR following 96-h treatment with non-targeting or CYP51-targeting pools of cell-permeable siRNAs. n = 2 wells per condition. n, GC–MS-based quantification of lanosterol levels in OPC-1 cells treated for 96 h with the indicated pooled siRNA reagents. n = 2 wells per condition. o, Percentage of MBP+ oligodendrocytes generated from a second, independent batch of OPCs (OPC-1) at 72 h following treatment with the indicated reagents. n = 3 wells per condition, with >1,000 cells analysed per well. p, Percentage of MBP+ oligodendrocytes generated from an independent derivation of OPCs at 72 h following treatment with exogenous lanosterol. n = 4 wells per condition except DMSO and ketoconazole (n = 8), with >1,000 cells analysed per well. q, Representative images of OPC-5 cells treated for 72 h with the indicated siRNA reagents and lanosterol. Nuclei are labelled with DAPI (blue), and oligodendrocytes are indicated by immunostaining for MBP (green). Scale bar, 100 μm. All bar graphs indicate mean $\pm$ s.d.; b, d, h, i, k, l, o and p are representative of two independent experiments, and all findings have been confirmed in a second independent derivation of OPCs (Fig. 1).

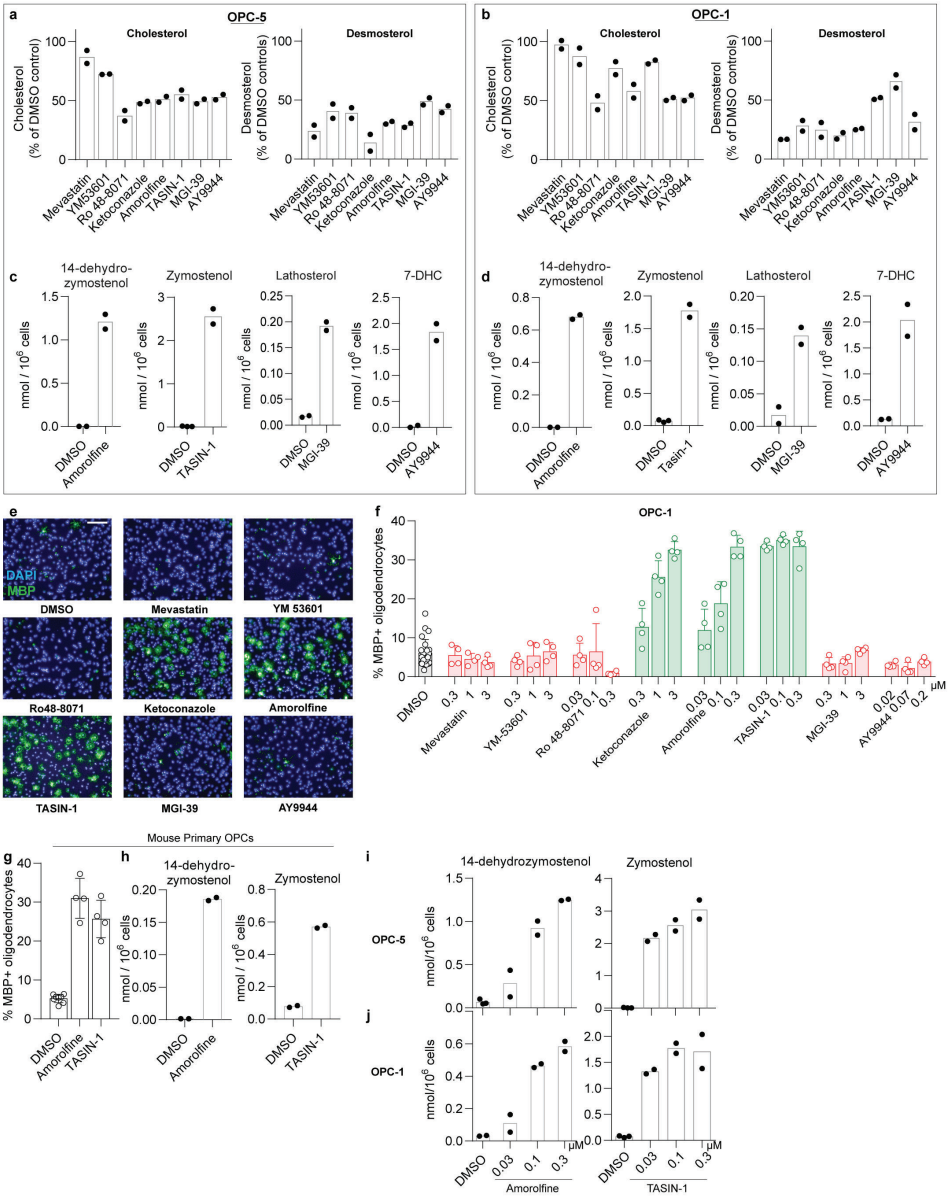

Figure 2.7: Extended Data Fig. 3 | Effect of small-molecule inhibition of the cholesterol biosynthesis pathway on enhancing oligodendrocyte formation. - Caption on next page

Extended Data Fig. 3 | Effect of small-molecule inhibition of the cholesterol biosynthesis pathway on enhancing oligodendrocyte formation. a, GC–MS-based quantification of sterol levels in OPCs (OPC-5) treated for 24 h with the indicated inhibitors of cholesterol biosynthesis. Left, cholesterol; right, desmosterol. n = 2 wells per condition. Inhibitors were used at the following doses unless otherwise noted: mevastatin, ketoconazole, MGI-39, 2.5 μM; YM53601, 2 μM; Ro 48-8071, amorolfine, TASIN-1, 100 nM; AY9944, 200 nM. b, GC–MS-based quantification of sterol levels in a second derivation of OPCs (OPC-1). Left, cholesterol; right, desmosterol. n = 2 wells per condition. c, GC–MS-based quantification of the sterol intermediates expected to accumulate following treatment of OPCs with the indicated inhibitors of cholesterol biosynthesis for 24 h. n = 2 wells per condition. d, GC–MS-based quantification of the sterol intermediates expected to accumulate following treatment of a second derivation of OPCs (OPC-1) with the indicated inhibitors of cholesterol biosynthesis for 24 h. n = 2 wells per condition. In c and d, no accumulation of other sterol intermediates indicative of off-target effects within the cholesterol pathway were observed (see Source Data). e, Representative images of OPC-5 cells treated for 72 h with the indicated small molecules. All treatments are at the highest concentration shown in Fig. 2b. Scale bar, 100 μm. f, Percentage of MBP+ oligodendrocytes generated from a second batch of OPCs (OPC-1) at 72 h following treatment with the indicated cholesterol pathway inhibitors. n = 4 wells per condition, except DMSO, n = 24, with >1,000 cells analysed per well. g, Percentage of MBP+ oligodendrocytes generated from mouse primary OPCs at 72 h following treatment with the indicated cholesterol pathway inhibitors at 300 nM. n = 4 wells per condition, except DMSO, n = 8, with >1,000 cells analysed per well. h, GC–MS-based quantification of sterol intermediate levels in mouse primary OPCs treated for 24 h with the indicated inhibitors of cholesterol biosynthesis at 300 nM. Left, 14-dehydrozymostenol levels following treatment with amorolfine; right, zymostenol levels following treatment with TASIN-1. n = 2 wells per condition. i, j, GC–MS-based quantification of sterol intermediate levels in OPC-5 (i) and OPC-1 (j) cells treated for 24 h with the indicated doses of inhibitors of cholesterol biosynthesis. Left, 14-dehydrozymostenol levels following treatment with amorolfine; right, zymostenol levels following treatment with TASIN-1. n = 2 wells per condition. Concentrations shown in i mirror those shown in f. All bar graphs indicate mean $\pm$ s.d., and a, c, e–h are representative of two independent experiments.

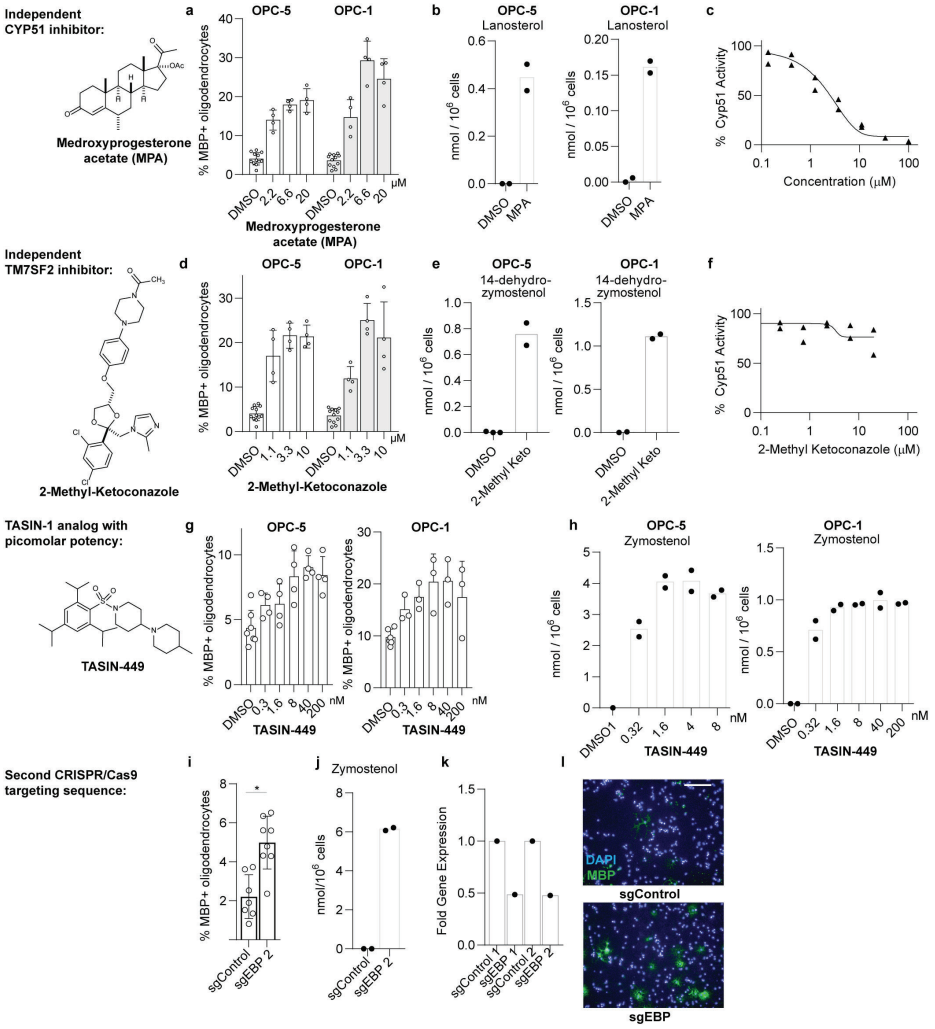

Figure 2.8: Extended Data Fig. 4 | Effect of independent chemical-genetic and genetic modulators of CYP51, sterol 14 reductase and EBP on oligodendrocyte formation and cholesterol biosynthesis. - Caption on next page

Extended Data Fig. 4 | Effect of independent chemical-genetic and genetic modulators of CYP51, sterol 14 reductase and EBP on oligodendrocyte formation and cholesterol biosynthesis. a, d, g, Percentage of MBP+ oligodendrocytes generated from two independent derivation of OPCs at 72 h following treatment with the indicated concentrations of medroxyprogesterone acetate (a), 2-methyl ketoconazole (d) or TASIN-449 (g). n = 4 wells per condition, except DMSO, n = 12 in a, d. In g, for OPC-5, n = 4 except DMSO, n = 7; for OPC-1, n = 3 except DMSO, n = 6. b, e, h, GC–MS-based quantification of sterol levels in two independent derivations of OPCs treated for 24 h with medroxyprogesterone acetate at 10 μM (b), 2-methyl ketoconazole at 2.5 μM (e) and TASIN-449 at the indicated concentrations (h). n = 2 wells per condition. c, f, Rat CYP51 enzymatic activity following treatment with varying concentrations of medroxyprogesterone acetate (c) and 2-methyl ketoconazole (f) as measured by LC–MS-based quantification of the CYP51 product FF-MAS. n = 2 independent enzymatic assays. i, Percentage of MBP+ oligodendrocytes generated from OPCs (OPC- 5) infected with lentivirus expressing Cas9 and an independent guide RNA targeting EBP (see also Fig. 2c). Eight wells per condition, with >1,000 cells analysed per well. Two-tailed Student's t-test, *P = 0.0009. j, Functional validation of CRISPR-based targeting of EBP with a second sgRNA using GC–MS-based quantification of zymostenol levels. n = 2 wells per condition. k, EBP mRNA levels measured by RT–qPCR in OPCs (OPC-5) infected with lentivirus expressing Cas9 and either of two guide RNAs targeting EBP. One well per condition, with results validated in an independent experiment. l, Representative images of the oligodendrocyte formation assay shown in Fig. 2c. Nuclei are labelled with DAPI (blue), and oligodendrocytes are indicated by immunostaining for MBP (green). Scale bar, 100 μm. All bar graphs indicate mean $\pm$ s.d., and a, d, g, i, k are representative of two independent experiments.

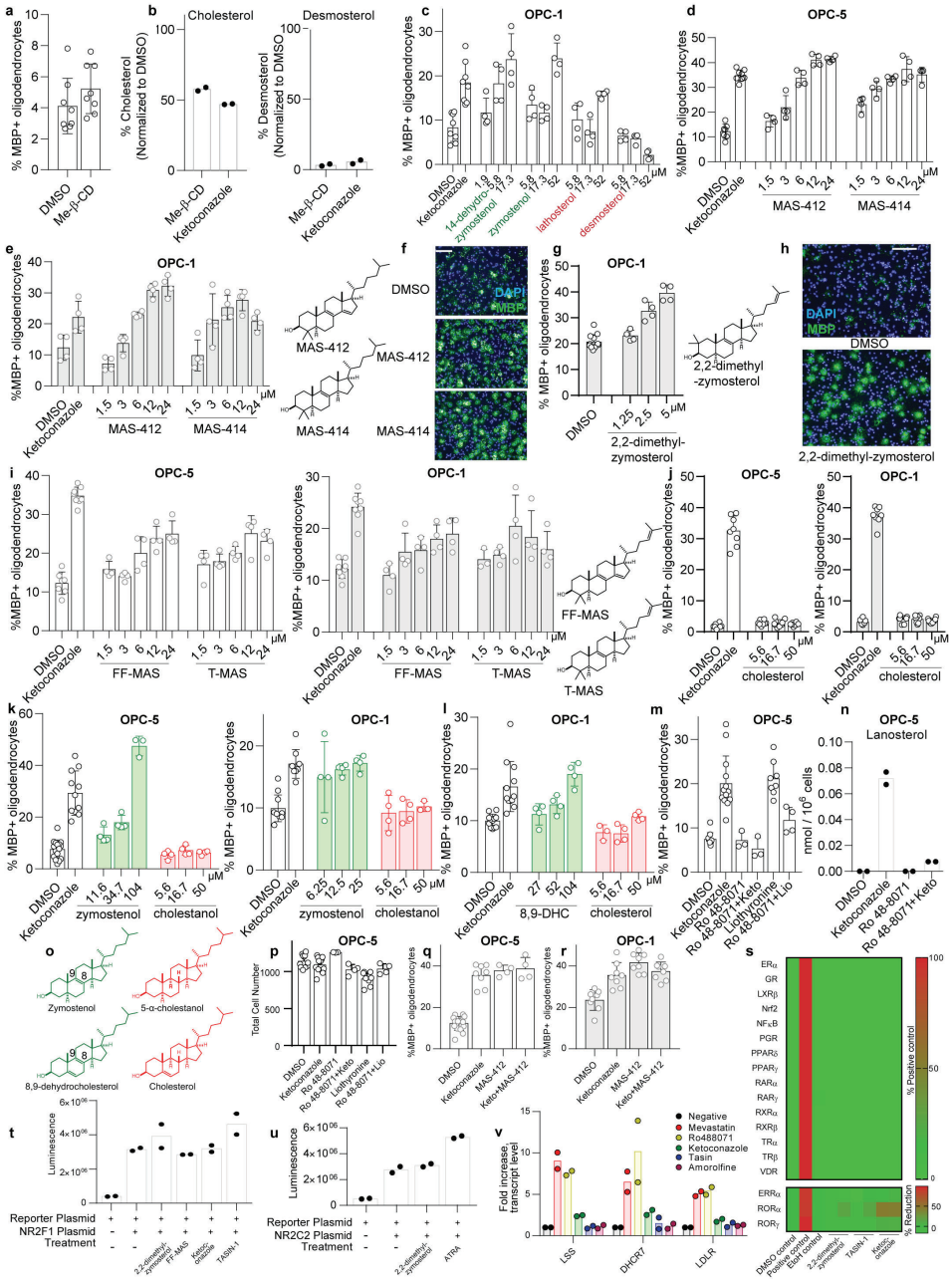

Figure 2.9: Extended Data Fig. 5 | Effect of 8,9-unsaturated sterols on oligodendrocyte formation. - Caption on next page

Extended Data Fig. 5 | Effect of 8,9-unsaturated sterols on oligodendrocyte formation. a, Percentage of MBP+ oligodendrocytes generated from OPCs (OPC-5) at 72 h following treatment with methyl β-cyclodextrin (1 mM) for 30 min at 37 ℃. n = 8 wells per condition, with >1,000 cells analysed per well. b, GC–MS-based quantification of cholesterol (left) and desmosterol (right) in OPCs (OPC-5) treated with methyl β-cyclodextrin (Me-β-CD) at 1 mM or ketoconazole at 2.5 μM. n = 2 wells per condition. c, d, Percentage of MBP+ oligodendrocytes generated from OPC-1 (c) and OPC-5 cells (d) at 72 h following treatment with the indicated purified sterol intermediates. n = 4 wells per condition, except n = 8 for DMSO and ketoconazole, with >1,000 cells analysed per well. Green text highlights metabolites that accumulate after treatments that enhance oligodendrocyte formation (Fig. 2e, Extended Data Fig. 3c). e, Percentage of MBP+ oligodendrocytes generated from OPC-1 cells at 72 h following treatment with MAS-412 and MAS-414. n = 4 wells per condition, with >1,000 cells analysed per well. f, Representative images of OPC5 cells treated for 72 h with DMSO, MAS-412, or MAS-414 (3 μM). Nuclei are labelled with DAPI (blue), and oligodendrocytes are indicated by immunostaining for MBP (green). Scale bar, 100 μm. g, Percentage of MBP+ oligodendrocytes generated from OPC-1 at 72 h following treatment with 2,2-dimethyl-zymosterol. n = 4 wells per condition except DMSO (n = 12), with >1,000 cells analysed per well. h, Representative images of OPC-5 cells treated for 72 h with vehicle and 2,2-dimethyl-zymosterol (2.5 μM). Nuclei are labelled with DAPI (blue), and oligodendrocytes are indicated by immunostaining for MBP (green). Scale bar, 100 μm. i, Percentage of MBP+ oligodendrocytes generated from OPC-5 (left) and OPC-1 (right) cells at 72 h following treatment with FF-MAS or T-MAS. n = 4 wells per condition except DMSO and ketoconazole (n = 8), with >1,000 cells analysed per well. j, Percentage of MBP+ oligodendrocytes generated from OPC-5 and OPC-1 OPCs at 72 h following treatment with the indicated concentrations of cholesterol. n = 8 wells per condition, with >1,000 cells analysed per well. k, l, Percentage of MBP+ oligodendrocytes generated from OPC-5 and OPC-1 cells at 72 h following treatment with the indicated concentrations of sterols that are structurally identical aside from the presence or absence of the 8,9 double bond (structures in o). n $\geq$ 3 wells per condition (see dot plots as replicate values vary by condition), with >1,000 cells analysed per well. m, Percentage of MBP+ oligodendrocytes generated from OPCs (OPC-5) at 72 h following treatment with the indicated small molecules or combinations of small molecules (ketoconazole, 2.5 μM; Ro 48-8071, 11 nM; liothyronine, 3 μM). n = 3 wells per condition, except DMSO n = 11, ketoconazole n = 13, liothyronine n = 8 & liothyronine + Ro 48-8071 n = 4, with >1,000 cells analysed per well. n, GC–MS-based quantification of lanosterol levels in OPCs (OPC-5) treated for 24 h with the indicated small molecules or combinations of small molecules at concentrations stated in m. n = 2 wells per condition. o, Structures of zymostenol, 8,9-dehydrocholesterol, 5α-cholestanol, and cholesterol. p, Total cell number as measured by counting of DAPI+ nuclei in the experiment presented in m. q, r, Percentage of MBP+ oligodendrocytes generated from OPCs (OPC5 and OPC-1) at 72 h following treatment with the indicated small molecules or combinations of small molecules in two independent batches of OPCs (ketoconazole, 2.5 μM; MAS412, 5 μM). In q, n = 16 for DMSO, 8 for ketoconazole, and 4 for remaining bars. In r, n = 8 wells per condition. s, Luciferase reporter assays were used to assess whether 2,2-dimethylzymosterol (5 μM),

ketoconazole (2.5 μM), and TASIN-1 (250 nM) modulate human ERα, GR, LXRβ, NFkB, NRF2, PGR, PPARδ, PPARγ, RARα, RARγ, RXRα, RXRβ, TRα, TRβ and VDR transcriptional activity in agonist mode and ERRα, RORα and RORγ in inverse-agonist mode. n = 2 wells per condition and n = 3 wells per positive control condition. t, Effects of sterols (2,2-dimethylzymosterol 5 μM, FF-MAS 10 μM) and small molecules (ketoconazole 2.5 μM, TASIN-1 100 nM) on the NR2F1-mediated activation of a NGFI-A promoter driven luciferase reporter. n = 2 wells per condition. u, Effects of 2,2-dimethylzymosterol (5 μM) on NR2C2-mediated activation of a NGFI-A promoter driven luciferase reporter in comparison to cells transfected with reporter only, untreated, or treated with a previously reported positive control (all-trans retinoic acid, ATRA, 5 μM). n = 2 wells per condition. v, LSS, DHCR7, LDLR mRNA levels measured by RT–qPCR following 24 h treatment with DMSO, mevastatin (2.5 μM), Ro 48-8071 (500 nM), ketoconazole (2.5 μM), TASIN-1 (100 nM), or amorolfine (100 nM). n = 2 wells. All bar graphs indicate mean $\pm$ s.d., and a–n and t–v are representative of two independent experiments.

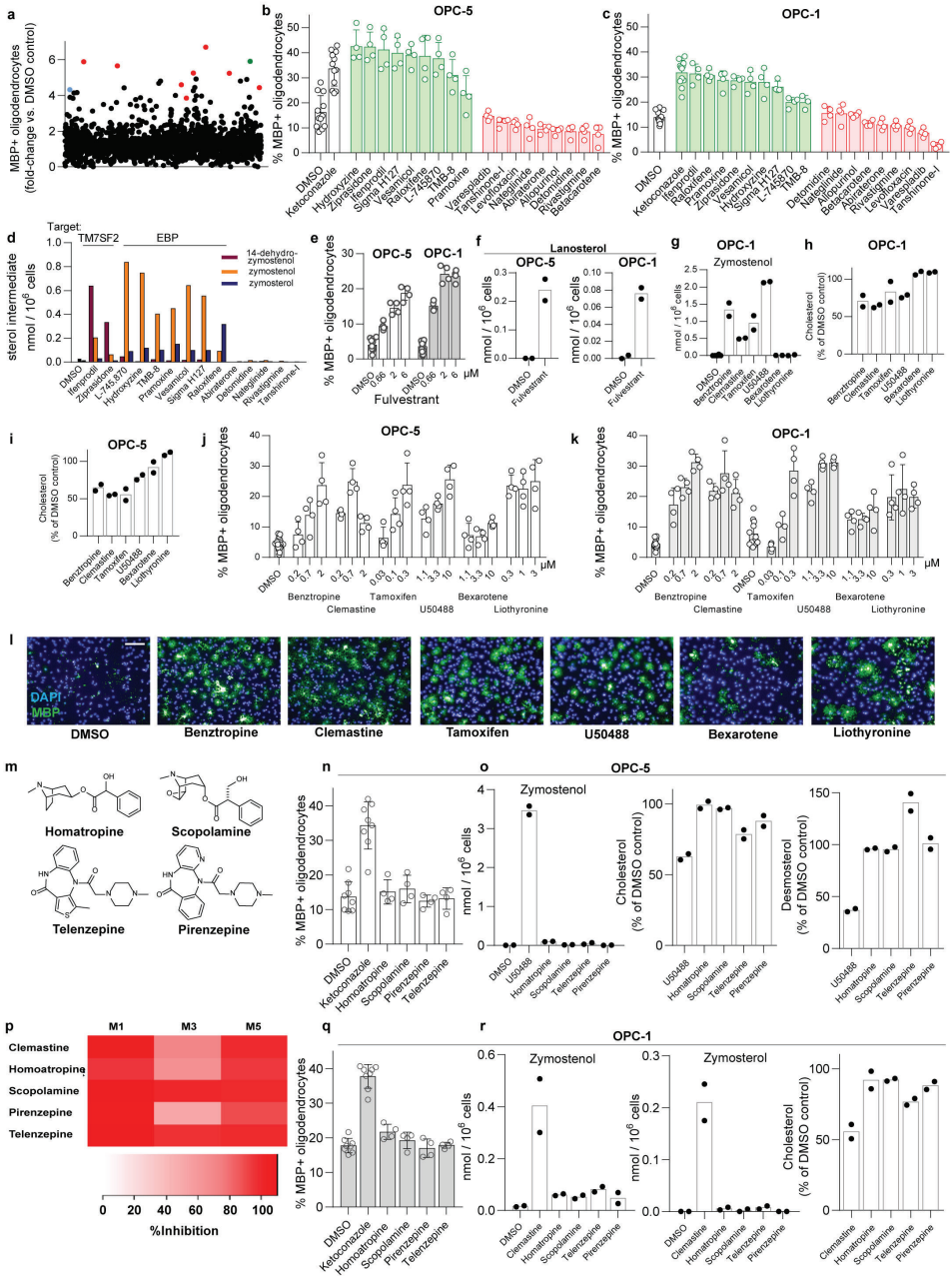

Figure 2.10: Extended Data Fig. 6 | Inhibiting CYP51, TM7SF2 and EBP is a unifying mechanism for many small-molecule enhancers of oligodendrocyte formation identified by high-throughput screening. - Caption on next page

Extended Data Fig. 6 | Inhibiting CYP51, TM7SF2 and EBP is a unifying mechanism for many small-molecule enhancers of oligodendrocyte formation identified by high-throughput screening. a, Percentage of MBP+ oligodendrocytes (relative to DMSO control wells) generated from OPCs (OPC-1 derivation) at 72 h following treatment with a library of 3,000 bioactive small molecules, each at 2 μM. Each dot represents the result for one small molecule in the library. Red, imidazole antifungals; blue, clemastine; green, EPZ005687, the top novel hit molecule (Extended Data Fig. 7). b, c, Percentage of MBP+ oligodendrocytes generated from OPCs (left: OPC-5; right: OPC-1) at 72 h following treatment with ketoconazole, nine top molecules identified by bioactives screening (green), and nine randomly chosen library members (red) at a uniform dose of 5 μM. n = 4 wells per condition except DMSO and ketoconazole, n = 12 wells, with >1,000 cells analysed per well. d, GC–MS-based quantification of zymosterol, zymostenol, and 14-dehydrozymostenol levels in a second batch of OPCs treated for 24 h with the indicated screening hits and randomly chosen library members at 2 μM. n = 1; for validation in a second derivation of OPCs, see Fig. 3a. Molecules are clustered by enzyme targeted (top labels). e, Percentage of MBP+ oligodendrocytes generated from OPCs at 72 h following treatment with the indicated doses of fulvestrant, one of the top 10 HTS hits. n = 4 wells per condition except DMSO, n = 12, with >1,000 cells analysed per well. f, GC–MS-based quantification of lanosterol levels in OPCs treated for 24 h with fulvestrant at 2 μM. n = 2 wells per condition. g–i, GC–MSbased quantification of metabolite levels in OPCs treated for 24 h with the indicated previously reported enhancers of oligodendrocyte formation at the following doses: benztropine, 2 μM; clemastine, 1 μM; tamoxifen, 100 nM; U50488, 5 μM; bexarotene, 1 μM; liothyronine, 3 μM. n = 2 wells per condition. j, k, Percentage of MBP+ oligodendrocytes generated from OPCs (OPC-5 left, OPC-1 right) at 72 h following treatment with the indicated previously reported enhancers of oligodendrocyte formation. n = 4 wells per condition, except DMSO n = 20 for OPC-5 and n = 12 for OPC-1, with >1,000 cells analysed per well. All doses are in μM. l, Representative images of OPCs treated for 72 h with the indicated small molecules. All treatments in l are at the highest concentration shown in j. Scale bar, 100 μm. m, Structures of muscarinic receptor antagonists used in this study. n, q, Percentage of MBP+ oligodendrocytes generated from OPCs (OPC-5: top, OPC-1: bottom) at 72 h following treatment with ketoconazole or the indicated muscarinic receptor modulators at 2 μM, the concentration used during screening. n = 4 wells per condition except DMSO and ketoconazole, n = 8, with >1,000 cells analysed per well. o, GC–MS-based quantification of three metabolite levels in OPC-5 OPCs treated for 24 h with U50488 (5 μM) or the indicated muscarinic receptor modulators (2 μM). Left, zymostenol; centre, cholesterol; right, desmosterol. n = 2 wells per condition. p, Heatmap indicating inhibition of muscarinic receptor isoforms M1, M3, and M5 by the indicated small molecules (2 μM) assayed using GeneBLAzer NFAT-bla CHO-K1 cells. n = 2 wells per condition. r, GC–MS-based quantification of three metabolite levels in OPC-1 OPCs treated for 24 h with clemastine (1 μM) or the indicated muscarinic receptor modulators at 2 μM. n = 2 wells per condition. Left, zymostenol; centre, zymosterol; right, cholesterol. Sigma H127, p-fluorohexahydro-sila-difenidol. All bar graphs indicate mean $\pm$ s.d., and b, c, e, i, j, k, n, q are representative of two independent experiments.

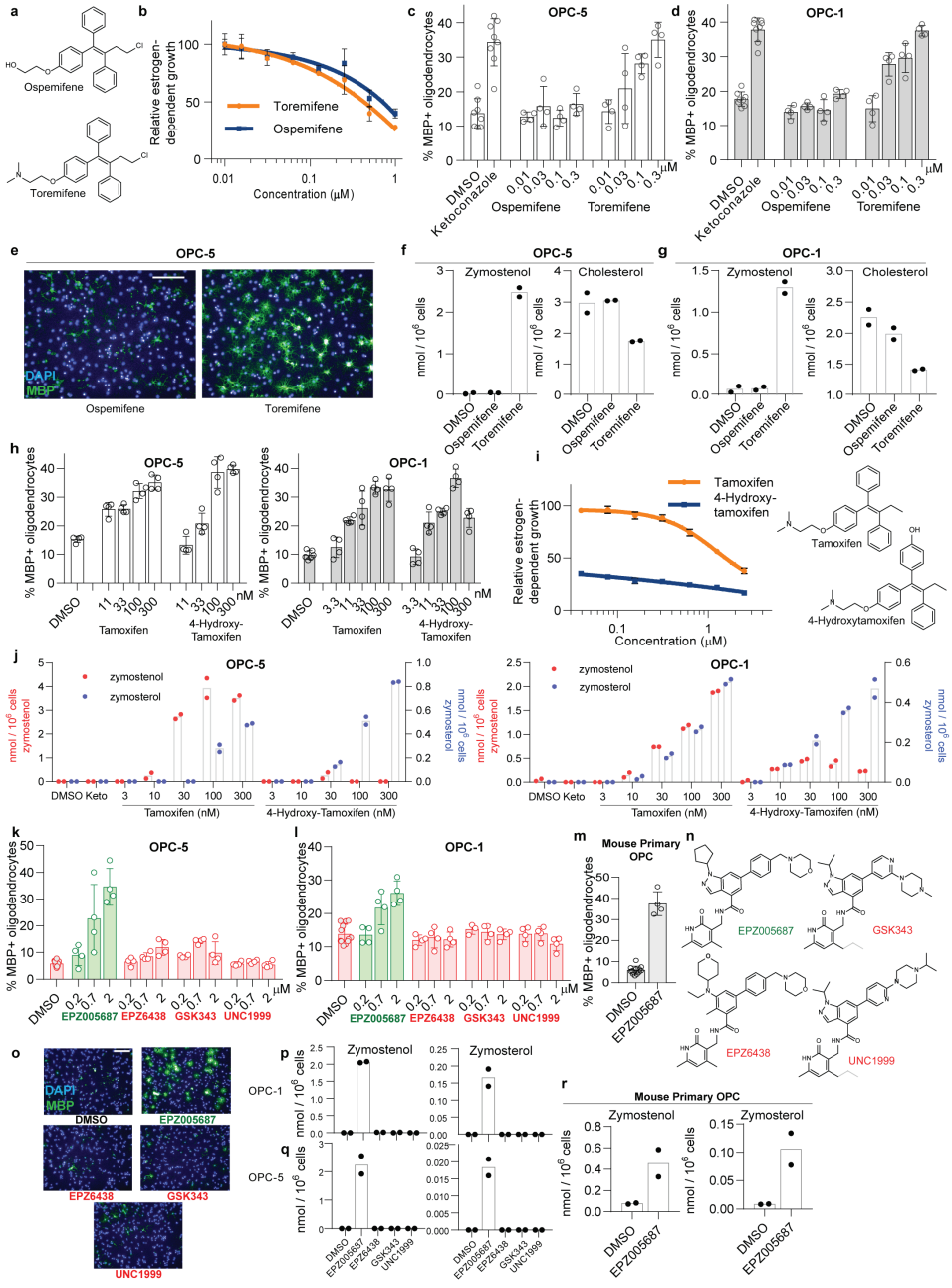

Figure 2.11: Extended Data Fig. 7 | Effect of selective oestrogen receptor modulators and EZH2 inhibitors on cellular EBP function and oligodendrocyte formation. - Caption on next page

Extended Data Fig. 7 | Effect of selective oestrogen receptor modulators and EZH2 inhibitors on cellular EBP function and oligodendrocyte formation. a, Structures of selective oestrogen receptor modulators used in this study. b, Effects of ospemifene and toremifene on the oestrogendependent growth of T47D cells. n = 3 wells per condition. c, d, Percentage of MBP+ oligodendrocytes generated from two independent batches of OPCs at 72 h following treatment with ospemifene and toremifene. n = 4 wells per condition except DMSO and ketoconazole, n = 8, with >1,000 cells analysed per well. e, Representative images of OPCs treated for 72 h with the indicated small molecules. All molecules were used at 300 nM. Scale bar, 100 μm. f, g, GC–MS-based quantification of two metabolite levels in OPCs treated for 24 h with ospemifene and toremifene at 300 nM. Left, zymostenol; right, cholesterol. n = 2 wells per condition. h, Percentage of MBP+ oligodendrocytes generated from two independent batches of OPCs at 72 h following treatment with tamoxifen and 4-hydroxytamoxifen. Left, OPC-5; right, OPC-1. n = 4 wells per condition, except DMSO, n = 6 for OPC-1 (right). i, Effects of tamoxifen and 4-hydroxytamoxifen on the oestrogen-dependent growth of T47D cells. n = 3 wells per condition. j, GC–MS-based quantification of zymostenol (left axis) and zymosterol levels (right axis) in OPC-5 and OPC-1 treated 24 h with tamoxifen and 4-hydroxytamoxifen at the indicated concentrations. n = 2 wells per condition. k, Percentage of MBP+ oligodendrocytes generated from OPCs at 72 h following treatment with the indicated structurally analogous EZH2 inhibitors. n = 4 wells per condition, except DMSO, n = 12, with >1,000 cells analysed per well. l, Percentage of MBP+ oligodendrocytes generated from a second batch of OPCs at 72 h following treatment with the indicated structurally analogous EZH2 inhibitors. n = 4 wells per condition, except DMSO, n = 12, with >1,000 cells analysed per well. m, Percentage of MBP+ oligodendrocytes generated from mouse primary OPCs at 72 h following treatment with EPZ005687. n = 4 wells per condition, except DMSO, n = 12, with >1,000 cells analysed per well. n, Structure of EPZ005687 and structurally analogous EZH2 inhibitors. o, Representative images of OPCs treated for 72 h with the indicated EZH2 inhibitors. All treatments are at 2 μM. Scale bar, 100 μm. p, GC–MS-based quantification of two sterol intermediates following treatment of OPCs with the indicated EZH2 inhibitors at 1 μM for 24 h. Left, zymostenol; right, zymosterol. n = 2 wells per condition. q, GC–MS-based quantification of two sterol intermediates following treatment of a second derivation of OPCs with the indicated EZH2 inhibitors at 1 μM for 24 h. Left, zymostenol; right, zymosterol. n = 2 wells per condition. r, GC–MS-based quantification of two sterol intermediates following treatment of mouse primary OPCs with EPZ005687 at 2 μM for 24 h. Left, zymostenol; right, zymosterol. n = 2 wells per condition. All bar graphs indicate mean $\pm$ s.d., and c, d, h, k–o, r are representative of two independent experiments.

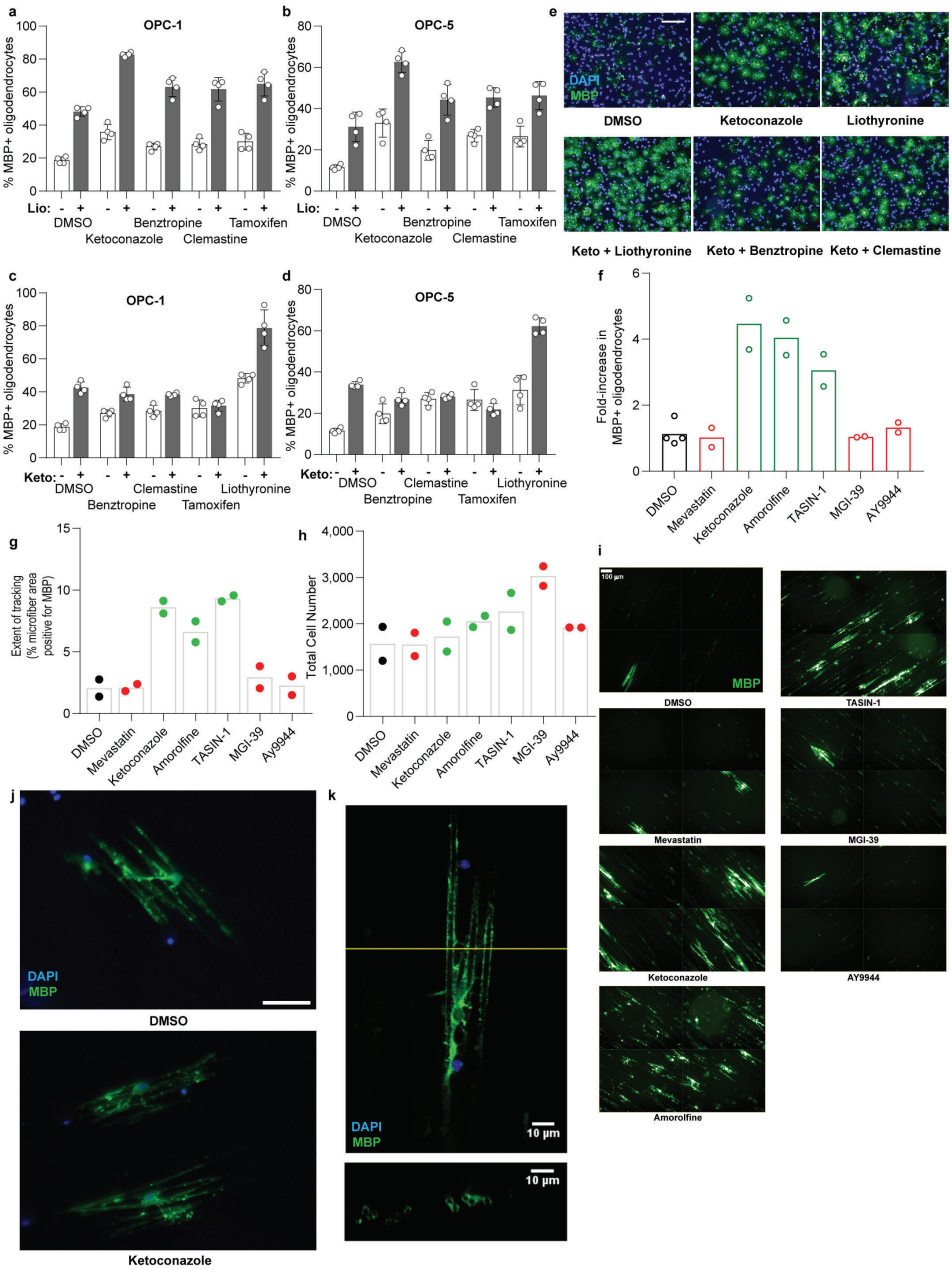

Figure 2.12: Extended Data Fig. 8 | Effect of combinations of small-molecule treatments on oligodendrocyte formation, and ability of oligodendrocytes to track along and wrap electrospun microfibres after single small-molecule treatments. - Caption on next page

Extended Data Fig. 8 | Effect of combinations of small-molecule treatments on oligodendrocyte formation, and ability of oligodendrocytes to track along and wrap electrospun microfibres after single small-molecule treatments. a, b, Percentage of MBP+ oligodendrocytes generated from OPCs (left, OPC-1; right, OPC-5) at 72 h following treatment with the indicated combinations of liothyronine and enhancers of oligodendrocyte formation. Unless noted, the following concentrations were used: ketoconazole, 2.5 μM; benztropine, 2 μM; clemastine 2 μM; tamoxifen 200 nM; liothyronine, 3 μM. n = 4 wells per treatment condition, with >1,000 cells analysed per well. Lio, liothyronine. c, d, Percentage of MBP+ oligodendrocytes generated from OPCs at 72 h following treatment with the indicated combinations of ketoconazole and enhancers of oligodendrocyte formation. n = 4 wells per treatment condition, with >1,000 cells analysed per well. e, Representative images of OPCs treated for 72 h with the indicated small molecules. Small-molecule concentrations are as in a. Scale bar, 100 μm. f, Fold-increase in MBP+ oligodendrocytes following plating of OPCs (OPC-5) onto microfibres and treatment for 14 days with the indicated pathway modulators. n = 2 wells per condition, except DMSO, n = 4. g, In an independent experiment, OPCs (OPC-5) were plated onto microfibres, treated with small molecules for 4 days, and fixed and stained after 14 days. The extent to which MBP+ oligodendrocytes tracked along the microfibre substrate was measured. n = 2 wells per condition. h, Total DAPI+ cell number in the experiment in g. i, Representative images highlighting tracking along the microfibre substrate. Each image is a montage of four separate images within the same well. Green, MBP. Scale bar, 100 μm. j, High-resolution images of MBP+ oligodendrocytes tracking along microfibres. Green, MBP; blue, DAPI. Ketoconazole, 2.5 μM. Scale bar, 50 μm. k, Confocal imaging of OPCs seeded onto aligned microfibres and treated for 14 days with ketoconazole (2.5 μM). The plane of the cross-section is highlighted in yellow and the cross-section, in which green fluorescence appears to encircle several microfibres, is shown in the bottom panel. Green, MBP; blue, DAPI. All bar graphs indicate mean $\pm$ s.d., and a–d are representative of two independent experiments.

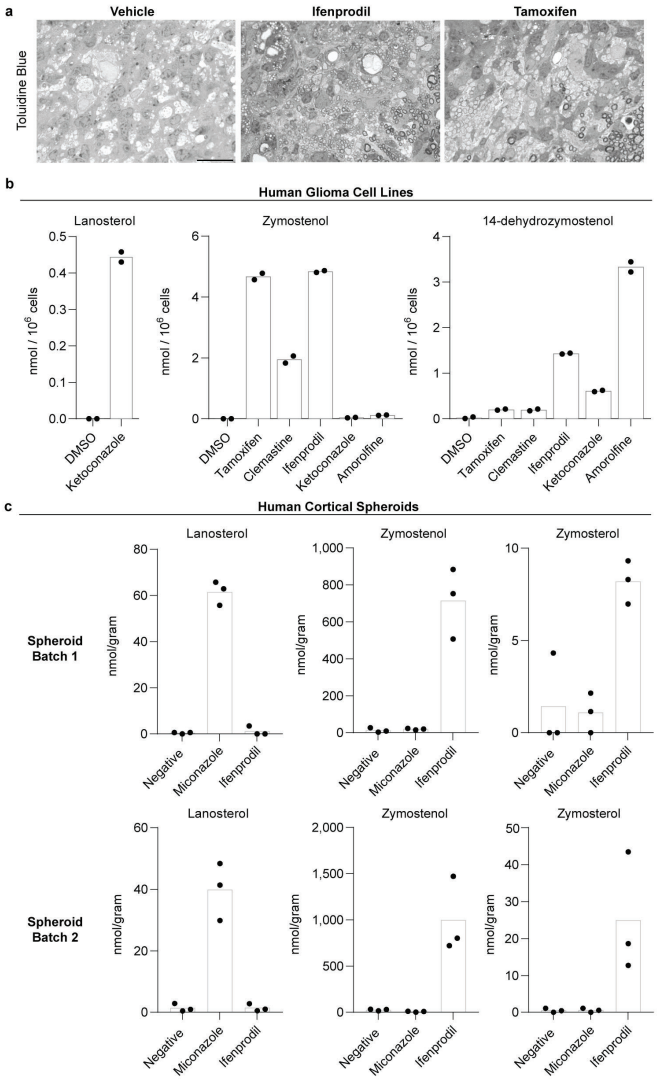

Figure 2.13: Extended Data Fig. 9 | Effect of oligodendrocyte-enhancing small molecules on sterol levels in human cells and human cortical spheroids. - Caption on next page

Extended Data Fig. 9 | Effect of oligodendrocyte-enhancing small molecules on sterol levels in human cells and human cortical spheroids. a, Representative images of toluidine blue-stained sections of LPClesioned dorsal spinal cord from mice treated for 8 days with ifenprodil (10 mg per kg) or tamoxifen (2 mg per kg). Scale bar, 20 μm. b, GC–MSbased quantification of three metabolite levels in human glioma cells (GBM528) treated for 24 h with the indicated small molecules at the following concentrations: tamoxifen, 100 nM; clemastine, 2 μM; ifenprodil, 2 μM; ketoconazole, 2.5 μM; amorolfine, 100 nM. Left, lanosterol; centre, zymostenol; right, 14-dehydrozymostenol. n = 2 wells per condition. c, GC–MS-based quantification of three metabolite levels in two independent batches of human cortical spheroids treated for 24 h with the indicated small molecules at 2 μM. Left, lanosterol; centre, zymostenol; right, zymosterol. n = 3 spheroids per condition; representative of two independent experiments.

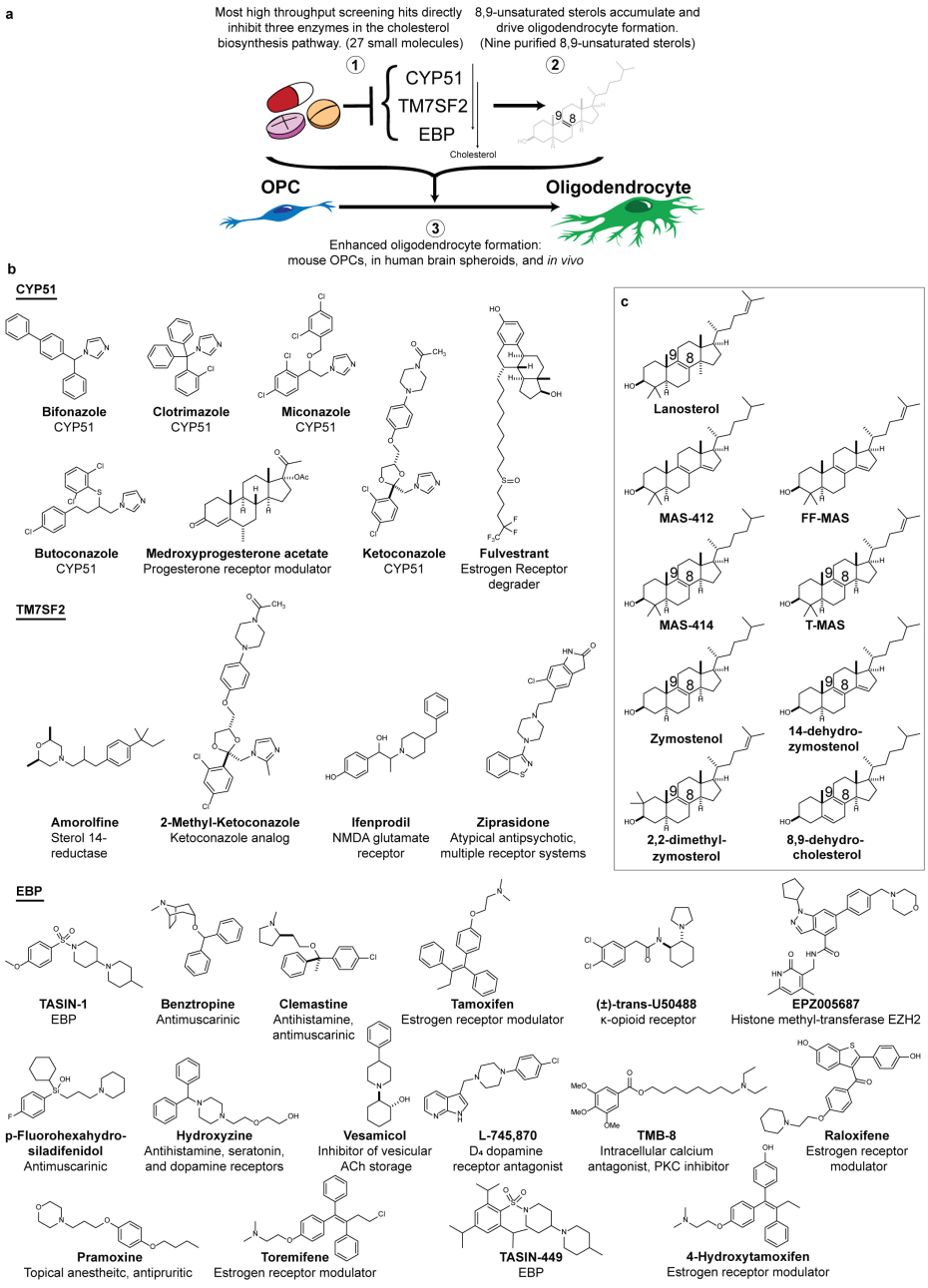

Figure 2.14: Extended Data Fig. 10 | Twenty-seven small molecules and nine purified 8,9-unsaturated sterols shown to enhance the formation of oligodendrocytes. - a, Schematic showing the proposed mechanism of action for enhanced oligodendrocyte formation by diverse small molecules. b, Molecules that enhance oligodendrocyte formation are grouped by enzyme inhibited (GC–MS analysis in OPCs): CYP51, top; sterol 14-reductase, centre; EBP, bottom. c, Purified 8,9-unsaturated sterols that enhance oligodendrocyte formation.

3

Modulation of lanosterol synthase drives 24,25-epoxysterol synthesis and oligodendrocyte formation

3.1 Introduction

Myelin is an essential component of the mammalian central nervous system (CNS) that enables saltatory conduction of action potentials and provides trophic support to axons. (66, 123) Loss of oligodendrocytes, the specialized glial cells whose membranes constitute myelin, underlies a number of neurological diseases including multiple sclerosis (MS). (45, 89) However, oligodendrocyte progenitor cells (OPCs), a stem cell population present in the CNS throughout life, can differentiate to form new oligodendrocytes that can replenish lost myelin. (51, 79) While this process of remyelination occurs to a limited extent in MS patients, it ultimately stalls, leading to disease progression. (33) As a result, future therapeutics that enhance the formation

of new oligodendrocytes and replace lost myelin have the potential to slow disease progression and limit disability in patients with MS.

To discover candidate remyelinating therapeutics, we and others have performed *in vitro* screens to identify small molecules that enhance oligodendrocyte formation from OPCs. (3, 38, 60, 71, 72, 88, 107, 122) Dozens of hit molecules have been identified in these screens, with many enhancing remyelination in leading preclinical animal models of MS. (38, 60, 71, 88, 107, 108, 122) One validated screening hit, clemastine, was shown to significantly increase axonal conduction velocity in demyelinated axons, a myelination-dependent phenotype in MS patients. (61) Recently, we reported that inhibition of the cholesterol biosynthesis enzymes CYP51, sterol 14-reductase, and EBP represents a unifying mechanism by which most oligodendrocyte-enhancing molecules, including clemastine, act. (3, 72) Inhibition of these enzymes causes cells to accumulate 8,9-unsaturated sterol precursors to cholesterol, which we showed are necessary and sufficient to enhance oligodendrocyte formation. (72) However, the structure-activity relationships governing the activity of 8,9-unsaturated sterols in OPCs and the sterol signaling mechanisms that ultimately induce the formation of oligodendrocytes remain unclear.

To identify 8,9-unsaturated sterols with increased potency in OPCs, we synthesized and evaluated a collection of 15 8,9-unsaturated sterols derived from lanosterol, the substrate of CYP51 previously shown to enhance oligo-

dendrocyte formation. (72) We noted that 24,25-epoxylanosterol promoted oligodendrocyte formation significantly more potently than lanosterol itself. However, OPCs metabolized 24,25-epoxylanosterol to 24,25-epoxycholesterol, which also promoted oligodendrocyte formation when supplied to OPCs in pure form. Notably, 24,25-epoxycholesterol lacks the 8,9-unsaturation, establishing a new structural feature of sterols that enhance the differentiation of OPCs to oligodendrocytes. Multiple approaches to enhancing epoxycholesterol levels in OPCs, including partial inhibition of the cholesterol biosynthesis enzyme LSS using genetic or small-molecule tools, also promote oligodendrocyte formation. While the mechanisms by which epoxycholesterol signals in OPCs remain unclear, we demonstrate that LXR signaling, a canonical target of epoxycholesterol, is unlikely to be involved. Together, these studies establish that sterols beyond 8,9-unsaturated sterols can promote the differentiation of OPCs to oligodendrocytes and validate LSS as a new druggable target within the cholesterol biosynthesis pathway for promoting remyelination. [1]

[1] This work was accomplished through the help of many including: Ryan M. Friedrich, Joel Sax, Dharmaraja Allimuthu, Farrah Gao, Adrianna M. Rivera-Leóon, Matthew Pleshinger, and Ilya Bederman

3.2 Results

3.2.1 24,25-epoxylanosterol promotes oligodendrocyte formation more potently than lanosterol

Our panel of 15 synthetic 8,9-unsaturated sterols (See fig. 3.5a) was first tested at two concentrations (2 and 0.4 μM) for their effects on oligodendrocyte formation from OPCs using our established high-content imaging assay (See fig. 3.1b). (72) The top four sterols promoting formation of mature, myelin basic protein-positive (MBP+) oligodendrocytes at 2 μM were next validated to enhance OPC differentiation in a dose-responsive manner (See fig. 3.1a,c). Because these molecules are all derivatives of lanosterol, the substrate for CYP51, we suspected some may inhibit cholesterol pathway enzymes previously validated for promoting oligodendrocyte formation: CYP51, sterol 14-reductase, and EBP. (3, 72) To evaluate potential inhibition of cholesterol pathway enzymes, we used GC-MS-based sterol profiling to simultaneously quantify levels of nine sterol intermediates between lanosterol and cholesterol. (72) We noted that CW0165 inhibited CYP51, as indicated by cellular accumulation of CYP51's substrate lanosterol (See fig. 3.1d). Notably, the 8,9-epoxy functionality generally appears to provide affinity for CYP51, as six other analogs containing this functionality also inhibited CYP51 and promoted oligodendrocyte formation, albeit with lower potency

(See fig. 3.1b, fig. 3.5b). By contrast, CW0191, which adds a morpholine to the lanosterol tail, led to accumulation of zymosterol, indicating inhibition of EBP (See fig. 3.1d). These sterols, like many other small molecules, appear to promote oligodendrocyte formation via inhibition of these previously-validated pathway enzymes.

Interestingly, CW0163 (24(R/S),25-epoxylanosterol) and CW0182 (24(R/S)-hydroxylanosterol) did not inhibit CYP51, sterol 14-reductase, or EBP in OPCs (See fig. 3.5c). Because 24-hydroxylanosterol showed significant cytotoxicity at the tested concentrations (See fig. 3.5d), we focused on epoxylanosterol. We synthesized the pure 24(*S*) and 24(*R*) diastereomers of 24,25-epoxylanosterol and evaluated their effects on oligodendrocyte formation. The C24 epimers of 24,25-epoxylanosterol showed comparable potency and were substantially more potent than lanosterol itself (See fig. 3.1e-f, fig. 3.5c).

3.2.2 24,25 epoxycholesterol promotes oligodendrocyte formation

24(*S*),25-epoxylanosterol is a naturally-occurring metabolite that arises from cyclization of diepoxysqualene by lanosterol synthase (LSS) (See fig. 3.2a). (124, 162) 24(*S*),25-epoxylanosterol can be metabolized to 24(*S*),25- epoxycholesterol via the epoxycholesterol shunt, which comprises the same se-

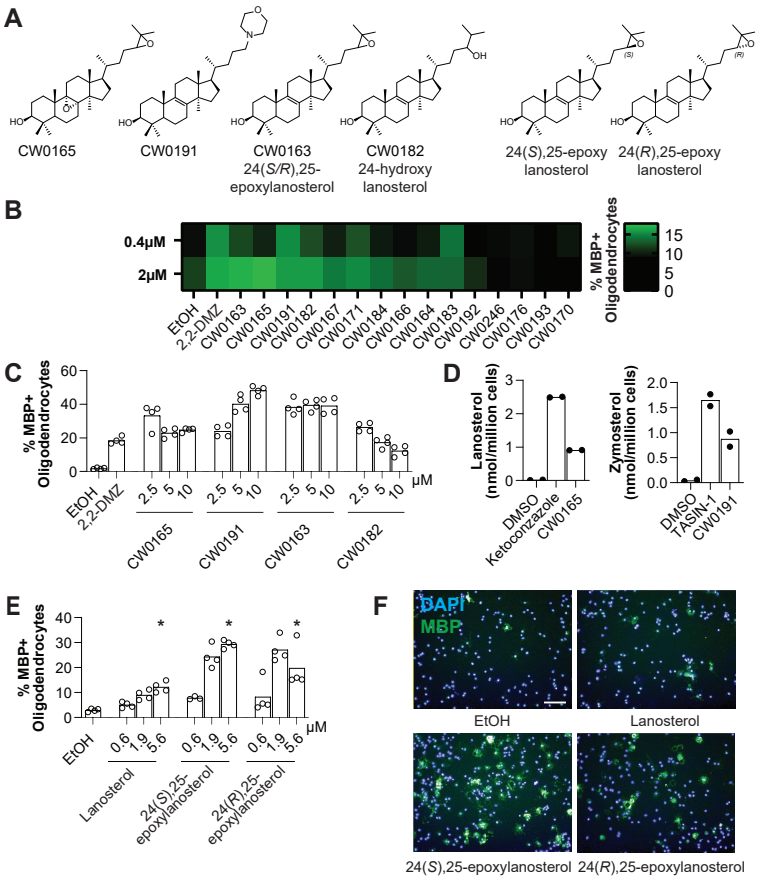

Figure 3.1: Evaluation of lanosterol structural variants reveals that epoxylanosterol promotes oligodendrocyte formation. - a, Structures of the top four lanosterol variants that promote oligodendrocyte formation and the two diastereomers of 24,25-epoxylanosterol. b, Heatmap showing the percentage of MBP+ oligodendrocytes 72 hours after treatment with each of the lanosterol variations at 0.4 and 2 μM. n = 4 wells per condition. 2,2-DMZ, a known 8,9-unsaturated sterol that promotes oligodendrocyte formation, 2.5 μM. c, Percentage of MBP+ oligodendrocytes 72 hours after treatment with the top oligodendrocyte formation enhancing 8,9-unsaturated sterol structural variants at the concentrations indicated. n = 4 wells per condition. 2,2-DMZ, 2.5 μM. d, GC-MS-based quantification of lanosterol and zymosterol in OPCs 24 hours after treatment with the indicated small molecules at 2 μM. n = 2 wells per condition. Ketoconazole, a canonical CYP51 inhibitor, 2.5 μM. TASIN-1, a selective EBP inhibitor, 1 μM. e, Percentage of MBP+ oligodendrocytes 72 hours after treatment with lanosterol, 24(*S*),25-epoxylanosterol, and 24(*R*),25-epoxylanosterol at the concentrations indicated. n = 4 wells per condition. *P = 0.0286; Mann-Whitney test in comparison to EtOH. f, Representative images of OPCs treated with lanosterol, 24(*S*),25-epoxylanosterol, and 24(*R*),25-epoxylanosterol at 5.6 μM. Nuclei are labelled with DAPI (blue) and oligodendrocytes are indicated by immunostaining for MBP (green). Scale bar, 100 μm. b, c, d, e are representative of two or more independent experiments.

quence of enzymes used to synthesize cholesterol (See fig. 3.2a). (146) Typically, epoxycholesterol synthesis is roughly one percent of cholesterol biosynthesis, and no other cellular route to epoxycholesterol is known. (18) We confirmed that exogenously supplied 24(*S*), 25-epoxylanosterol fluxed over 24 hours to epoxycholesterol in OPCs (See fig. 3.2b) and that inhibition of EBP or sterol 14-reductase prevented this flux (See fig. 3.2c). Interestingly, the unnatural diastereomer 24(*R*),25-epoxylanosterol also gave rise to lower amounts of an epoxycholesterol product (See fig. 3.2b). The flux of epoxylanosterol to epoxycholesterol suggested that the oligodendrocyte-enhancing effects of epoxylanosterol may in part be mediated by epoxycholesterol. To assess this possibility, we synthesized 24(*R*) and 24(*S*),25-epoxycholesterol and evaluated their effects on OPC differentiation. Both epimers of epoxycholesterol led to enhanced oligodendrocyte formation without inhibiting CYP51, sterol 14-reductase, or EBP (See fig. 3.2d-e, fig. 3.6a). Two additional synthetic sterols containing the 24,25-epoxide functionality also promoted oligodendrocyte formation (See fig. 3.6b) without inhibiting cholesterol pathway enzymes (See fig. 3.6c), suggesting that the 24,25-epoxide is a new structural feature shared among several oligodendrocyte-formation-enhancing sterols. This result marked the first instance in which sterols lacking the 8,9-unsaturation promoted oligodendrocyte formation and demonstrates that sterol signaling axes beyond inhibition of CYP51, sterol 14-reductase, and EBP can enhance the OPC differentiation process.

3.2.3 Genetic and biochemical manipulations favoring epoxycholesterol synthesis promote oligodendrocyte formation

Given that exogenously-supplied 24,25-epoxycholesterol promoted oligodendrocyte formation, we wondered if increasing the levels of endogenous 24,25-epoxycholesterol would also cause enhanced oligodendrocyte formation. To evaluate this possibility, we used two complementary genetic approaches to enhance the production of epoxycholesterol in OPCs. First, we suppressed LSS enzymatic function in OPCs. Past work demonstrated that partial inhibition of LSS leads to increased flux through the epoxycholesterol shunt, and increased epoxycholesterol levels (See fig. 3.2a). (12, 18, 40, 100, 140, 160, 162) By contrast, complete inhibition of LSS prevents the synthesis of all sterols. To suppress LSS function, we established a line of OPCs stably expressing Cas9 and used electroporation to deliver synthetic CRISPR guide RNAs targeting LSS. After electroporation, we cultured OPCs for 48, 72, or 96 hours prior to inducing their differentiation. This approach enabled us to empirically determine time points at which partial LSS inhibition leads to enhanced oligodendrocyte formation (See fig. 3.3a). In two independent experiments, LSS suppression led to enhanced formation of mature oligodendrocytes after culturing for either 72 or 96 hours prior to measuring the percentage of MBP+ oligodendrocytes (See fig. 3.3b-c, fig. 3.6d). Critically,

these time points also showed clear elevation of epoxycholesterol levels and a 45-65$\%$ reduction in LSS transcript levels (See fig. 3.3d-e).

As a contrasting genetic manipulation to increase epoxycholesterol synthesis, we overexpressed squalene epoxidase (SQLE) in OPCs to favor the production of diepoxysqualene and thus epoxycholesterol (See fig. 3.2a).20 OPCs expressing Myc-tagged SQLE gave rise to more mature oligodendrocytes within the Myc+ population than OPCs expressing Myc-tagged GFP (See fig. 3.3f). Together, these genetic manipulations targeting LSS and SQLE demonstrate that increasing flux through the epoxycholesterol pathway enhances oligodendrocyte formation.

As a biochemical approach to increase flux through the epoxycholesterol pathway, we treated OPCs with dioxidosqualene, the first committed metabolite in the epoxycholesterol biosynthesis pathway (See fig. 3.2a). At non-toxic concentrations of dioxidosqualene, we observed dose-responsive increases in oligodendrocyte formation (See fig. 3.3h, fig. 3.6e). Importantly, 24,25-epoxycholesterol levels were elevated following dioxidosqualene treatment at 1.2 μM, the maximally effective dose for enhancing oligodendrocyte formation (See fig. 3.3i, fig. 3.6f). Overall, these genetic and metabolite supplementation experiments demonstrate that increasing flux through the epoxycholesterol biosynthesis pathway enhances oligodendrocyte formation.

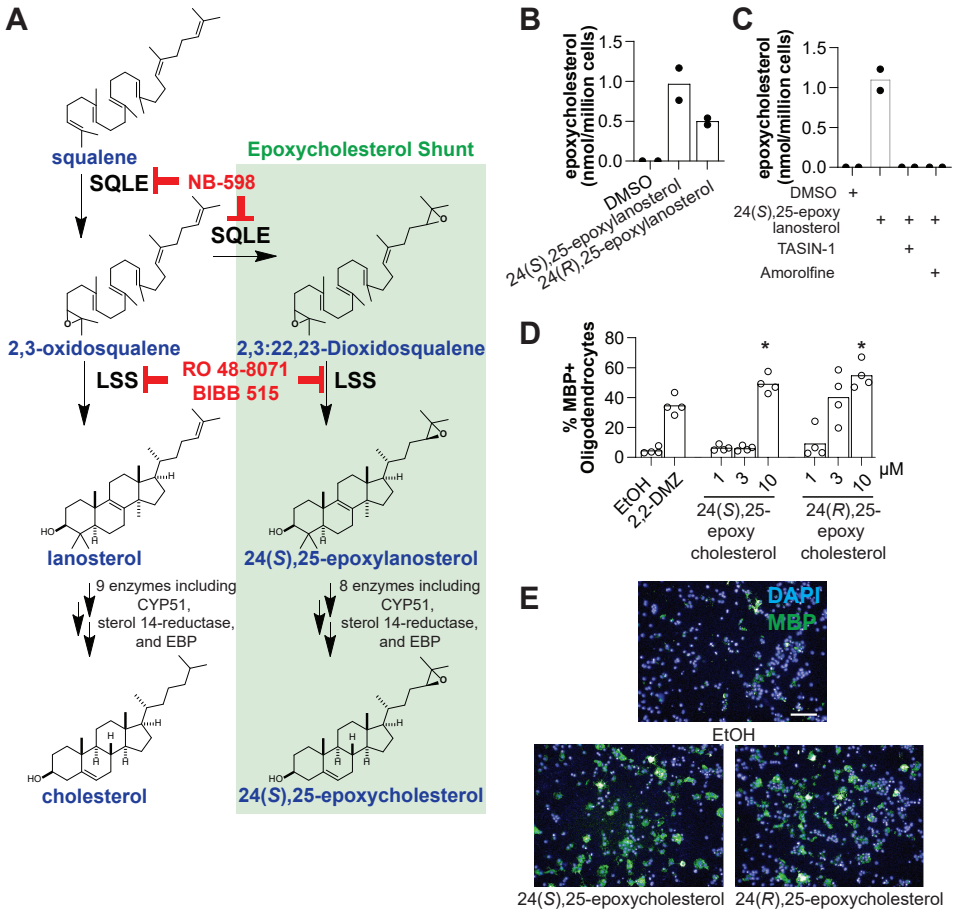

Figure 3.2: Epoxycholesterol promotes oligodendrocyte formation. - a, Schematic of the post-squalene cholesterol biosynthesis pathway. Ro 48-8071 and BIBB 515 are LSS inhibitors. NB-598 is an SQLE inhibitor. b, GC-MS based quantification of epoxycholesterol in OPCs 24 hours after treatment with 24(*S*),25-epoxylanosterol and 24(*R*),25-epoxylanosterol (10 μM each). n = 2 wells per condition. c, GC-MS based quantification of epoxycholesterol in OPCs 24 hours after treatment with 24(*S*),25-epoxylanosterol (10 μM) alone or in combination with TASIN-1 (10 μM), a selective EBP inhibitor, or Amorolfine (5 μM), a sterol-14 reductase inhibiting positive control. d, Percentage of MBP+ oligodendrocytes 72 hours after treatment with 24(*S*),25-epoxycholesterol, and 24(*R*),25-epoxycholesterol at the concentrations indicated. n = 4 wells per condition. 2,2-DMZ, an 8,9-unsaturated sterol positive control, 10 μM. *P = 0.0286; Mann-Whitney test. d, Representative images of OPCs treated with 24(*S*),25-epoxycholesterol, and 24(*R*),25-epoxycholesterol at 10 μM. Nuclei are labelled with DAPI (blue) and oligodendrocytes are indicated by immunostaining for MBP (green). Scale bar, 100 μm. b, d are representative of two or more independent experiments.

3.2.4 Small-molecule inhibition of LSS increases epoxycholesterol levels and enhances oligodendrocyte formation

To achieve more granular control over the extent of LSS inhibition, we next turned to small-molecule inhibitors of LSS. We began by characterizing two previously-reported potent and selective LSS inhibitors, Ro 48-8071 and BIBB 515 (See fig. 3.2a). (34, 42, 94) Evaluation of these inhibitors across a wide concentration range using both LC-MS and GC-MS methods revealed increases in epoxycholesterol that followed a bell-shaped dose-response pattern, with maximal elevation of epoxycholesterol from 5 to 50 nM (See fig. 3.4a-c). Both the potency and the bell-shaped dose-response pattern, which results from high inhibitor concentrations that inhibit LSS fully and prevent synthesis of all sterols, are closely aligned with past reports. (12, 18, 40, 100, 140, 160, 162) Critically, for both LSS inhibitors, increases in oligodendrocyte formation closely mirrored effects on epoxycholesterol levels, including the unusual bell-shaped dose-response pattern (See fig. 3.4a-c, fig. 3.7a). At higher concentrations at which epoxycholesterol levels decrease, dose-responsive increases in the epoxysqualene substrate of LSS were also observed, likely indicating near-complete inhibition of LSS (See fig. 3.7b). As a specificity control, we also evaluated NB-598, an inhibitor of squalene epoxidase (SQLE). (125) SQLE lies immediately upstream of LSS

and was not characterized in our earlier evaluation of cholesterol pathway inhibitors (See fig. 3.2a). (72) While we confirmed that NB-598 led to elevated levels of its substrate squalene in OPCs, no positive effect was seen on oligodendrocyte formation (See fig. 3.7g-j). These results highlight LSS as a unique pivot point in cholesterol biosynthesis whose partial inhibition can shift pathway flux toward epoxycholesterol and drive oligodendrocyte formation.

Since inhibition of late cholesterol pathway enzymes is a surprisingly common off-target cellular activity of many known bioactive small molecules, we wondered whether LSS inhibition could underlie any other small molecules' oligodendrocyte-enhancing abilities. (81) In a dose-responsive evaluation of several selective inhibitors of the M1 muscarinic receptor, a target previously implicated in driving oligodendrocyte formation,11 we noted that VU 025503533 uniquely enhanced oligodendrocyte formation (See fig. 3.4d, fig. 3.7c). However, increased formation of oligodendrocytes occurred only at concentrations more than 10-fold higher than its reported cellular EC50 for the M1 receptor, suggesting a potential off-target effect in OPCs. (52) While no accumulation of 8,9-unsaturated sterols was observed following treatment of OPCs with VU 0255035, we noted that VU 0255035 bore significant structural similarity to 4-piperazinopyridine-containing potent and selective LSS inhibitors (See fig. 3.7j). (19, 20, 137) Sterol profiling revealed that VU 0255035 indeed induced the accumulation of epoxycholesterol in

OPCs, and concentrations of VU 0255035 that maximized epoxycholesterol levels also maximized oligodendrocyte formation (See fig. 3.4e, See fig. 3.7d). Subsequent studies identified three additional bioactive small molecules that inhibit LSS in OPCs as an off-target effect, leading to epoxycholesterol accumulation and enhanced formation of oligodendrocytes: AGI-6780, fenhexamid, and ciproxifan (See fig. 3.7e-f,j). Together these genetic and chemical-genetic studies support LSS as a fourth enzyme within the cholesterol biosynthesis pathway whose inhibition enhances oligodendrocyte formation.

3.2.5 24,25-epoxysterols and 8,9-unsaturated sterols are independent classes of pro-differentiation sterols

Given the interdependent nature of the cholesterol and epoxycholesterol biosynthesis pathways, 8,9-unsaturated sterol accumulation could potentially alter 24,25-epoxycholesterol levels and vice versa. To evaluate this possibility, we assessed whether treating OPCs with purified 8,9-unsaturated sterols or inhibitors of CYP51, sterol 14-reductase, or EBP might induce accumulation of epoxycholesterol. Neither the unnatural 8,9-unsaturated sterol 2,2-dimethylzymosterol or a variety of enzyme inhibitors led to elevated levels of epoxycholesterol as measured by both GC-MS and LC-MS methods (See fig. 3.8a-b). Together with our previous observation that 24,25-

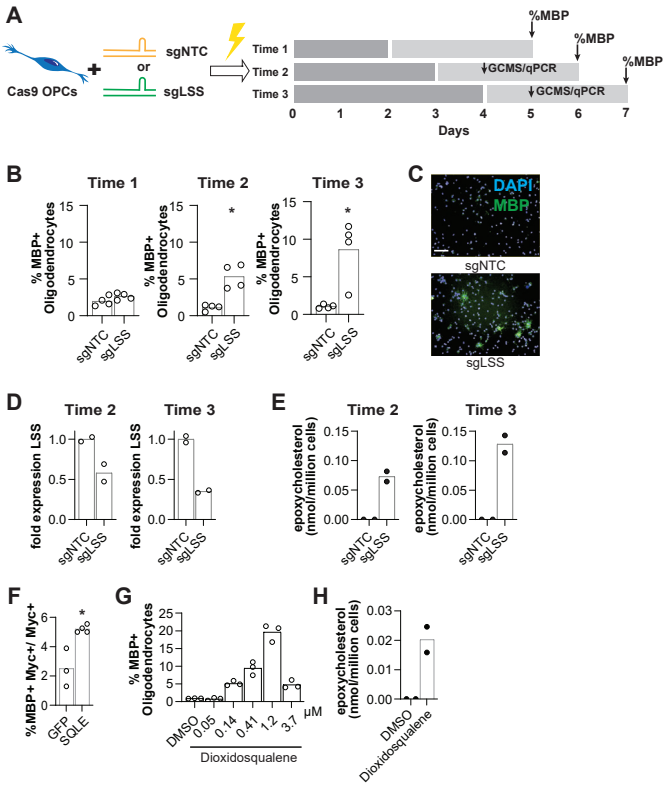

Figure 3.3: Increasing flux toward epoxycholesterol promotes oligodendrocyte formation. - a, Schematic demonstrating the experimental setup for CRISPR mediated LSS depletion. b, Percentage of MBP+ oligodendrocytes from Cas9-expressing OPCs electroporated with CRISPR guideRNA targeting LSS. OPCs were cultured for 48, 72, or 96 hours respectively prior to replating in differentiation media. MBP+ oligodendrocyte formation was then assessed after 72 hours. n = 4 wells per condition. *P = 0.0286; Mann-Whitney test. c, Representative images of the Time 3 condition. Nuclei are labelled with DAPI (blue) and oligodendrocytes are indicated by immunostaining for MBP (green). Scale bar, 100 μm. d, Fold-change in gene expression of LSS in OPCs transfected with sgRNA targeting LSS. Cells were cultured for 72 or 96 h following electroporation, replated in differentiation media, and analyzed 24 hours after replating. n = 2 wells per condition per condition. e, GC-MS based quantitation of epoxycholesterol in OPCs transfected with sgRNA targeting LSS 24 hours after growth factor withdrawal for the indicated timepoints. n = 2 wells per condition. f, Percentage of MBP+ oligodendrocytes among Myc+ cells 72 hours after OPCs were transfected with either a Myc-tagged SQLE or Myc-tagged GFP ORF. n = 3-4 replicates each comprising >2,000 cells. *P = 0.0286; Mann-Whitney test. g, Percentage of MBP+ oligodendrocytes 72 hours after treatment with dioxidosqualene at the concentrations indicated. n = 3 wells per condition. h, GC-MS based quantification of epoxycholesterol in OPCs 24 hours after treatment with dioxidosqualene at 1.22 μM. n = 2 well per condition. b, e, f, g are representative of two independent experiments.

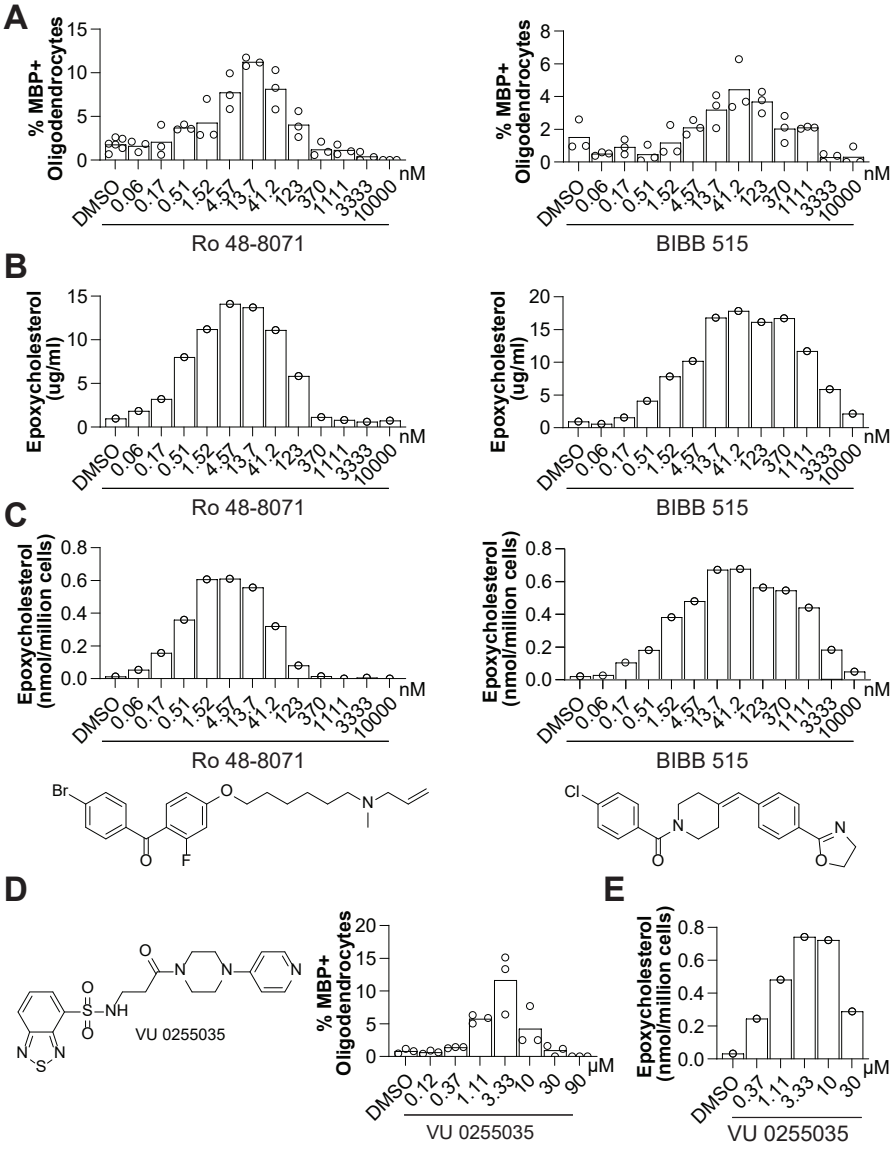

Figure 3.4: LSS-inhibiting small molecules promote oligodendrocyte formation. - a, Percentage of MBP+ oligodendrocytes 72 hours after treatment with Ro 48-8071 or BIBB 515 at the concentrations indicated. n = 3 wells per condition. b, LC-MS based quantification of epoxycholesterol in OPCs 24 hours after treatment with Ro 48-8071 or BIBB 515 at the concentrations indicated. n = 1 well per condition. c, GC-MS based quantification of epoxycholesterol in OPCs 24 hours after treatment with Ro 48-8071 or BIBB 515 at the concentrations indicated. n = 1 well per condition. d, Percentage of MBP+ oligodendrocytes 72 hours after treatment with VU 0255035 at the concentrations indicated. n = 3 wells per condition. e, LC-MS based quantification of epoxycholesterol in OPCs 24 hours after treatment with VU 0255035 at the concentrations indicated, as measured by GC-MS. n = 1 well per condition. a, b, d are representative of two or more independent experiments.

epoxycholesterol does not induce 8,9-unsaturated sterol accumulation (See fig. 3.6a), these data indicate that accumulation of 8,9-unsaturated sterols or 24,25-epoxycholesterol represent independent sterol structural series that both promote oligodendrocyte formation.

3.2.6 Modulation of LXR does not enhance oligodendrocyte formation

Finally, we examined whether epoxycholesterol's known cellular binding partners mediate its effects on oligodendrocyte formation. As epoxycholesterol has been widely studied as an agonist of the LXR nuclear receptors, we began by evaluating a panel of four LXR agonists and antagonists.38 Notably, neither the agonists nor antagonists were capable of driving enhanced oligodendrocyte formation (See fig. 3.8c). Naturally-occurring oxysterols have also been described as LXR modulators. (119) We evaluated a panel of six oxysterols in our OPC differentiation assay and noted some, but not all, showed modest increases in oligodendrocyte formation (See fig. 3.8d). Importantly, LXR agonists and antagonists increased and decreased, respectively, the activity of a luciferase-based LXR reporter construct in OPCs, indicating that increasing or decreasing LXR transcriptional activity in OPCs has little effect on their differentiation to oligodendrocytes (See fig. 3.8e). These results, along with our previously published LXR profiling experiments, sug-

gest that LXR is unlikely to be involved the signaling downstream of either 24,25-epoxycholesterol or 8,9-unsaturated sterols. (72)

3.3 Discussion

Our previous work showed that most small-molecule enhancers of oligodendrocyte formation increase 8,9-unsaturated sterol levels in OPCs to enhance remyelination *in vitro* and *in vivo*. (3, 72) However, beyond the 8,9-unsaturation, the sterol structural features associated with enhanced oligodendrocyte formation were unexplored. In this work, we describe 24,25-epoxylanosterol, 24,25-epoxycholesterol, and related epoxysterols as promoting oligodendrocyte formation. Both epoxylanosterol and epoxycholesterol are synthesized endogenously in OPCs via the epoxycholesterol shunt pathway. Diverse small-molecule, biochemical, and genetic approaches that increase flux through the epoxycholesterol shunt lead to elevated 24,25-epoxycholesterol levels and promote oligodendrocyte formation. Notably, 24,25-epoxycholesterol is one of several sterols identified here that lack an 8,9-unsaturation yet enhance oligodendrocyte formation, indicating that a broader range of sterols than previously recognized can promote oligodendrocyte formation. Remarkably, cholesterol, which only differs from epoxycholesterol by addition of an oxygen atom, does not drive oligodendrocyte formation. Together these observations highlight the 24,25-epoxide as a novel

structural feature of sterols that enhance oligodendrocyte formation and suggest the possibility that additional oxysterols may also influence oligodendrocyte formation.

While purified 8,9-unsaturated precursors to cholesterol face challenges to drug development, including low potency, poor solubility, and rapid metabolism to cholesterol, oxidized derivatives of these sterols may offer greater promise. Oxysterols show improved aqueous solubility and in many cases cross the blood brain barrier. (14) Additionally, epoxylanosterol offers significantly enhanced potency for enhancing oligodendrocyte formation relative to lanosterol. Further optimization of these or other sterol derivatives could yield potent, drug-like molecules that directly enhance remyelination without modulating cholesterol biosynthesis. In oligodendrocytes, 24,25-epoxycholesterol is synthesized endogenously via the epoxycholesterol shunt pathway which runs parallel to the post-squalene cholesterol biosynthesis pathway. The epoxycholesterol shunt typically accounts for less than one percent of cholesterol pathway flux(18) and its contributions to cellular function are arguably underexplored relative to the Bloch and Kandutsch–Russell pathways of cholesterol biosynthesis. However, our work for the first time demonstrates that increasing flux through the epoxycholesterol shunt significantly enhances oligodendrocyte formation. Several genetic and biochemical approaches support this conclusion, including targeting of LSS using CRISPR and supplementation of OPCs with dioxidosqualene. In addition, several oligodendrocyte-

enhancing small molecules partially inhibit LSS to increase 24,25- epoxycholesterol levels. These LSS-inhibiting small molecules represent four distinct structural scaffolds, and their ability to enhance epoxycholesterol correlates closely with their ability to promote oligodendrocyte formation. Overall, numerous genetic and chemical-genetic approaches demonstrate that LSS inhibition leads to enhanced oligodendrocyte formation by increasing flux through the epoxycholesterol shunt.

Some past studies have noted that LSS inhibitors can have neutral or inhibitory effects on oligodendrocyte formation and myelination, albeit at concentrations that may not drive flux through the epoxycholesterol shunt. While we had previously assessed the effects of Ro 48-8071 in OPCs, the concentrations tested did not substantially affect epoxycholesterol levels. (72) Similarly, treating rat primary OPCs with Ro 48-8071 did not lead to enhanced oligodendrocyte formation or myelin gene expression; however, the effects on epoxycholesterol levels at these concentrations was not determined. (98) Previous work in zebrafish correlated LSS inhibitor treatment with decreased myelination, but neither brain nor peripheral epoxycholesterol levels were determined. (101) In summary, while LSS represents a new target for remyelinating small molecules, the bell-shaped concentration-response requires careful titration of LSS inhibition to ensure increased flux through the epoxycholesterol shunt.

This work suggests two novel approaches for advancing future ‘remyeli-

nating therapeutics'. The first is the development of LSS inhibitors. While the blood brain barrier penetrance of existing LSS inhibitors is yet-untested, these molecules frequently show high affinity for LSS and are well poised for further medicinal chemistry optimization. Additionally, serum and brain levels of 24,25-epoxycholesterol represent a ready biomarker of target engagement to guide the optimization of dosing regimens in preclinical models and clinical trials. Second, as discussed above, optimized oxidized sterols may also prove useful therapeutically as modulators of oligodendrocytes formation *in vivo*. Both LSS inhibitors and 24,25-epoxycholesterol or other oxysterol derivatives may represent promising starting points for future development efforts.

Overall, this work highlights 24,25-epoxycholesterol, the epoxycholesterol shunt, and LSS as novel players for promoting oligodendrocyte formation. In addition to an 8,9-unsaturation, a 24,25-epoxide functionality may also contribute to a sterol's ability to drive oligodendrocyte formation. Further, LSS unexpectedly represents a fourth druggable target in the cholesterol biosynthesis pathway whose inhibition promotes oligodendrocyte formation. This work expands upon and strengthens the links between sterol signaling, cholesterol biosynthesis enzymes, and enhanced oligodendrocyte formation.

3.4 Methods

Small molecules/Reagents: The identity and purity of key small molecules were authenticated by LC–MS. The following compounds were purchased from Cayman Chemicals: Ro 48-8071, BIBB 515, 20-hydroxycholesterol, 27-hydroxycholesterol, 22(S)-hydroxycholesterol, 22(R)-hydroxycholesterol, 24-hydroxycholesterol, 25- hydroxycholesterol, T0901317, GW 3965, WAY252623, SR9238. Fenhexamid was purchased from Sigma-Aldrich. VU 0255035 was purchased from Fisher. NB-598 was purchased from MedChemExpress. AGI-6780 was pulled from the L1700 Selleck Library. Ciproxifan was pulled from the LOPAC1280 library. The following standards were purchased from Toronto research chemicals: dioxidosqualene, monoepoxysqualene, squalene. Details pertaining to all controls and GC-MS standards, was reported previously. (72)

Mouse OPC preparation: iPSC-derived OPCs were previously obtained using *in vitro* differentiation protocols and culture conditions 43. OPCs were expanded in the presence of PDGF and FGF and frozen down in aliquots. OPCs were thawed into growth conditions for one passage before use in further assays. Cultures were regularly tested and shown to be mycoplasma free and authenticated on the basis of immunopositivity for OPC markers (Olig2, Sox10) and ability to differentiate to MBP+ oligodendrocytes in the presence of thyroid hormone.

Mouse OPC culture: OPCs were grown and expanded in poly-ornithine (PO) and laminin-coated flasks with growth medium (DMEM/F12 supplemented with N2-MAX (R&D Systems), B-27 (ThermoFisher), GlutaMax (Gibco), FGF2 (10 μg/mL, R&D systems, 233-FB-025) and PDGF-AA (10 μg/mL, R&D systems, 233-AA-050) before harvesting for plating. OPCs *in vitro* phenotypic assay: OPCs were seeded onto 96-well CellCarrierUltra plates (PerkinElmer) coated with poly-D-lysine and laminin (Sigma, L2020; 15 μg/mL) using multi-channel pipet. For the experiment, 40,000 cells were seeded per well. Cells were incubated under standard conditions (37℃, 5% CO2) for 3 days and fixed with 4% paraformaldehyde (PFA) in phosphate buffered saline (PBS) for 20 min. Fixed plates were washed with PBS (100 μL per well) twice, permeabilized with 0.1% Triton X-100 and blocked with 10% donkey serum (v/v) in PBS for 40 min. Then, cells were labelled with an anti-MBP antibody (Abcam, ab7349; 1:200) for 16 h at 4℃ followed by detection with Alexa Fluor conjugated secondary antibodies (1:500) for 45 min. Nuclei were visualized by DAPI staining (Sigma; 1 μg/mL). During washing steps, PBS was added using a multi-channel pipet and aspiration was performed using Biotek EL406 washer dispenser (Biotek) equipped with a 96-well aspiration manifold.

High-content imaging and analysis: During hit validation experiments, plates were imaged on the Operetta High Content Imaging and Analysis system (PerkinElmer) and a set of 6 fields captured from each well resulting

in an average of 1,200 cells being scored per well. Analysis (PerkinElmer Harmony and Columbus software) began by identifying live nuclei stained by DAPI; that is, those traced nuclei that were between 55-250 μm2 in area which excludes picnotic nuclei. Each traced nucleus region was then expanded by 50$\%$ and cross-referenced with the mature myelin protein (MBP) stain to identify oligodendrocyte nuclei, and from this the percentage of oligodendrocytes was calculated.

GC/MS-based sterol profiling: EpiSC-derived OPCs were plated at 1 million cells per mL in PDL- and laminin-coated six well plates with differentiation media. After 24 h, cells rinsed with PBS, and frozen. For sterol analyses, cells were lysed in hexane (Sigma-Aldrich) for 10 min. Cholesterol-d7 standard (25,26,26,26,27,27,27-2H7-cholesterol, Cambridge Isotope Laboratories) was added before drying under nitrogen stream and derivatization with 55 μL of bis(trimethylsilyl) trifluoroacetamide/ trimethylchlorosilane to form trimethylsilyl derivatives. Following derivatization at 60 ℃ for 20 min, 2 μL was analyzed by gas chromatography/mass spectrometry using an Agilent 5973 Network Mass Selective Detector equipped with a 6890 gas chromatograph system and a HP-5MS capillary column (60 m x 0.25 mm x 0.25 μm). Samples were injected in splitless mode and analyzed using electron impact ionization. Ion fragment peaks were integrated to calculate sterol abundance, and quantitation was relative to cholesterol-d7. The following m/z ion fragments were used to quantitate each metabolite: cholesterol-d7

(465), cholesterol (368), zymostenol (458), zymosterol (456), desmosterol (456, 343), lanosterol (393), lathosterol (458), 14-dehydrozymostenol (456), epoxycholesterol (382), epoxylanosterol (409). Calibration curves were generated by injecting varying concentrations of sterol standards and maintaining a fixed amount of cholesterol-D7.

LC/MS-based epoxycholesterol measurements: OPCs were plated at 1 million cells per mL in PDL- and laminin-coated six well plates with differentiation media. After 24 h, cells rinsed with PBS, and frozen. Cells were lysed in hexane (Sigma-Aldrich) for 10 min. Cholesterol-d7 standard (25,26,26,26,27,27,27-2H7-cholesterol, Cambridge Isotope Laboratories) and 1 mL of saline were added to the well and transferred to a glass vial. This was vortexed and the top layer isolated and dried in a new glass vial. Picolinate derivatization, chromatographic separation, and mass spectrometric detection were performed as reported previously. (70) A Linear Ion Trap Quadrupole LC/MS/MS Mass Spectrometer (AB Sciex Instruments, Model #: 1022643-C) equipped with a Kinetex Phenylhexyl HPLC column (Phenomenex, Inc., 2.6 μm, 50 x 2 mm) was used for detection with mobile phase A being water and 0.1% formic acid and mobile phase B being acetonitirile with 0.07% formic acid. Peaks from selective reaction monitoring were integrated to calculate sterol abundance, and quantitation was relative to cholesterol-d7.

CRISPR LSS experiment: Cas9 containing OPCs were generated using

the previous described lentivirus protocol. (85) Hek293T cells were transfected using Lenti-x shots as per the manufacturer's protocol (Clontech). After 4 h, the media was changed to OPC media for collection of virus. 48 h later the media was collected, supplemented with FGF, PDGF, and protamine sulfate (Sigma, 8 μg/mL), and used to transduce OPCs. 24 h later the media was changed to non-virus containing media for 48 h. Cells underwent two 48 h stretches of puromycin selection (Invitrogen). Cells were allowed to recover for several passages prior to being aliquoted and frozen down. Cells were thawed one passage prior to electroporation. crRNA and tracrRNA were purchased from Dharmacon (NTC and LSS) and electroporated into OPCs using the Basic Nucleofector Kit for Primary Mammalian Glial Cells and Nucleofector 2b Device by following standard manufacturer's protocol. Cells were allowed to recover for 48-96 hours in growth media prior to being plated for GC-MS, differentiation experiments, and qPCR.

SQLE overexpression: Myc tagged GFP and Myc tagged SQLE constructs were purchased from Origene and 1ug of DNA was delivered to OPCs using the Basic Nucleofector Kit for Primary Mammalian Glial Cells and Nucleofector 2b Device by following standard manufacturer's protocol.

LXR Luciferase Assay: The ABCA1 promoter luciferase reporter was purchased from Addgene (Plasmid #86442). 1 ug of DNA was delivered to OPCs using the Nucleofector Kit for Primary Mammalian Glial Cells and the Nucleofector 2b Device by following standard manufacturer's protocol.

Transformed OPCs were seeded at 50,000 cells per well on 96-well CellCarrierUltra plates (PerkinElmer) coated with poly-D-lysine and laminin (Sigma, L2020; 15 μg/mL) using multi-channel pipet and treated with small molecules. Cells were incubated under standard conditions (37℃, 5$\%$ CO2) for 2 days. Cells were lysed using the Bright-Glo luciferase assay system (Promega, E2620) and were analyzed using a Synergy Neo2 High Performance plate reader.

3.5 Supplement

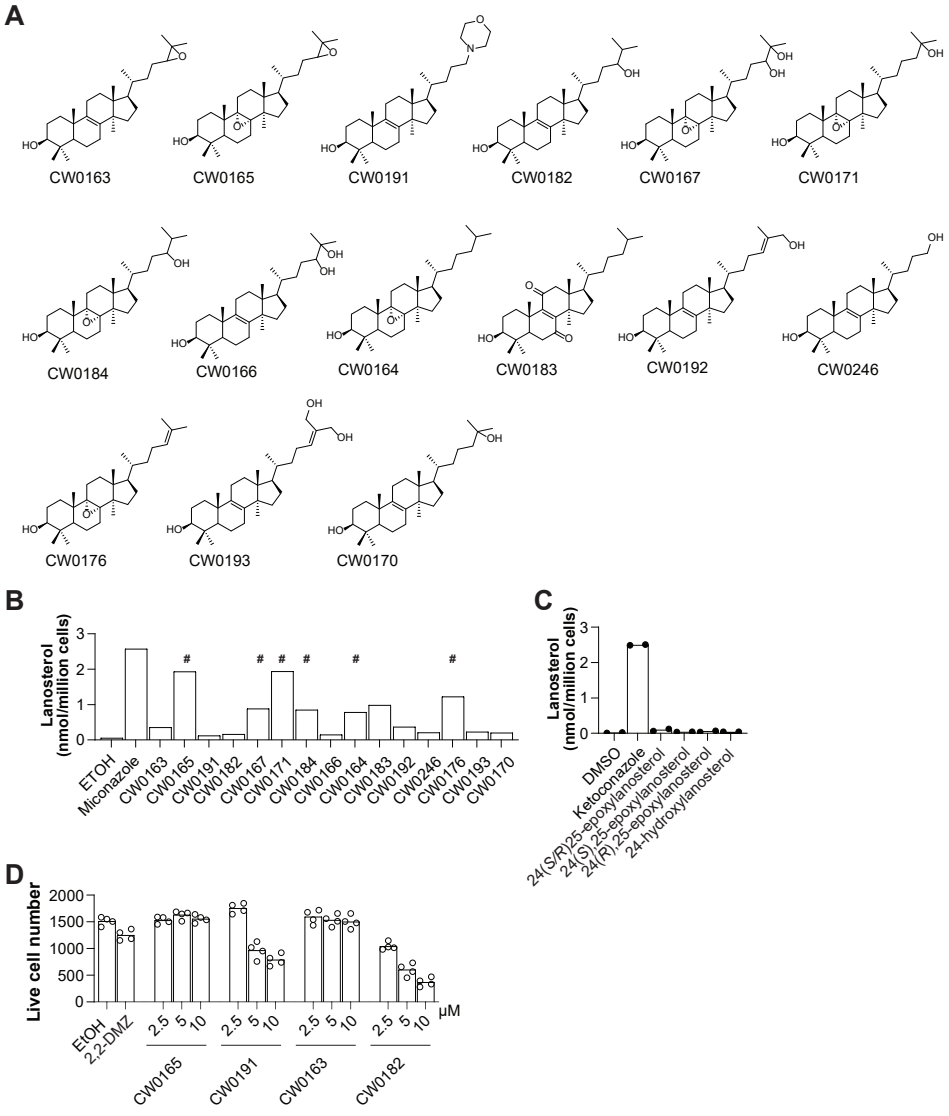

Figure 3.5: ED 1 - Caption on next page

Supplement for Fig 1. a, Structures of lanosterol variants tested in preliminary structural screen. b, GC-MS based quantification of lanosterol in OPCs 24 hours after treatment with the lanosterol variants. n = 1 well per condition. # indicates 8,9-epoxysterols. Miconazole, a CYP51-inhibiting positive control, 5 μM. c, GC-MS based quantification of lanosterol in OPCs 24 hours after treatment with indicated sterols at 10 μM. n = 2 wells per condition. Ketoconazole, a CYP51-inhibiting positive control, 2.5 μM. d, Number of live cells 72 hours after treatment with each top four lanosterol variants that promote oligodendrocyte formation at the concentrations indicated. n = 4 wells per condition. 2,2-DMZ, 2.5 μM c, d, are representative of two or more independent experiments.

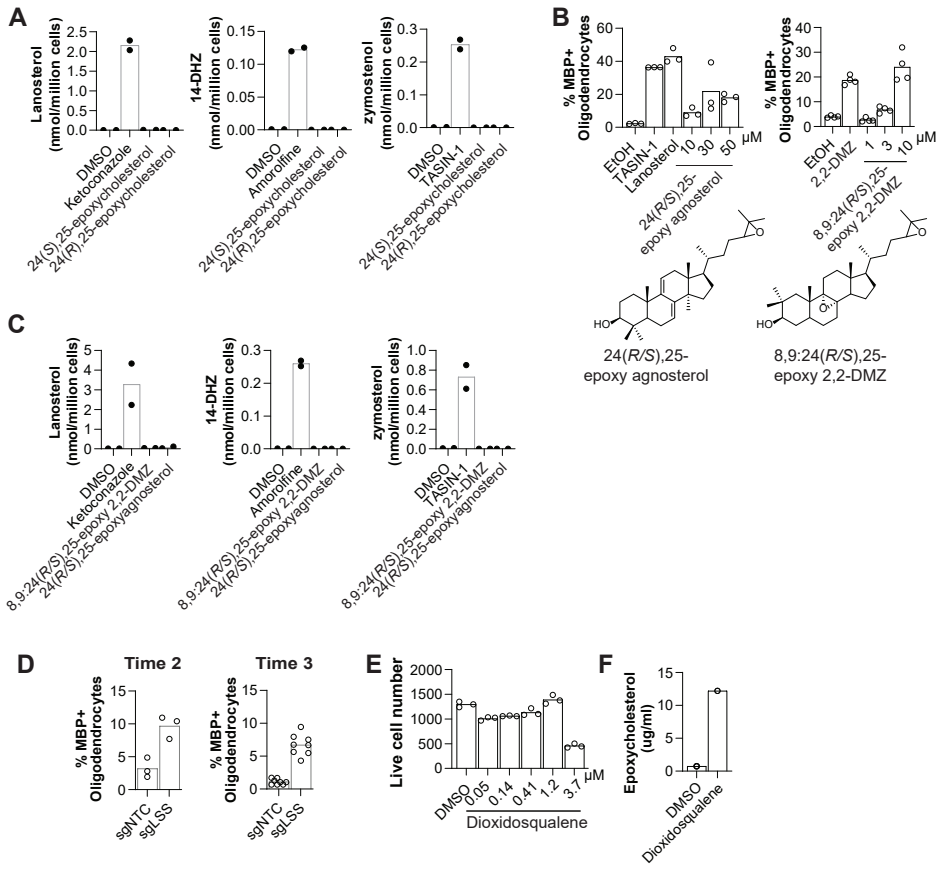

Figure 3.6: ED 2 - Caption on next page

Supplement for Fig 2-3. a, GC-MS based quantification of lanosterol, 14-DHZ, and zymostenol in OPCs 24 hours after treatment with the 24(*S*),25-epoxycholesterol or 24(*R*),25-epoxycholesterol to evaluate inhibition of CYP51, sterol-14 reductase, and EBP. n = 2 wells per condition. Ketoconazole, 2.5 μM. Amorolfine, a sterol-14 reductase inhibiting positive control, 0.6 μM. TASIN-1, 1 μM. b, Percentage of MBP+ oligodendrocytes 72 hours after treatment with 24,25-epoxide-containing sterols at the indicated concentrations. n = 3-4 wells per condition. TASIN-1, 1 μM. Lanosterol, 30 μM. 2,2-DMZ, 10 μM. c, GC-MS based quantification of lanosterol, 14-DHZ, and zymostenol in OPCs 24 hours after treatment with 8,9:24,25(*R/S*)-epoxy 2,2-DMZ at 10 μM, 24,25(*R/S*)-epoxyagnosterol at 50 μM. Ketoconazole, 2.5 μM. Amorolfine, 0.6 μM. TASIN-1, 1 μM. d, Independent experiment measuring percentage of MBP+ oligodendrocytes from Cas9-expressing OPCs electroporated with CRISPR guideRNA targeting LSS. OPCs were cultured for 72 (Time 2) or 96 hours (Time 3) prior to replating in differentiation media. MBP+ oligodendrocyte formation was then assessed after 72 hours. n = 3-6 wells per condition. e, Number of live cells 72 hours after treatment with dioxidosqualene at the concentrations indicated. n = 3 wells per condition. f, LC-MS based quantification of epoxycholesterol in OPCs 24 hours after treatment with dioxidosqualene at 1.2 μM. n = 1 well per condition. a, b, c, e are representative of two or more independent experiments.

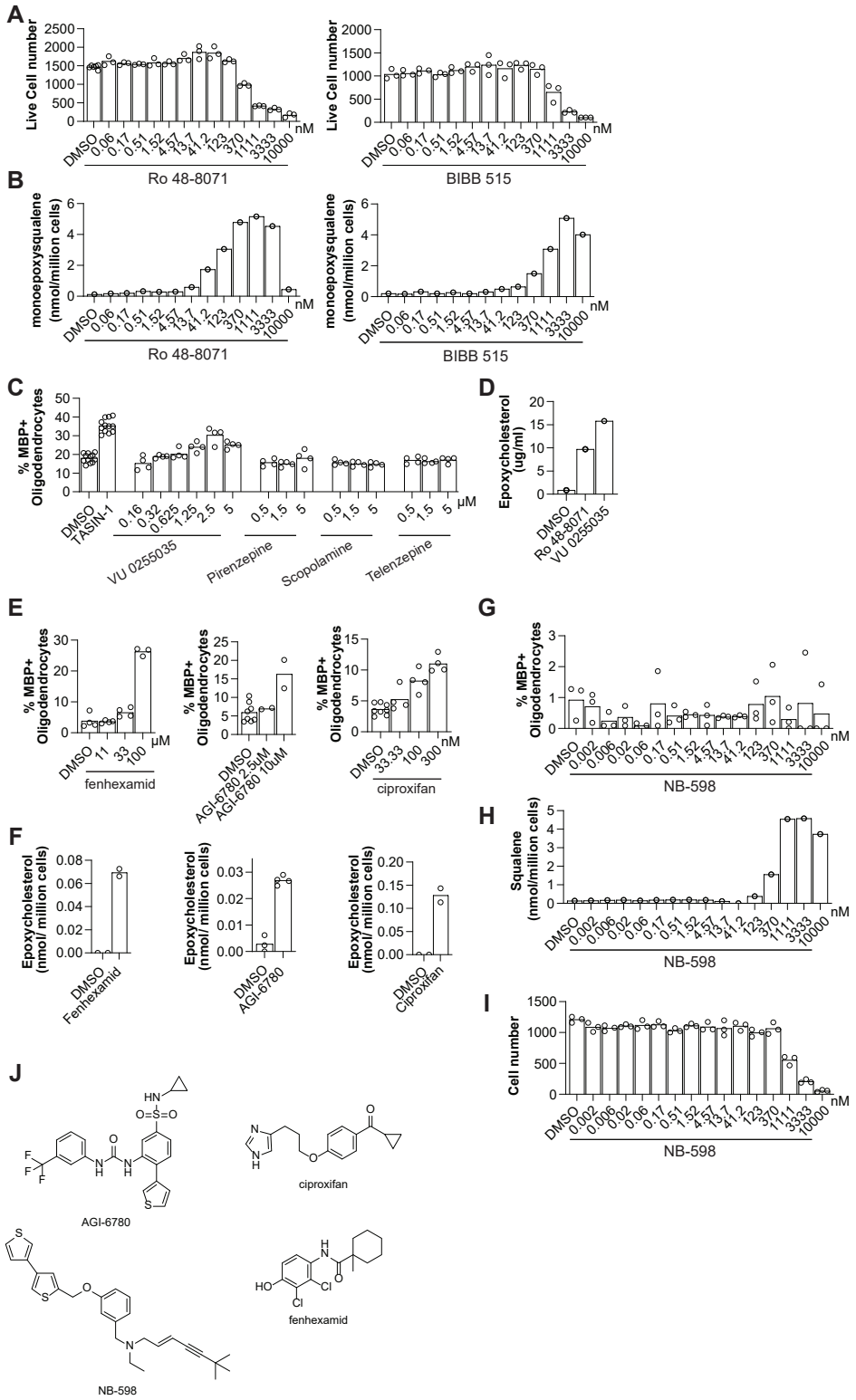

Figure 3.7: ED 3 - Caption on next page

Supplement for Fig 4. a, Live cell number 72 hours after treatment with Ro 48-8071 or BIBB 515 at the concentrations indicated. n = 3 wells per condition. b, GC-MS based quantification of levels of monoepoxysqualene in OPCs 24 hours after treatment with Ro 48-8071 or BIBB 515 at the concentrations indicated. n = 1 well per condition. c, Percentage of MBP+ oligodendrocytes 72 hours after treatment with various muscarinic receptor modulators at the concentrations indicated. n = 3 wells per condition. TASIN-1 is 0.1 μM. d, LC-MS based quantification of epoxycholesterol in OPCs 24 hours after treatment with VU 0255035 at 2.5 μM and Ro 48-8071 at 13.7 nM. n = 1 well per condition. e, Percentage of MBP+ oligodendrocytes after 72 hours after treatment with indicated small molecules at concentrations indicated. AGI-6780 is an isocitrate dehydrogenase inhibitor that was near the hit threshold in our published screen. (72) Fenhexamid was profiled because it has been described as an inhibitor of the yeast homolog of the cholesterol biosynthesis enzyme HSD17B7. (36) Ciproxifan is a histamine H3 antagonist identified in the course of additional screening efforts. n = 2-8 wells per condition. f, GC-MS based quantification of levels of epoxycholesterol in OPCs after 24 hours treated with the indicated small molecules at the indicated concentrations. n = 2-4 wells per condition. g, Percentage of MBP+ oligodendrocytes after 72 hours of treatment with NB-598 at the concentrations indicated. n = 3 wells per condition. h, GC-MS based quantification of squalene in OPCs 24 hours after treatment with NB-598 at the concentrations indicated. n = 1 well per condition. i, Live cell number after 72 hours of treatment with NB-598 at the concentrations indicated. n = 3 wells per condition. j, Structures of AGI-6780, ciproxifan, NB-598, and fenhexamid. a, e, f, g, I are representative of two or more independent experiments.

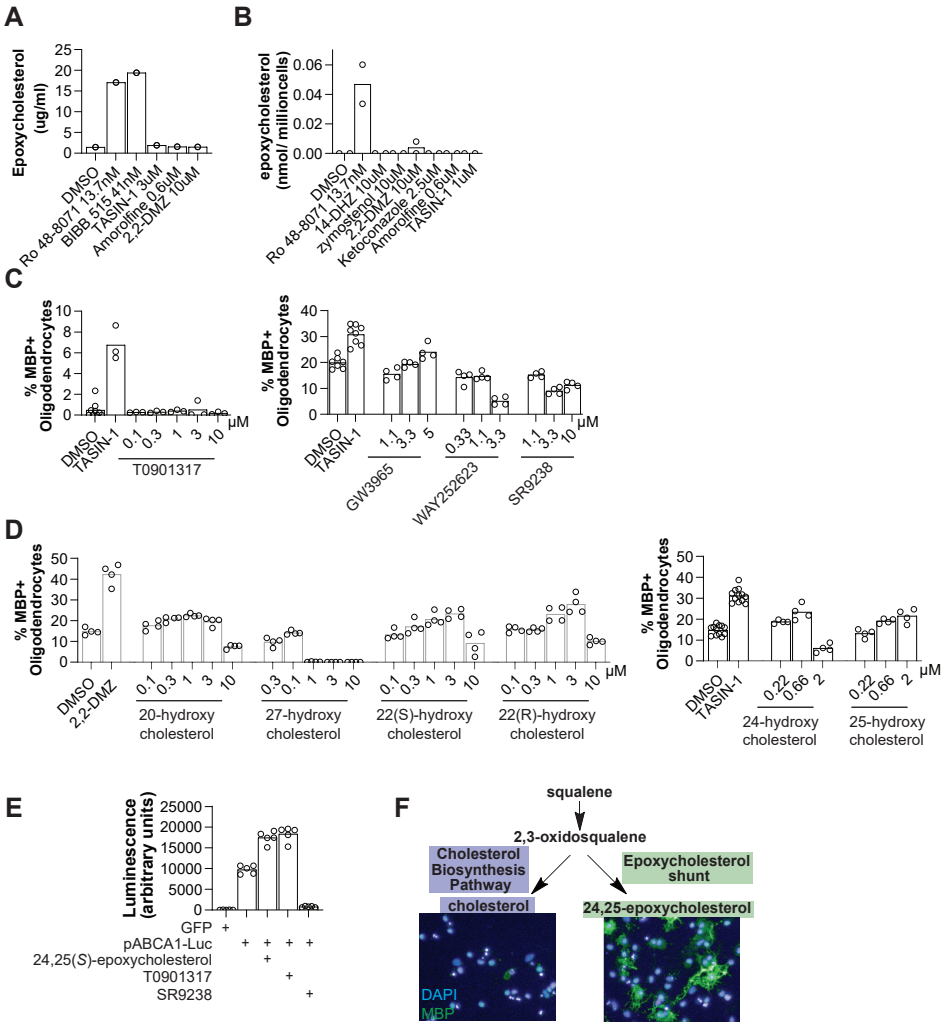

Figure 3.8: ED 4 - Caption on next page

24,25-epoxide is an independent structural feature of oligodendrocyte-enhancing sterols and LXR is unlikely to mediate their effects. a, LC-MS based quantification of epoxycholesterol in OPCs 24 hours after treatment with compounds at concentrations indicated. n = 1 well per condition. b, GC-MS based quantification of epoxycholesterol in OPCs 24 hours after treatment with compounds at concentrations indicated. n = 2 wells per condition. c, Percentage of MBP+ oligodendrocytes after 72 hours of treatment with LXR modulators at concentrations indicated. TASIN-1 at 1 μM. n = 3-4 wells per condition. d, Percentage of MBP+ oligodendrocytes after 72 hours of treatment with oxysterols at concentrations indicated. 2,2-DMZ at 2.5 μM and TASIN-1 at 1 μM. n $\geq$ 4 wells per condition. e, Effects of epoxycholesterol (10 μM) and other LXR modulators (T0901317 3 μM, SR9238 10 μM) on the activation of an ABCA1 promoter-driven luciferase reporter. n = 5 wells per condition. f, Summary diagram. Increasing flux through the epoxycholesterol shunt enhances oligodendrocyte formation by increasing 24,25-epoxycholesterol levels. c, d, e are representative of two or more independent experiments.

4

Discussion and future work

4.1 Summary and significance of the current study

Loss of myelin is the defining characteristic and the primary cause of disability in patients with demyelinating disorders, such as those with multiple sclerosis (MS). Myelin is a lipid-rich membrane of oligodendrocyte cells, which wraps neuronal axons and allows for saltatory conduction between neurons. While it is well known that myelin is essential for brain homeostasis, there are no FDA-approved remyelinating therapeutics that could alleviate symptoms caused by myelin loss. In the central nervous system (CNS) of adult mammals, oligodendrocytes arise from oligodendrocyte progenitor cells (OPCs). The ability to generate new oligodendendrocytes capable of remyelinating bare axons makes OPCs a potential target for remyelinating therapies. Therefore, to discover novel therapies for demyelinating disorders, we used chemical-genetic screening to discover small molecules that promote the formation of new oligodendrocytes from OPCs.

Confusingly, the annotated targets of the high-throughput screening hits were either not expressed in OPCs or did not align with known oligodendrocyte biology. Yet generation of potent small-molecules for clinical translation is streamlined immensely when a small-molecules' cellular target is known. Therefore, we set out to understand the mechanism by which the OPC screening hits promote oligodendrocyte formation.

We initially focused on the cholesterol biosynthesis pathway, because miconazole is a screening hit that is known to inhibit this pathway and well-validated to promote remyelination *in vivo*. We then determined that the vast majority of pro-myelinating small molecules identified by screening promote oligodendrocyte formation, not through their canonical targets, but through one of four enzymes in the cholesterol biosynthesis pathway: LSS, CYP51, sterol-14-reductase, or EBP. In several models, genetic and pharmacological inhibition of these enzymes promotes oligodendrocyte formation and myelination. Inhibition of CYP51, sterol-14-reductase, or EBP causes an accumulation of the 8,9-unsaturated sterol substrates of each enzyme. The 8,9-unsaturated sterols are sufficient to drive oligodendrocyte formation and necessary for the effects of the small molecule screening hits. By contrast, *partial* inhibition of LSS drives oligodendroctye formation through a distinct mechanism, increasing flux through the epoxycholesterol shunt pathway and subsequent accumulation of 24,25-epoxycholesterol.

We found that acute inhibition of the post-squalene cholesterol biosyn-

thesis pathway at LSS, CYP51, sterol-14-reductase, or EBP, promotes myelin formation by inducing a 'sterol shift' to either 8,9-unsaturated sterols or 24,25-epoxycholesterol. These findings do not contradict previous work showing inhibition of pre-squalene cholesterol biosynthesis pathway leads to hypomyelination *in vivo*. (143) Inhibition of the pre-squalene cholesterol biosynthesis pathway is likely detrimental to oligodendrocyte formation as it blocks the biosynthesis of all cellular sterols, including 8,9-unsaturated sterols and 24,25-epoxycholesterol. Our findings upend the established dogma that blocking cholesterol biosynthesis at any step is detrimental to oligodendrocyte formation.

Collectively, our results define a unifying sterol-based mechanism of action for most known small molecule enhancers of oligodendrocyte formation. We used *in vitro* and *in vivo* tools to demonstrate that modulating the sterol landscape in OPCs can enhance the formation of oligodendrocytes and point to new therapeutic targets, potent inhibitors for these targets, and metabolite-based biomarkers to accelerate the development of optimal remyelinating therapeutics.

4.2 Inhibition of the post-squalene cholesterol biosynthesis pathway as a therapeutic strategy

Inhibition of the cholesterol biosynthesis pathway is a novel and unifying mechanism for many remyelinating small molecules. In this section, we will discuss concepts related to the clinical translation of these small-molecules. Topics include: most promising targets, reduction of off-target effects, potential challenges to *in vivo* use, and strategies for overcoming these challenges.

4.2.1 EBP is the ideal clinical target for therapeutic translation

While this work describes four pro-myelinating targets (CYP51, Sterol-14-reductase, EBP, and LSS), there is a hierarchy in terms of their clinical translatability. CYP51 is a part of the larger cytochrome p450 family of enzymes that metabolize many different types of drugs in the liver. (92) CYP51 inhibitors are likely to interfere with the metabolism of other medications the patients are taking and therefore are not ideal clinically. LSS is also not an ideal therapeutic target as only partial inhibition of LSS is associated with elevated levels of 24,25-epoxycholesterol; the therapeutic window for drugs

targeting LSS is likely to be narrow. Further, robust inhibition of LSS leads to the accumulation of toxic metabolites epoxysqualene, diepoxysqualene, squalene, and pre-squalene. (119) Sterol-14-reductase activity is shared between two proteins: TM7SF2 and LBR. LBR is a bi-functional protein whose nuclear domain is involved with the organization of DNA on the periphery of the nucleus. (128) It is currently unclear how modulation of LBR's sterol binding domain affects its function in the nucleus. (78) Additionally, in our screening, sterol-14-reductase and LSS are the two enzymes for which we found the least number of drugs, which suggest that they might be more difficult to target therapeutically.

In contrast, there are no reports of EBP's involvement in other cellular functions besides the cholesterol biosynthesis pathway. The vast majority of our screening hits inhibit EBP; this intrinsically high druggability could facilitate the development of potent inhibitors that lack off-target effects. Unlike other metabolites, zymostenol and zymosterol accumulation is not associated with any negative phenotypes. Lastly, EBP is the most validated target *in vivo*; several labs showed that small-molecules that inhibit EBP (such as tamoxifen, clemastine, benztropine, and obazedoxifene) enhance remyelination in almost all leading myelination and remyelination models. (38, 60, 107, 138). Therefore, given the current data, EBP likely represents the best target for clinical translation.

4.2.1.1 Reducing off target effects by counter screening

Unfortunately, the off-target effects of EBP inhibiting small-molecules could hamper their use clinically. The remyelinating small-molecules discovered through drug repurposing screens retain an affinity for their canonical targets (such as the muscarinic receptor, estrogen receptor, or kappa opioid receptor), despite affecting oligodendrocyte formation through inhibition of EBP. Their activity is non-selective; they affect both the cholesterol biosynthesis pathway and their annotated target. This additional cellular activity may lead to unwanted side effects. To identify more selective EBP inhibitors, we screened a library of 10,000 structurally-diverse small-molecules for their ability to enhance oligodendrocyte formation and inhibit the cholesterol biosynthesis pathway. This screen revealed several novel scaffolds that promoted oligodendrocyte formation through inhibition of EBP and lack affinity for the muscarinic receptor, estrogen receptor, and kappa-opioid receptor(3). (See fig. 4.1)

4.2.1.2 Potential EBP inhibitors already in clinical trials

Beyond the small-molecules described in the previous chapters, there are likely more small molecules that function through inhibition of EBP. Instead of exhaustively annotating every possible EBP inhibitor, I suggest we focus on drugs poised for clinical trials as remyelinating therapies. These small molecules could serve as pilot studies for how EBP inhibitors will fare clin-

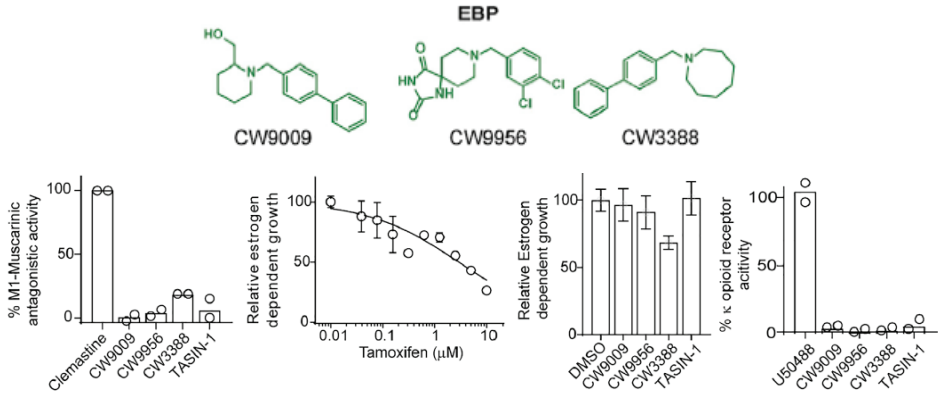

Figure 4.1: Avoid common off-targets of EBP inhibiting small molecules - Top hits from a screen of 10,000 small-molecules which promote oligodendrocyte formation, block EBP, and do not inhibit the annotated targets from the previous screen.

ically and perhaps address some of the challenges I discussed in the previous sections. One example is clemastine, which inhibits EBP to enhance oligodendrocyte formation. In phase II clinical trials, clemastine improved quantitative metrics of myelination in the eye but did not improve patient symptoms. (83)

Three small molecules which are in clinical trials and might be EBP inhibitors are quetiapine, domperidone, and GSK239512. (83) Further, quetiapine modulates cholesterol homeostasis in OPCs, promotes oligodendrocyte formation in an additive manner with T3, and drives phenotypic effects in OPCs identical to those seen with other cholesterol biosynthesis pathway inhibitors. (30) If we establish these as EBP inhibitors, any unexpected issues that arise during their clinical testing could foreshadow issues that novel EBP inhibitors might also have.

4.2.2 Challenges to Clinical translation

4.2.2.1 Contribution of adult OPCs to remyelination

In rodent models, adult OPCs are reproducibly able to differentiate and remyelinate bare axons in a variety of contexts. Despite this, there remains controversy regarding the ability of human adult OPCs to generate new oligodendrocytes and myelin. Transplanted adult humans OPCs can remyelinate rodent axons in *in vivo* models. (159) Studies in postmortem brains of MS patients indicated that there are OPCs in most acute and chronic MS lesions until very late in the disease. (33) Additionally, there is remyelination on the periphery of chronic lesions. (33) In contrast, a recent study found that in MS patients, there is no generation of new oligodendrocytes. (167) Instead, they found that existing oligodendrocytes are generating more myelin for remyelination. (167) This study raises questions regarding whether resident OPCs are capable of generating new oligodendendrocytes in adult humans.

Regardless, even if adult human OPCs do not spontaneously differentiate, remyelinating small-molecules may still stimulate them to generate new oligodendrocytes. The remyelinating small-molecules currently in clinical trials will more directly address if endogenous human OPCs are a viable source of new remyelinating oligodendrocytes. (83)

4.2.2.2 Myelination Block

In MS, there are two phases: relapsing-remitting MS (RRMS) and secondary progressive MS. In RRMS, the neuronal axons are remyelinated, albeit slowly and imperfectly. The sterol-modulating molecules promote remyelination in models of RRMS, such as EAE and cuprizone. In secondary progressive MS, there is a failure to remyelinate; each new immune attack on oligodendrocytes leaves the neuronal axons permanently bare. Interestingly, in most chronic lesions, PLP and MOG staining indicate oligodendrocyte differentiation in the lesioned area, but these oligodendrocytes do not myelinate. (33) It is unclear if sterol-modulating molecules will be able to contribute to the myelination failure seen in secondary progressive MS.

The reason that OPCs fail to remyelinate in chronic lesions is unknown, making it challenging to model. (54, 76, 99) Potential contributory factors include: elevated growth factors, myelin debris, and chronic inflammatory signal. (54) Hypothetically, we could test the sterol-modulating pro-myelinating small-molecules in the context of these inhibitory signals to understand the potential of these drugs in secondary progressive MS. However, given how little we know about what is contributing to the inhibitory milieu *in vivo*, the best test would be to see how the EBP-inhibiting small-molecules fare clinically.

If the EBP inhibitors fail to improve remyelination in the clinic, it may indi-

cate that the cellular and *in vivo* models used do not recapitulate the necessary features of MS pathology. To test if adult human OPCs have an intrinsic ability to form new oligodendrocytes and myelinate, we could isolate OPCs from MS patients in parallel with healthy controls to compare OPCs' intrinsic remyelinating potential in the context of microfibers. This experiment should be feasible: the protocols for isolation of primary human OPCs exist, as do the protocols for culturing iPSC derived human OPCs. (104, 159) Ultimately, studying purified human OPCs could clarify if the myelination block seen in MS is an OPC intrinsic or extrinsic phenomena.

4.2.3 Treatment of genetic disorders affecting cholesterol and myelination

Beyond the treatment of adult-onset demyelinating disorders such as MS, EBP inhibiting small-molecules could be helpful in other disorders affecting myelin. Given the importance of cholesterol in myelin, it is unsurprising that there are genetic disorders that affect cholesterol homeostasis and lead to hypomyelination, such as Smith-Lemli-Optiz syndrome (SLOS) and Niemann-Pick disease type C (NPC). Currently, there are no treatments for the neurological symptoms in either SLOS or NPC.

4.2.3.1 Smith-Lemli-Opitz syndrome

SLOS is an autosomal recessive disorder that is due to mutations in the enzyme DHCR7. SLOS leads to a large number of abnormalities in the development and growth of peripheral organs, musculoskeletal patterning, and neurological abnormalities. (142) In the brain, in addition to delayed myelin maturation, there can be agenesis of the corpus callosum, hypoplastic cerebellum, and lissencephaly. (142) Mice with complete DHCR7 knockout have severe neurological impairments and hypomyelination. (142) Biochemically, this mutation leads to decreased cholesterol levels and an accumulation of four sterol metabolites: 7-DHC, 7-DHD, 8-DHC, and 8-DHD. 7-DHC and 7-DHD are the classical substrates for DHCR7, which EBP isomerizes to 8-DHC and 8-DHD. (142) (fig 1.4) Both the accumulation of the metabolites and the decreased levels of cholesterol contribute to different aspects of the SLOS phenotype (142). Previously, HMGCR inhibitors were tested in SLOS mouse models and found to improve many SLOS phenotypes but failed to improve neurological phenotypes. (142)

Given that current approaches fail to alleviate the neurological symptoms of patients with SLOS, therapeutics in this area are especially needed. High-throughput LC-MS-based screening identified small-molecules that prevent the accumulation of the toxic substrate of DHCR7, 7-DHC. (81, 153) The hits of these screens overlapped with small molecules that enhance oligodendro-

cyte formation through inhibition of CYP51, sterol-14-reductase, and EBP. The overlap in the pro-myelinating screens and the cholesterol biosynthesis screens was one of the first clues that the pro-myelinating drugs might be functioning through inhibition of the cholesterol biosynthesis pathway. However, in terms of SLOS treatment, the inhibitors of CYP51, sterol-14 reductase, and EBP are doubly intriguing: it is possible that inhibiting EBP would not only prevent the accumulation of 7DHC (a toxic metabolite that generates reactive oxygen species), and, simultaneously, promote oligodendrocyte formation. Blocking 7-DHC production may prevent further damage to the CNS while accumulating 8,9-unsaturated sterols could promote oligodendrocyte formation to alleviate the hypomyelination/demyelination phenotype.

4.2.3.2 Niemann-Pick Disease type C

NPC is an autosomal recessive lipid trafficking and storage disorder, which presents clinically with physical deterioration and neurodegeneration. The neurodegeneration is characterized clinically by ataxia and dementia, which mirrors the pathological findings of cerebral and cerebellar atrophy. (142) Notably, there is concurrent hypoplasia of white matter in human patients. (142) The disease is due to mutations in the genes NPC1 and NPC2, which are involved in the export of cholesterol from late endosomes/lysosomes. The most distinctive histological feature of this disorder is foamy deposits of lipids such as sphingomyelin, cholesterol, and gangliosides. (142) In addi-

tion to other symptoms, mice with NPC1 mutations exhibit impaired oligodendrocyte maturation, dysmyelination, and demyelination. (142)

There are currently no therapeutics available that alleviate the neurological symptoms of NPC. While treatment with cyclodextrin, a sterol-depleting molecule, leads to improved outcomes in peripheral symptoms of NPC in mouse models, systemic cyclodextrin failed to improve neurological symptoms clinically (142). However, given the hypomyelination components of NPC, EBP inhibitors may be beneficial to not only block cholesterol synthesis, but also remyelinate the hypomyelinated portions of the patients' brains. Additionally, given that the 8,9-unsaturated sterols can be trafficked via an NPC1/NPC2 independent pathway, shifting the sterol pool away from cholesterol and toward 8,9-unsaturated sterols might prevent the lysosomal cholesterol accumulation. (87, 95, 166) Other researchers have performed a small molecule screen for drugs that promote clearance of cholesterol from lysosomal compartment in patient cell lines. However, this work used filipin (a non-selective sterol dye) and therefore, may not have been sensitive to subtle shifts in sterol pools. (134) Further, the reported screen focused on drugs that promote clearance of cholesterol as opposed to drugs that prevent further cholesterol accumulation. (134) Therefore, an area that might be worth further exploring is the application of EBP inhibitors in Niemann-pick disease type C.

4.3 Relevance to endogenous myelination cues

4.3.1 Plausible role for sterols as pro-differentiation signals in developmental myelination

The role of 8,9-unsaturated sterols, 24,25-epoxycholesterol, and other oxysterols in developmental or *in vivo* OPC differentiation is a topic that remains unexplored. Previous studies of sterols in myelination focused solely on cholesterol. (143) Yet small-molecules that increase 8,9-unsaturated sterols reproducibly accelerate developmental myelination *in vivo*, suggesting that sterols besides cholesterol may play a role in this process. In classic studies of myelination, rising levels of cholesterol and myelination are so tightly correlated that they are considered interchangeable. (31, 65, 136) However, it is possible that, opposed to cholesterol itself being the biomarker that ties to myelination, the pro-differentiation sterols, such as the 8,9-unsaturated sterols or 24,25-epoxycholesterol, could instead be a biomarker of increased flux through the cholesterol biosynthesis that trigger endogenous OPCs to differentiate and initiate myelination.

There are several lines of evidence that support the idea that oligodendrocyte formation-enhancing-sterols may be involved in the endogenous OPC differention and myelination. Firstly, if this hypothesis is true, the levels of the pro-differentiation sterols should rise before the onset of myelination.

While the levels of these sterols have not been measured directly, the peak rate of flux through the cholesterol biosynthesis pathway in mouse brains is in the first five days post-birth, which slightly precedes the onset of detectable MBP protein levels, supporting our hypothesis. (31, 136) Further, as myelin is cholesterol-enriched and deficits in total cholesterol have been linked with delays in myelination, (143) it would make sense for OPCs to have a mechanism of detecting ongoing cholesterol synthesis rates prior to the onset of differentiation. Lastly, cholesterol can not cross the blood-brain barrier; this makes OPCs especially dependent on the rate of local cholesterol synthesis. (1)

Either 8,9-unsaturated sterols or 24,25-epoxycholesterol could be acting as signaling molecules in differentiation as they all promote differentiation *in vitro*. However, of all the known pro-differentiation sterols, the levels of 24,25-epoxycholesterol are the most abundant in newborn mice, suggesting that it is the most likely sterol to act as a readout of local cholesterol biosynthesis and triggering endogenous oligodendrocyte formation. (109)

Preliminary experiments support the idea that 24,25-epoxycholesterol may be involved in endogenous myelination cues. Using *in vitro* experiments, we found that 24,25-epoxycholesterol accumulates during differentiation in parallel with the 8,9-unsaturated sterols and cholesterol, albeit at very low levels. (see fig. 4.2) To determine if the endogenous epoxycholesterol levels affect oligodendrocyte formation, we overexpressed LSS, which leads

to preferential flux through the cholesterol biosynthesis pathway, decreasing 24,25-epoxycholesterol levels. While the overall differentiation percentages are low, the effect is reproducible: overexpressing LSS leads to decreased oligodendrocyte formation, suggesting that the endogenous levels of epoxycholesterol in OPCs could dictate baseline differentiation levels. (see fig. 4.2)

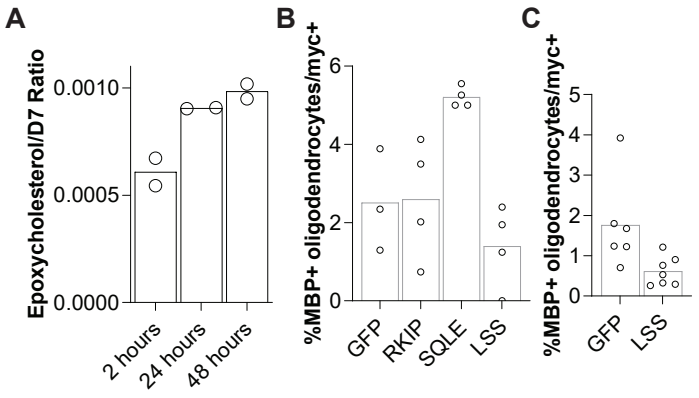

Figure 4.2: Epoxycholesterol in Differentiation - A) Epoxycholesterol increases during differentiation of OPCs to oligodendrocytes. B) %MBP+ oligodendrocytes of myc+ cells with overexpression of myc tagged GFP, RKIP, SQLE, and LSS. RKIP is a unrelated protein control to ensure consistency in the background. C) An independent experiment of (B)

Previous *in vivo* studies showed that blocking the formation of both cholesterol and epoxycholesterol *in vivo* delays myelination dramatically. (143) To interrogate if 24,25-epoxycholesterol is involved in endogenous differentiation and myelination cues *in vivo*, we could use an LSS minigene overexpression construct to drive the formation of cholesterol over epoxycholesterol. While SQLE overexpression would increase 24,25-epoxycholesterol and drive precocious myelination, it may also decrease cholesterol synthe-

sis, which could be a confounding factor. Further work in this area could provide novel insight into the role of sterols in *in vivo* cell fate decision making.

4.3.2 Contribution of Astrocytes

In vitro we use almost pure populations of OPCs in serum-free media, which forces the OPCs to generate cholesterol endogenously. However, it is less clear which cell type generates cholesterol for myelin in the brain. Studies have been published both in support of OPCs synthesizing cholesterol and OPCs acquiring their cholesterol from exogenous sources. (27, 143) Likewise, the origin of the pro-differentiation sterols *in vivo* could be either the OPC themselves or other cells in the brain such as astrocytes. Primary astrocytes, which are known to contribute to OPC sterol pools, secrete epoxycholesterol in parallel with cholesterol. (27, 163) Additionally, media conditioned by astrocytes promotes oligodendrocyte formation *ex-vivo*. (158) In mice where cholesterol homeostasis is perturbed selectively in astrocytes via genetic tools, there is a delay in myelination. (27) These findings suggest that astrocytes could trigger OPCs to differentiate *in vivo* via the following model:

1. Astrocytes increase cholesterol biosynthesis, leading to a rise in pro-differentiation sterols such as 24,25-epoxycholesterol.

2. These pro-differentiation sterols are delivered to OPCs (possibly via vesicles).

3. The pro-differentiation sterols trigger the progression of OPCs to oligodendrocytes, beginning the process of myelination.

The critical experiment to study this hypothesis would be to conditionally overexpress LSS in astrocytes, which would limit their production of epoxycholesterol, and determine if there is a delay in developmental myelination. A control experiment would be to conditionally overexpress LSS in oligodendrocytes and determine what the effects are there. Both genetic modifications would likely delay myelination as the OPCs are likely agnostic to the source of epoxycholesterol. However, I would conjecture that the effect would be more significant with LSS overexpression in astrocytes as astrocytes are known to produce large amounts of cholesterol *in vivo*.

4.4 Potential signaling mechanisms for 8,9- unsaturated sterols

There is increasing evidence that the sterols in the post-squalene cholesterol biosynthesis pathway can act as signaling molecules in a variety of biological contexts. (165) The notion that the various intermediates in this pathway have distinct signaling roles is further supported by the observa-

tion that human diseases relating to each of the enzymes in the cholesterol biosynthesis pathway present with heterogeneous phenotypes. (1) However, the majority of research in this area is highly focused on SREBP and LXR, as they are well-established sterol-interacting partners. Chapters 2 and 3 suggest that SREBP and LXR are not mediating the effects of either the 8,9-unsaturated sterols or 24,25-epoxycholesterol to promote oligodendrocyte formation. Therefore, the actual mechanism by which these sterols act is unclear. To address this question, we have tried several biased and unbiased approaches with limited success. Therefore, we generated new genetic approaches that will streamline future work in this area.

4.4.1 Biased Approaches

This section addresses the mechanism of pro-differentiation sterols by focusing on experiments that evaluate the contribution of pathways known to affect oligodendrocyte formation or established sterol interacting partners. It is not wholly encompassing but instead addresses concepts that have been raised by others in the field, and thus the results might be interesting to a broader audience. None of the ideas have been exhaustively explored, yet each negative result makes that specific mechanism less likely to be the "real" mechanism and moves it down the hypothetical list of possible mechanisms.

4.4.1.1 Hypotheses based on oligodendrocyte literature

There are a dozen hypotheses that are explored in chapters 2 and 3, using a variety of approaches including pathway profiling, luciferase reporters, and small molecules. In the following section, we used the same tools to explore several more. Importantly, hypotheses based on gene targets not expressed in OPCs, according to both RNAseq data from primary OPCs and RNAseq data from our own OPC model, are immediately rejected. (171)

First, we used commercially available reporter cell line profiling to ask if pro-differentiation small molecules are affecting various canonical signalling pathways. (see fig. 4.3) Based on these experiments, we were initially excited about the PI3K/AKT/FOXO3 pathway because in agonist-mode, the pro-differentiation small-molecules were all leading to decreased signaling through this pathway. However, the effect did not retest when the assay was rerun in antagonist mode. (see fig. 4.3)

We also sought to test if our drugs and sterols might be directly interacting with proteins previously described to modulate oligodendrocyte formation. CHRM1 is an annotated target of several pro-differentiation small-molecules and has previously been thought to regulate oligodendrocyte formation. (107) GPR17 is a sterol binding GPCR whose inhibition has been shown to promote oligodendrocyte formation. (90) We used pathway profiling to determine that 8,9-unsaturated sterols do not bind to either of these

targets. (see fig.4.4, 4.5) We also treated OPCs with a GPR17 antagonist called HAMI3379 to determine if modulating GPR17 promotes oligodendrocyte formation in our hands. We tested it alone and in combination with two pro-differentiation small-molecules: Tasin-1 (an EBP inhibitor) or liothyronine (a thyroid hormone analog). HAMI3379 showed no effect on oligodendrocyte formation in any condition. (see fig.4.5) (90)

GPR30 has also been described as being a potential target of pro- differentiation selective estrogen modulators such as Tamoxifen and shown to affect remyelination *in vivo*. (68) G15, a GPR30 antagonist, did not affect oligodendrocyte formation, either alone or in combination with 22-DMZ or Liothyronine. (see fig. 4.6) Decreases in differentiation with G15 were attributable to toxicity at higher concentrations.

Lingo-1 is a cell surface receptor whose inhibition is thought to promote oligodendrocyte formation *in vivo*. (172) We tested a Lingo-1 antibody to see if Lingo-1 was in any way involved in the mechanism of our 8,9-unsaturated sterols but again, saw no effect. (see fig. 4.7)

There has also been some speculation that PLP might be involved in the pro-differentiation phenotype seen with our drugs. Importantly, PLP is known to interact with cholesterol in lipid rafts directly . (157) The levels of cholesterol and PLP are interdependent in oligodendrocytes. (157) To test if PLP was involved in the mechanism of our pro-differentiation small molecules, we tested the pro-differentiation small-molecules in OPCs with a

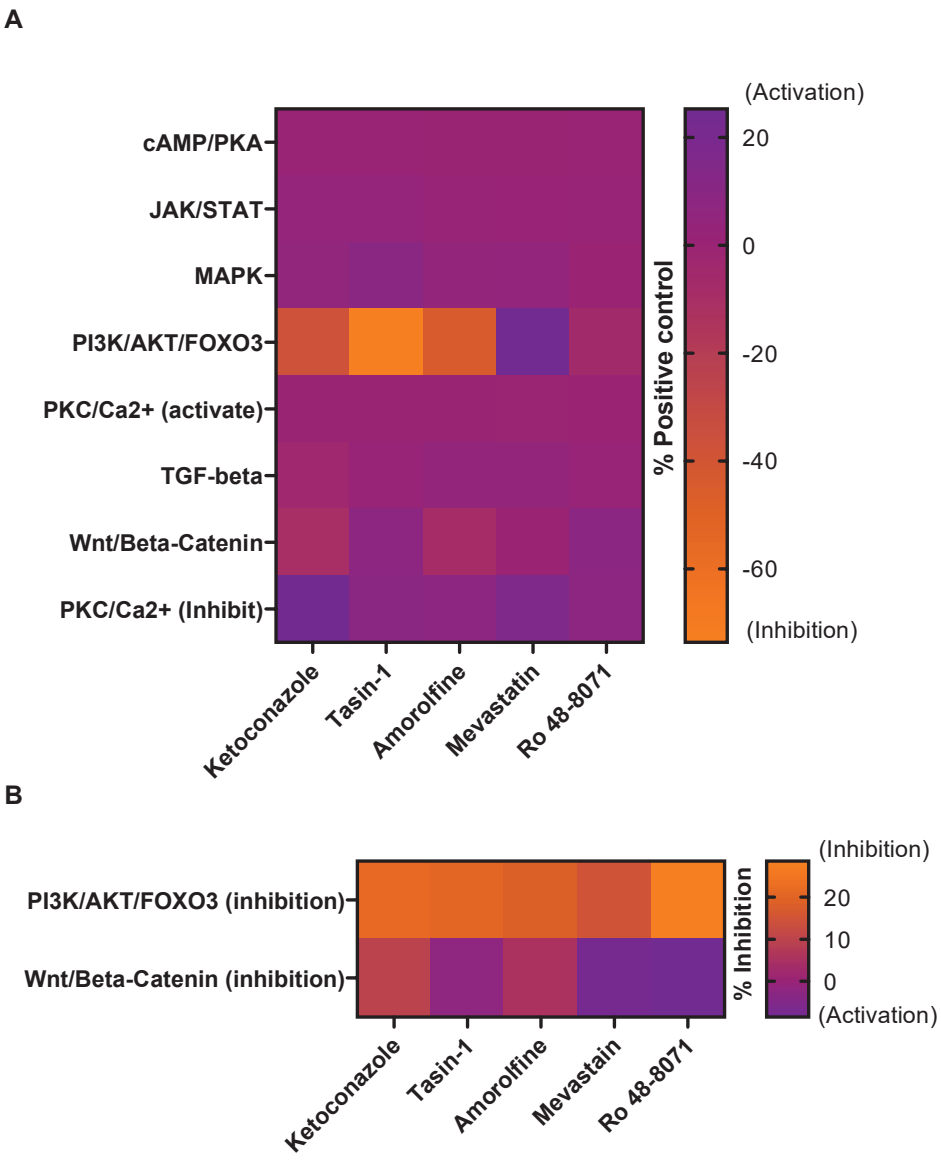

Figure 4.3: Screen of Signalling Pathways - A selection of small molecules: Ketoconazole at 2.5uM, Tasin-1 0.3uM, Amorolfine 0.3uM, Mevastatin 2.5uM, Ro 48-8071 0.1uM. Each square is the mean of two replicates. All conditions are relative to a positive control.

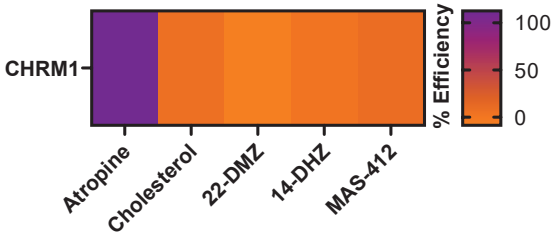

Figure 4.4: CHRM1 binding assay - A commercial screen showed no binding of all sterols to the CHRM1 receptor at 5uM

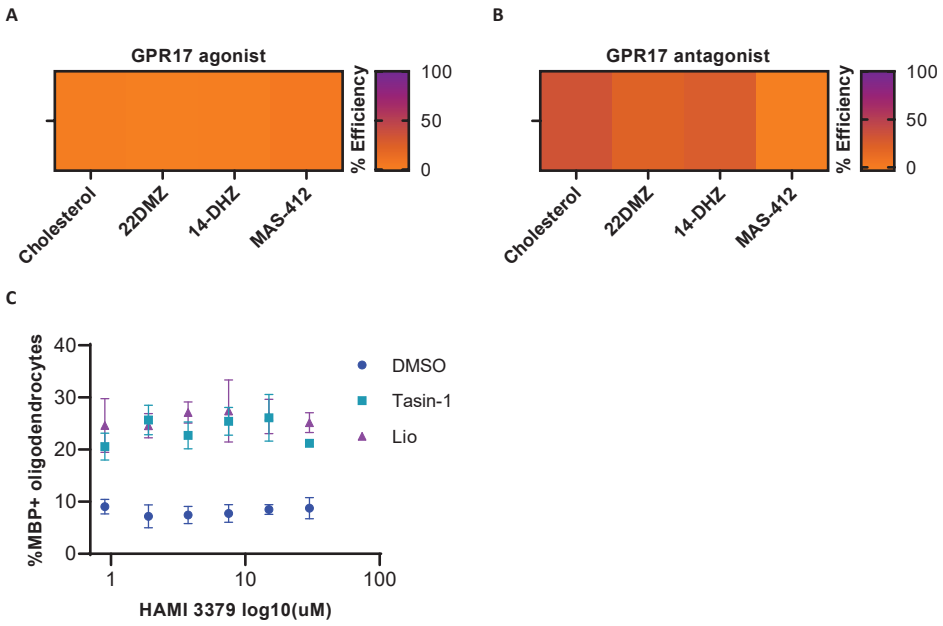

Figure 4.5: GPR17 related experiments - A) and B) are direct binding assays for GPR17 that show no binding for 22-DMZ, 14-DHZ, MAS-412, or cholesterol in either agonist or antagonist mode. Each square is representative of two replicates. C) Is a dose response curve of HAMI3379 alone or in combination with Tasin-1 and Liothyronine (Lio) showing no effect in differentiation. This is representative of two independent runs.

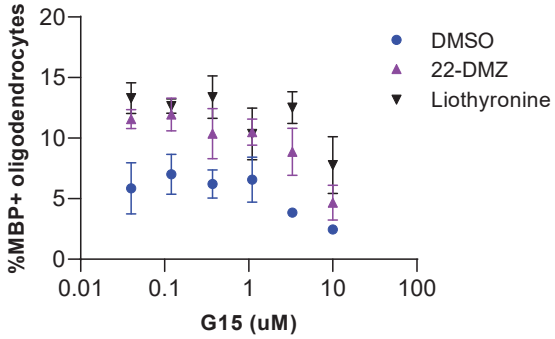

Figure 4.6: GPR30 antagonist - G15 is a GPR30 antagonist that was tested in dose response with and without 22-DMZ or Liothyronine and showed no selective effect on differentiation. Decreases in differentiation were attributable to toxicity.

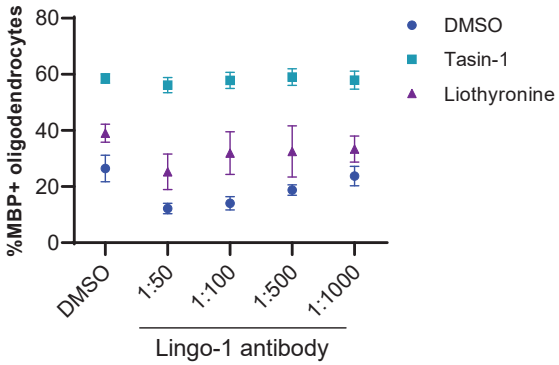

Figure 4.7: Lingo-1 antibody - Lingo-1 antibody did not show any effect on differentiation alone or in combination with Tasin-1 or Liothyronine.

homozygous mutation in exon three of PLP-1 that leads to PLP degradation. However, both the wild type cells and the PLP mutant cells had increased levels of oligodendrocyte formation in response to the sterol modulating small-molecules. Separately, our collaborators had done a drug screen in PLP mutant cells for small molecules that promote oligodendrocyte formation. (43) Their top small-molecules had high concordance with top small-molecules done in wild-type lines. In fact, we validated their top small-molecule Ro 25–6981, as a sterol-14-reductase inhibitor both *in vitro* and *in vivo*. Overall, these results suggest that PLP is not directly involved in the mechanism of our pro-differentiation sterols.

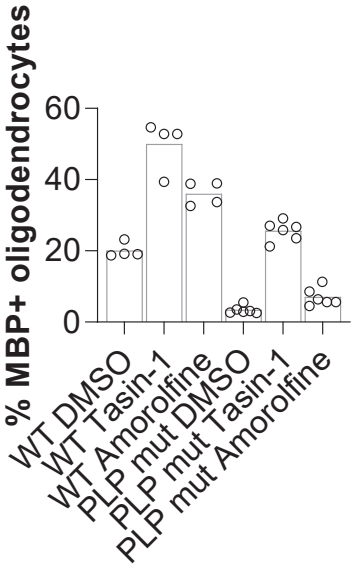

Figure 4.8: PLP mutated cells - Mutating PLP doesn't prevent the Tasin-1 or Amorolfine from promoting oligodendrocyte formation.

4.4.1.2 Hypotheses based on sterol literature

Broadly, pro-myelinating sterols could be exerting their effects through changes in membrane properties, most commonly referred to as membrane fluidity. Previously studies showed that lanosterol increases membrane fluidity in macrophages, and an EBP inhibitor increases membrane fluidity in red blood cells. (4, 151) Biochemically, lanosterol and zymosterol affect membrane fluidity differently than desmosterol and cholesterol. (48) However, there is disagreement in the field on this matter. (152) To address if pathway modulating small molecules increase membrane fluidity in OPCs, we used a fluidity sensitive dye called laurdan. Preliminary data showed that both CYP51 inhibitors and HMGCR inhibitors lead to increases in membrane fluidity, suggesting that these effects are likely due to cholesterol depletion as opposed to the accumulation of 8,9-unsaturated sterols. However, this assay is not trivial to execute, highly noisy, and very low throughput. To test if membrane fluidity is linked with oligodendrocyte formation using an orthogonal approach, we increased membrane fluidity using two reagents: n-heptanol and benzyl alcohol. Despite increasing membrane fluidity, as measured by the laurdan assay, neither significantly increased differentiation in our hands. However, these approaches are agnostic to nuances such as lipid rafts and differences between intracellular compartments; sub-cellular alterations in membrane fluidity could still be contributing to the effects of

pro-differentiation sterols.

If membrane fluidity were a mechanism of promoting oligodendrocyte formation, we would expect a subset of the small molecule drug screening hits to promote oligodendrocyte formation to inhibit separate pathways to affect membrane fluidity, such as sphingolipids. Given that none of the hits we have tested affect alternative pathways that could modulate membrane fluidity, it is less likely that membrane fluidity is involved in the effects of 8,9-unsaturated sterols. Instead, there is an increasing body of literature regarding proteins that directly sense the composition of lipids in a membrane, as opposed to indirectly measuring the lipid composition through fluidity. (5) Given that small changes in sterols lead to starkly different effects on oligodendrocyte formation, it seems more likely that a specific protein interacts with the pro-differentiation sterols to mediate their effects.

It is possible that the enzyme LBR is mediating the effects on oligodendrocyte formation. LBR is known to bind 8,9-unsaturated sterols due to its role as a sterol-14-reductase enzyme in the cholesterol biosynthesis pathway. It also has direct access to DNA and transcriptional machinery as a component of the inner nuclear membrane. (78, 128) Currently, it is unknown if the sterol-binding domain and the DNA-binding domain of LBR affect each other's activity. (78) However, given that both domains of LBR are highly conserved among vertebrates, and the sterol binding domain is redundant with TM7SF2, it is likely that there is an evolutionary reason to keep LBR

with both domains. (129) Therefore, pro-differentiation sterols may interact with the sterol binding domain of LBR, leading to structural change in the nuclear domain of LBR, that contribute to the differentiation phenotype. The only qualm with the hypothesis that LBR is involved in downstream signaling of the pro-differentiation sterols is that 2,2-DMZ does not lead to any 14DHZ accumulation. This observation suggests that 2,2-DMZ does not interact with the enzymatic domains of TM7SF2/LBR, which contradicts the idea that 2,2-DMZ could be binding LBR to mediate its effects on oligodendrocyte formation. While we have not ruled out that 2,2-DMZ might have a differential binding affinity for TM7SF2 versus LBR, it still makes this hypothesis less tractable. To determine if 2,2-DMZ and LBR are interacting, we could use a cellular thermal shift assay. This approach measures the thermal stability of a protein in the presence or absence of a particular ligand.

Other potential candidates for promoting oligodendrocyte formation are proteins that are structurally similar to enzymes in the cholesterol biosynthesis pathway. For example, the binding pockets of both sigmar1 and sigmar2 are all structurally similar to EBP and expressed in OPCs. Preliminary results suggest that sigmar1 and sigmar2 are not involved mediating the effects on oligodendrocyte formation. We tested (+)pentazocine, a small molecule that selectively affects the activity of the sigmar1 over sigmar2 and EBP, and found that it had no effect on oligodendrocyte formation alone or in combination with other pro-differentiation small molecules. (see fig 4.9) We also

tested siRNA mediated transcript depletion of both sigmar1 and sigmar2; in two independent experiments, there was no selective effect on oligodendrocyte formation with or without pro-differentiation small-molecules. (see fig.4.10)

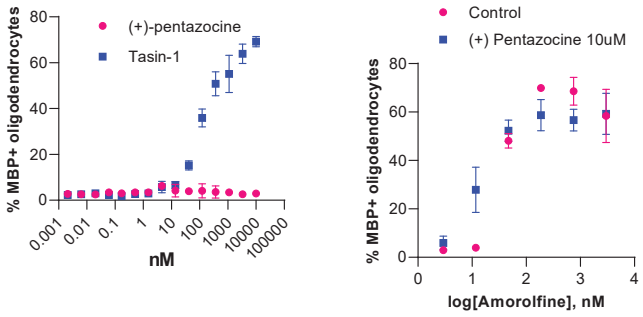

Figure 4.9: Selective sigmar1 small-molecule - (+)-pentazocine does not have any effect on oligodendrocyte formation either alone or in combination with amorolfine.

Epoxycholesterol has its own set of known interacting partners, which we have previously explored, including LXR, INSIG/SREBP, and GPR17. (119) However, there exists another family of proteins that are known to bind epoxycholesterol called the oxysterol binding proteins (OSBPs). Interestingly, one of the OSBPs, OSBPL1a, is highly up-regulated in differentiating OPCs. (171) We performed preliminary experiments to deplete transcript levels of the top five most expressed OSBPs in the context of various differentiation driving small molecules. Broadly, it seems that treating OPCs with siRNA targeting OSBPs decreases oligodendrocyte formation even in the presence of pro-differentiation signals. This effect is not selective for 8,9-unsaturated sterols, as differentiation also decreased in liothyronine treated

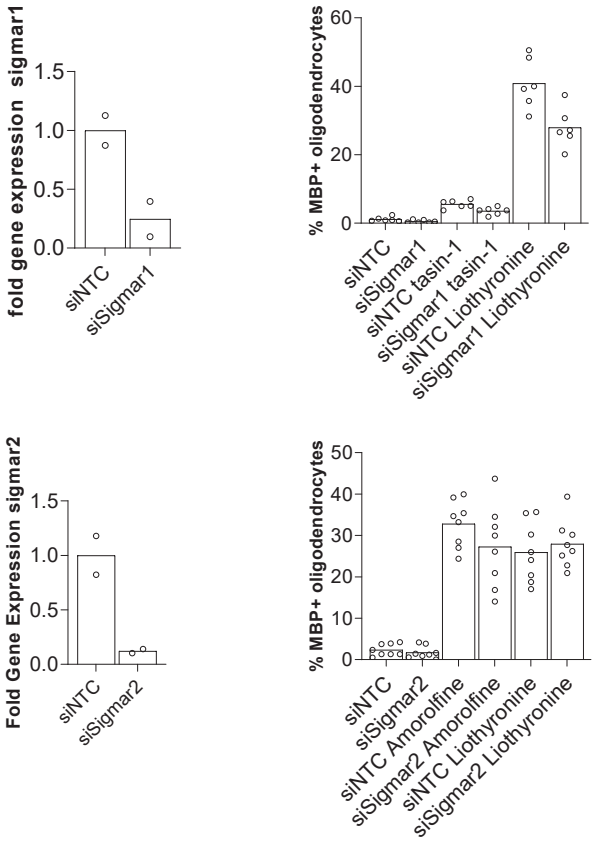

Figure 4.10: sigmar1 and sigmar2 knockdown - Knockingdown sigmar1 or sigmar2 alone and in combination with Tasin-1 or liothyronine .

OPCs. (see fig 4.11)

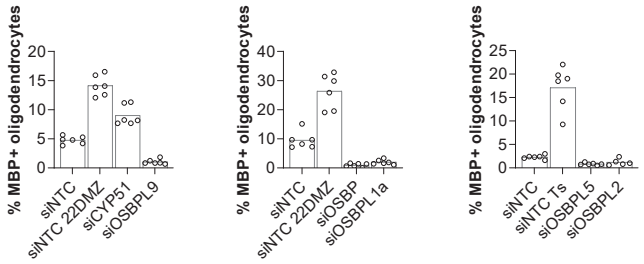

Figure 4.11: Oxysterol binding Proteins - Knocking down the top five OSBPs decreases differentiation. Transcript depletion of CYP51 reproduces to promote oligodendrocyte formation.

4.4.1.3 Generation of Genetic tools for more rapid hypothesis analysis

One challenge we faced in trying to determine the mechanism by which the pro-differentiation sterols function was that the existing genetic tools for OPCs were not ideal with regards to throughput nor kinetics. siRNA leads to a robust and rapid depletion of transcript levels. However, for some targets we were unable to see functional effects on the protein of interest, likely due to variability in protein turnover. In contrast, our established methods for lentiviral infection of OPCs with CRISPR targeting reagents take three weeks, which is far too long when studying changes in metabolic pathways. (85) Therefore, we sought to implement a technique that allowed us to genetically manipulate OPCs with more temporal control.

To address this, we generated a protocol for CRISPR mediated mutation of target genes using electroporation. First, we used lentivirus to generate

OPCs that constitutively express Cas9. Then we used electroporation to deliver commercially available synthetic hairpin sgRNA into the Cas9 OPCs for the gene of interest. We optimized the electroporation so that transfection efficiency is effectively 100$\%$. This approach was used in chapter 3 to determine when exactly LSS knockdown leads to 24,25-epoxycholesterol accumulation. Neither the siRNA approach nor the lentivirus CRISPR was able to capture the precise timeframe associated with partial LSS inhibiton and 24,25-epoxycholesterol accumulation. With the CRISPR electroporation approach we were able to test multiple timepoints and monitor the temporal accumulation of 24,25-epoxycholesterol, which indicated the best time to perform the differentiation assay to see effects on oligodendrocyte formation. The approach takes less than 3 days and the reagents cost less than $\$$200 per gene, allowing us to test many hypotheses rapidly and cheaply.

We then wanted to generate approaches that allow us to ask if an increase in the expression of certain genes affects oligodendrocyte formation. To address this, we generated a CRISPRa OPC line into which we can electroporate hairpin sgRNA to increase transcription of the target gene. The over-expression happens very quickly due to the constitutive expression dCAS9-VPR. (see fig 4.12 for an overexpression example) The challenge with this approach is that it has minimal effects on genes that are already highly expressed. Therefore, we also optimized a CMV driven plasmid overexpression protocol that utilized MYC staining to determine which cells con-

tain the plasmid of interest. These methods allow us to overexpress genes robustly regardless of their endogenous expression level.

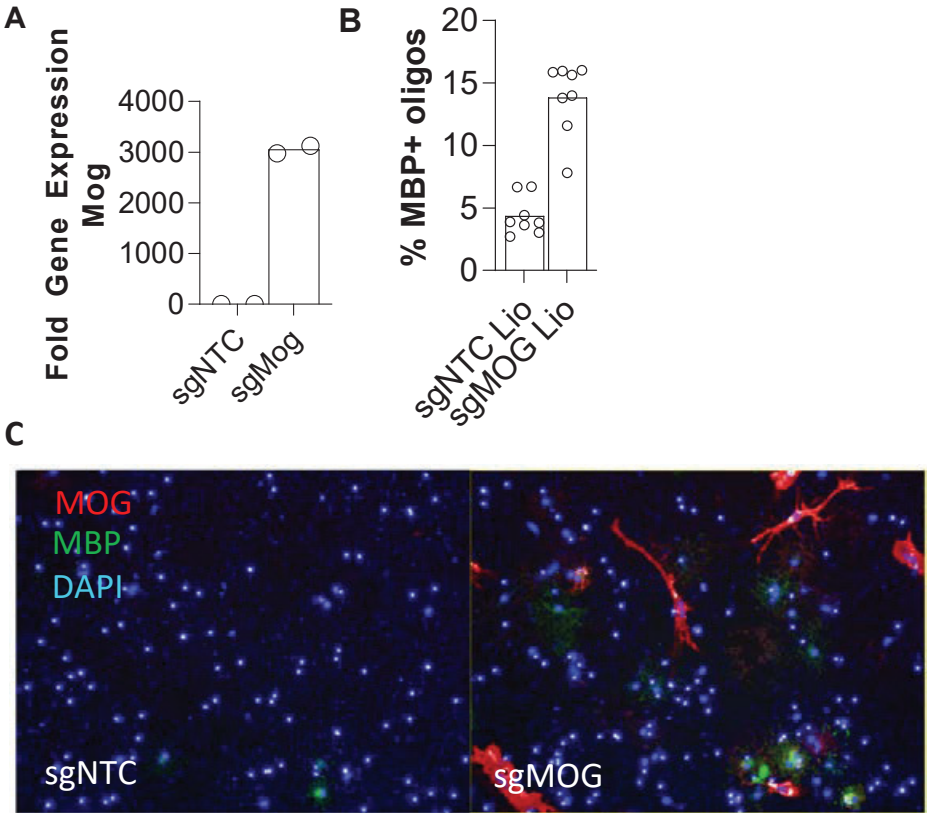

Figure 4.12: Electroporation based CRISPRa for MOG - A) In less than 72 hours there is robust increase in MOG expression. C) Protein overexpression was confirmed with antibody staining. B) MOG overexpression increase the percentage of MBP+ oligodendrocytes.

These tools I have optimized for use in OPCs will allow us to get a better understanding of the role of various genes in oligodendrocyte formation on a more appropriate timescale.

4.4.2 Unbiased Approaches

To date, few papers use unbiased approaches to determine the mechanism of action of intermediates in the cholesterol biosynthesis pathway regardless of phenotype. The three types of unbiased approaches that have identified the target of sterol-like small molecules are transcriptional profiling, photoaffinity pull-down, and genetic screening. (67, 149)

4.4.2.1 RNAseq

We performed RNAseq experiments for three timepoints throughout the differentiation of OPCs treated with 8,9 unsaturated sterols, cholesterol, and a variety of pro-differentiation small-molecules. Surprisingly, the RNAseq revealed that the genes differentially expressed between 48 hours and 24 hours in OPCs treated with 2,2-DMZ almost completely overlap with genes differentially expressed in the untreated differentiating control in the same time frame. In contrast, in OPCs treated with liothyronine, there were substantial differences in gene expression between 48 and 24 hours that differed from the untreated controls. This observation supports the idea that liothyronine and 8,9-unsaturated sterols do not work via the same mechanism, which was evident in chapter 2 based on combination experiments. The gene expression signature in response to the 8,9-unsaturated sterols makes it less likely that the 8,9-unsaturated sterols are promoting oligodendrocyte formation by directly affecting a single transcription factor such as nuclear

hormone receptors, LXR, or SREBP. Unfortunately, the RNAseq did not help us nominate any specific mechanism for how the 8,9-unsaturated sterols promote oligodendrocyte formation. Some drawbacks of this experiment are that the cells were not sorted based on cell state before sequencing; therefore, the cellular heterogeneity may have masked subtle changes in gene expression.

4.4.2.2 Genetic Screening

Another common approach to identify the target of small-molecules is genetic screening. These approaches ideally assess the whole genome and determine if transcript depletion or mutation of genes affects the phenotype of the small molecule. One advantage of this approach is that it can illuminate either direct targets or signaling pathways involved in the mechanism of a small molecule. The genetic screening approaches commonly used for mammalian cells are siRNA screening or CRISPR screening.

For siRNA screening, we needed a high-throughput way of transfecting OPCs. We have been able to miniaturize the electroporation protocol into a 96-well format. Therefore, we are currently beginning to screen a siRNA library targeting 48 sterol binding proteins to see if transcript depletion of these targets affects oligodendrocyte formation driven by 8,9-unsaturated sterols. However, due to the cost of electroporation reagents and the need for replicates with siRNA screening, whole-genome siRNA screening is cur-

rently unfeasible for OPCs. Another complication is that the differentiation assay is only three days, which may not be enough time for protein turnover, especially for membrane-bound proteins.

For CRISPR screening, one challenge is that mature oligodendrocytes are highly multiprocessed and, therefore, difficult to detach and sort based on membrane markers. To overcome this issue, we could instead focus on isolating the nuclei instead of the whole cells. We could then stain the nuclei for a nucleus specific mature oligodendrocyte marker, before flow-sorting to separate the mature and immature nuclei. A key area of optimization would be to find a nucleus stain specific for mature oligodendrocytes, possibilities include nuclear proteins (such as cleaved MYRF or NKX6.2) or membrane proteins (such as MBP or MOG). Currently, our lentivirus CRISPR approach has an antibiotic selection step, which lengthens the assay by a week. To address this, we could use a GFP tagged plasmid and only isolate cells that have nuclear GFP signal. Nevertheless, optimizing a CRISPR screen for this purpose would be a time-consuming undertaking that may, or may not, yield the direct target of the sterols.

4.4.2.3 Click Sterols

The most direct way to determine the interacting partners of a small-molecule is by using photoaffinity pull-down reagents. This approach has been successfully used for other sterol-like small molecules to identify sterol interact-

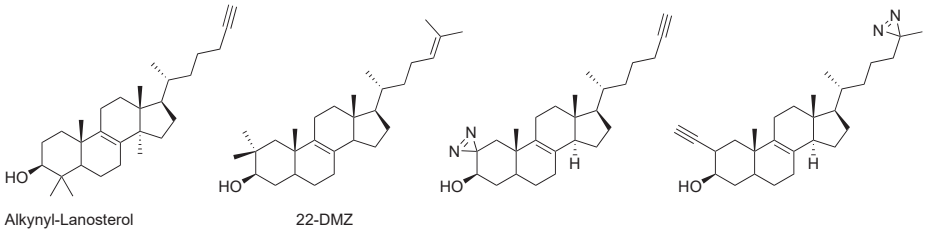

Figure 4.13: Ideal Pulldown Sterols - Alkynyl lanosterol and 2,2-DMZ demonstrate two sites of modification that would allow us to add an alkyne and diazirine to an 8,9-unsaturated sterol to generate two potential pull-down sterols for unbiased target identification.

ing partners. (23, 149) These molecules are chemically modified to contain two groups: one that allows for crosslinking with proteins and another for crosslinking to a bead for purification. The specific functional groups can vary; however, the least bulky functional groups that fulfill these criteria are a diazirine for UV affinity labeling and alkyne for click chemistry isolation. The read-out is typically protein mass-spectrometry to determine which protein fragments are most commonly crosslinked to the small molecule. The biggest hurdle in these types of experiments is generating a small molecule that fulfills the required criteria. For us, this means a candidate pull-down sterol needs to:

- contain an alkyne
- contain a diazirine
- enhance oligodendrocyte formation
- not block CYP51, sterol-14-reductase, EBP, or LSS

- not be metabolized into an inactive metabolite

Previous work has highlighted that the introduction of an alkyne on the tail of lanosterol does not prevent lanosterol from being metabolized, indicating that this alkyne-lanosterol would fulfill three out of the five criteria. (149) Given that 2,2-DMZ promotes differentiation, it does not block the enzymes in the cholesterol biosynthesis pathway, nor is it further metabolized by enzymes in the cholesterol biosynthesis pathway, I propose the following sterols as a possible click-sterol which could fulfill all five criteria. (see fig. 4.13) The potential draw-back of pull-down sterols is that they do not necessarily inform about the downstream signaling that leads to the given phenotype. However, of all of the mechanistic approaches, the pull-down approach is the one most likely to give us a tractable lead.

4.5 Interrogate other pathway members

We have defined several targets for pro-myelin therapies including: LSS, CYP51, sterol-14 reductase, and EBP. However, we still need to determine if these encompass the full spectrum of pro-myelinating targets within the cholesterol biosynthesis pathway. Our initial experiments were limited to enzymes for which there are selective small molecule inhibitors. However, we can now use genetic approaches to explore targets that lack selective inhibitors.

4.5.1 Sterol-14-reductase: TM7SF2/LBR

In chapter 2, we showed that sterol-14 reductase inhibition with small molecules leads to increased levels of 8,9-unsaturated sterols and promotes oligodendrocyte formation. However, it is less clear which protein is mediating in this effect. The enzymatic activity of sterol-14 reductase is shared by two proteins TM7SF2 and LBR. (78) TM7SF2's only known function is as a sterol-14 reductase enzyme in the cholesterol biosynthesis pathway. In contrast, LBR is a bi-functional protein with two domains: an enzymatically active transmembrane domain and a nuclear domain which is involved with the organization of the DNA. (78) There is disagreement in the field about the ability of these two enzymes to compensate for one another in mammalian cells, likely due to differences in expression level in various tissue types and variability in the availability of exogenous sterols. (29, 150, 155) In the context of high or low exogenous sterol availability the relative expression levels of TM7SF2 and LBR change. (29) Therefore, it would be interesting to know if in OPCs TM7SF2 or LBR is the dominant mediator of the pro-differentiation phenotype seen with sterol-14 reductase inhibition. Practically, we can study this using CRISPR electroporation. Further, if only one of these proteins is responsible for the phenotypic effects seen, it may be beneficial to design small molecules that selectively inhibit either TM7SF2 or LBR.

4.5.2 C-4 demethylation complex

The C-4 demethylation complex lies between sterol-14 reductase and EBP in the cholesterol biosynthesis pathway and consists of three enzymes: SC4MOL, HSD17B7, and NSDHL. The enzyme complex acts twice to demethylate the C-4 position of sterols sequentially. Our previous work shows that T-MAS promotes oligodendrocyte formation without inhibiting any of the established targets (CYP51, sterol-14 reductase, EBP, or LSS). Lentivirus based CRISPR targeting of SC4MOL leads to the accumulation of T-MAS and promotes oligodendrocyte formation. (See fig. 4.14) Therefore, it is plausible that the C4DMC enzymes represent three further targets for enhancing oligodendrocyte formation. In addition to being a hormone, 17- hydroxyprogesterone is a known SC4MOL inhibitor that promotes oligodendrocyte formation. (55) (See fig. 4.14) There currently exist no commercially available selective inhibitors of these enzymes for mammalian cells and limited commercially available sterol standards for the substrates of these enzymes. However, evaluation of the C-4 demethylation complex enzymes as targets for promoting oligodendrocyte formation should be relatively straight forward using the previously described genetic tools.

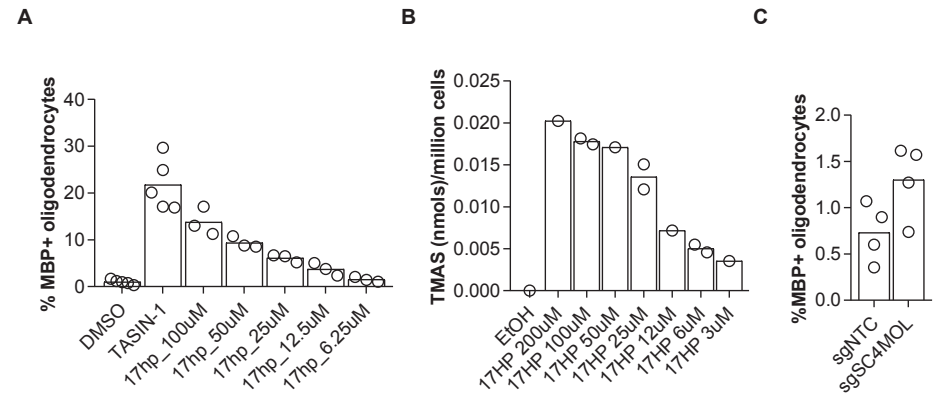

Figure 4.14: SC4MOL as a potential target - 17-hydroxyprogesterone enhances oligodendrocyte formation and inhibits SC4MOL. SC4MOL mutation, promotes oligodendrocyte formation

4.6 Insights into the Cholesterol biosynthesis pathway

One challenge of this work is that 8,9-unsaturated sterols are also small-molecules that can have effects on the cholesterol biosynthesis pathway in unexpected ways. Therefore, it is essential to parse if pro-differentiation sterols are working directly to promote oligodendrocyte formation or indirectly via inhibition of CYP51, sterol-14-reductase, or EBP. In analyzing this data, I noticed two subtle phenomena that may have gone underappreciated in previous research regarding the metabolites of the cholesterol biosynthesis pathway.

4.6.1 Natural metabolites block other steps in cholesterol biosynthesis pathway

Firstly, metabolites that are considered endogenous to the cholesterol biosynthesis pathway can function as inhibitors of other steps within the post-squalene pathway. We treated OPCs with each of the pro-differentiation 8,9-unsaturated sterols in chapter 2 and found that two of them block enzymes upstream in the pathway. Specifically, dihydro-FF-MAS and dihydro-T-MAS lead to the accumulation of lanosterol in addition to being further metabolized in the pathway. Conceptually, this is not surprising given that dihydro-FF-MAS is the product of CYP51 and dihydro-T-MAS differs from dihydro-FF-MAS only by a double bond at the C14 position. However, this effect happened at concentrations of dihydro-FF-MAS and dihydro-T-MAS are far above the range typically seen physiologically; it is unlikely that they are relevant at physiologic concentrations. However, it suggests that the effects exogenous natural metabolites on the cholesterol biosynthesis pathway should be determined before the interpretation of phenotypic consequences in other assays.

4.6.2 14-DHZ may be a non-canonical natural metabolite

Previous work had shown that with sterol-14-reductase inhibition *in vitro*, there is an accumulation of the 14-DHZs as opposed to accumulation an

of FF-MAS and dihydro-FF-MAS. (See chapter 1) However, this may not be an artifact of small molecule treatment or genetic experiments alone, but instead represent the natural tendency of the C4DMC to metabolize FF-MAS and dihydro-FF-MAS, as opposed to sterol-14 reductase which is suggested by the Bloch and Kandutsch-Russell pathways. While not described in the literature, there are several lines of evidence that support this idea:

- 14-DHZ can flux through the pathway. In OPCs treated with 14-DHZ, there is an increase in the downstream metabolites: zymostenol and lathosterol.
- 14-DHZ is detectable endogenously in untreated OPCs.
- OPCs treated with exogenous FF-MAS and dihydro-FF-MAS, have increased levels of 14-dehydrozymosterol and 14-dehydrozymostenol.
- In OPCs treated with very potent EBP inhibitors, there is 14DHZ accumulation, as would be expected if EBP is fully inhibited and the metabolites are accumulating upstream.

While none of these observations are conclusive, in combination, they suggest that the order of enzymes in the cholesterol biosynthesis pathway may not always follow the classical Bloch or Kandutsch-Russell pathways. Instead, it is possible that FF-MAS and dihydro-FF-MAS are metabolized by either sterol-14-reductase or C4DMC depending on the cell type. In unperturbed OPCs, C4DMC could act before sterol-14-reductase.

Unfortunately, our current sterol measurements are steady-state measurements. To get accurate measurements of flux through this portion of the pathway, we need to do experiments with C13 labeling or deuterium labeling at shorter timepoints. Also, biochemical assays could clarify the relative affinity for FF-MAS and dehydro-FF-MAS by C4DMC versus sterol-14-reductase. Lastly, 14-DHZ should be purified from OPCs to conclusively establish it as a natural metabolite of the cholesterol biosynthesis pathway.

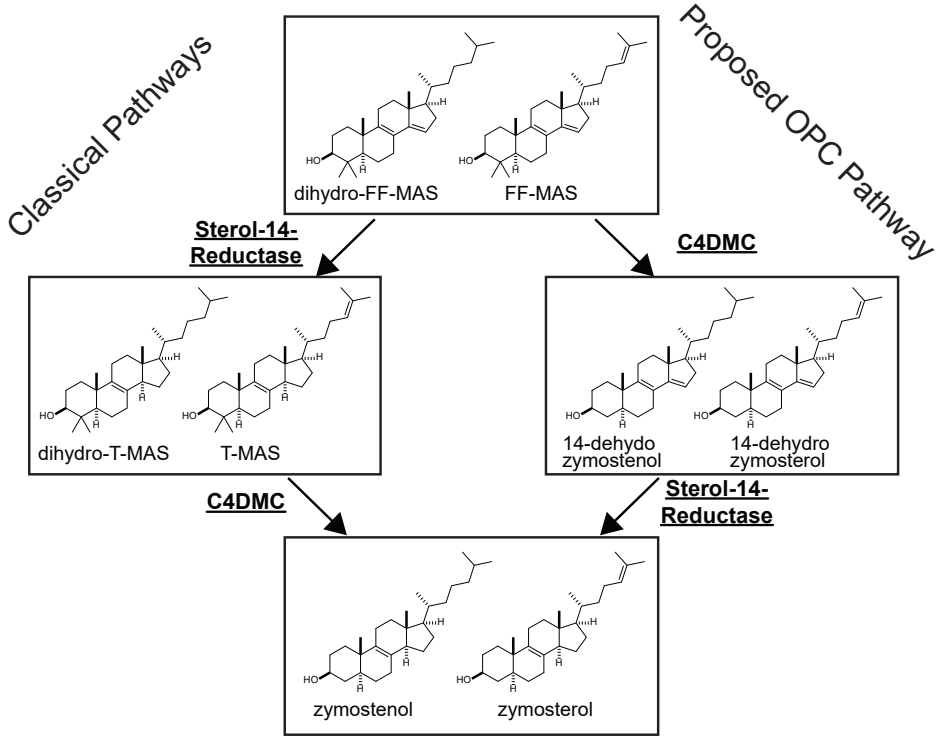

Figure 4.15: Alternative order of Sterol-14-reductase and C4DMC for OPCs - Diagram indicating the classical order of enzymes in the cholesterol biosynthesis pathway (left) versus the proposed pathway, (right).

4.7 Conclusion

Foundational work in rodents highlighted OPCs as a potential target for therapies that aim to improve myelin production after demyelinating insults. High-throughput drug screening delineated dozens of small molecules that promote oligodendrocyte formation from OPCs, both in vitro and in vivo. Our work identified that inhibition of four enzymes in the cholesterol biosynthesis pathway is a common mechanism of these pro-differentiation and pro-myelination small molecules. Inhibition of these enzymes leads to accumulation of sterol metabolites that are sufficient to promote oligodendrocyte formation. Structure-function-relationship studies of the sterols highlighted the epoxycholesterol synthesis pathway as a novel pathway contributing to oligodendrocyte formation. Inhibition of CYP51, sterol-14 reductase, and EBP enhanced remyelination in mouse models of multiple sclerosis. Therefore, small molecules that inhibit these enzymes are candidates for clinical translation. Interestingly, one EBP inhibiting compound, clemastine, improves physiological metrics of demyelination in multiple sclerosis patients, but it was unable to improve the symptoms of these patients. However, this study did not determine whether the dose used of clemastine was optimally inhibiting EBP. Therefore, the success of EBP inhibition as a therapeutic strategy has yet to be determined. The most direct way of establishing the utility of sterol modulating therapeutics for remyelination is to test them in further clin-

ical trials. Given that inhibition of enzymes in the postsqualene portion of the cholesterol biosynthesis pathway leads to precocious myelination in development, the sterol metabolites may be contributing to endogenous cues that trigger oligodendrocyte formation and myelination in vivo. The mechanism by which the sterol metabolites lead to enhanced oligodendrocyte formation is completely unknown. We have explored many of the most likely mechanism given known sterol and oligodenderocyte biology. However, it is likely that these metabolites are functioning through novel biological approaches that have yet to be described in the literature. Therefore, I strongly advocate for the use of pull-down sterols as an approach to determine the interacting proteins of the pro-differentiation sterols. Then, genetic tools can be used to establish the involvement of each protein on the oligodendrocyte formation phenotype. Other targets in the cholesterol biosynthesis pathway may be novel targets for enhanced oligodendrocyte formation that can be further explored using genetic tools. Exploration of the cholesterol biosynthesis pathway has highlighted that metabolites in this pathway can act both as substrates and inhibitors of enzymes. Further, metabolites that accumulate upon enzymatic inhibition may represent natural metabolites in OPCs under physiologic conditions.

In conclusion, we have shown that inhibition of the post-squalene cholesterol biosynthesis pathway is a novel therapeutic strategy to enhance remyelination. This mechanism is shared between most known small-molecules

that enhance oligodendrocyte formation. Yet, beyond the obvious therapeutic applications, this work opens the door to a slew of new questions surrounding both oligodendrocyte biology, sterol signaling mechanisms, and the cholesterol biosynthesis pathway. While we achieved our primary goal of determining the mechanism of action of the oligodendrocyte formation enhancing small-molecules, instead of closing the chapter on this area of work, it has opened our eyes to a whole new world of possible questions.

References

[1] AČIMOVIČ, J. & ROZMAN, D. (2013). Steroidal triterpenes of cholesterol synthesis. *Molecules*, **18**, 4002–4017. 12, 13, 14, 132, 136

[2] AHFELDT, T., LITTERMAN, N.K. & RUBIN, L.L. (2017). Studying human disease using human neurons. *Brain Research*, **1656**, 40–48. 1

[3] ALLIMUTHU, D., HUBLER, Z., NAJM, F.J., TANG, H., BEDERMAN, I., SEIBEL, W., TESAR, P.J. & ADAMS, D.J. (2019). Diverse chemical scaffolds enhance oligodendrocyte formation by inhibiting CYP51, TM7sf2, or EBP. *Cell Chemical Biology*, **26**, 593–599.e4. 85, 87, 100, 123

[4] ARALDI, E., FERNÁNDEZ-FUERTES, M., CANFRÁN-DUQUE, A., TANG, W., CLINE, G.W., MADRIGAL-MATUTE, J., POBER, J.S., LASUNCIÓN, M.A., WU, D., FERNÁNDEZ-HERNANDO, C. & SUÁREZ, Y. (2017). Lanosterol modulates TLR4-mediated innate immune responses in macrophages. *Cell Reports*, **19**, 2743–2755. 143

[5] BALLWEG, S., SEZGIN, E., DOKTOROVA, M., COVINO, R., REINHARD, J., WUNNICKE, D., HÄNELT, I., LEVENTAL, I., HUMMER, G. & ERNST, R. (2020). Regulation of lipid saturation without sensing membrane fluidity. *Nature Communications*, **11**. 144

[6] BARATEIRO, A. & FERNANDES, A. (2014). Temporal oligodendrocyte lineage progression: In vitro models of proliferation, differentiation and myelination. *Biochimica et Biophysica Acta (BBA) - Molecular Cell Research*, **1843**, 1917 – 1929. 9

[7] BATTA, A.K., TINT, G.S., SHEFER, S., ABUELO, D. & SALEN, G. (1995). Identification of 8-dehydrocholesterol (cholesta-5,8-dien-3 beta-ol) in patients with Smith-Lemli-Opitz syndrome. *J. Lipid Res.*, **36**, 705–713. 15

[8] BAUMANN, N. & PHAM-DINH, D. (2001). Biology of oligodendrocyte and myelin in the mammalian central nervous system. *Physiological Reviews*, **81**, 871–927. 2, 3

[9] BECHLER, M.E., BYRNE, L. & FFRENCH CONSTANT, C. (2015). CNS myelin sheath lengths are an intrinsic property of oligodendrocytes. *Current Biology*, **25**, 2411–2416. 37

[10] BENNETT, J.L. & STÜVE, O. (2009). Update on inflammation, neurodegeneration, and immunoregulation in multiple sclerosis. *Clinical Neuropharmacology*, **32**, 121–132. 4

[11] BERGER, J., MOSER, H.W. & FORSS-PETTER, S. (2001). Leukodystrophies: recent developments in genetics, molecular biology, pathogenesis and treatment. *Current Opinion in Neurology*, **14**, 305–312. 3

[12] BEYEA, M.M., HESLOP, C.L., SAWYEZ, C.G., EDWARDS, J.Y., MARKLE, J.G., HEGELE, R.A. & HUFF, M.W. (2006). Selective up-regulation of LXR-regulated GenesABCA1, ABCG1, andAPOEin macrophages through increased endogenous synthesis of 24(s), 25-epoxycholesterol. *Journal of Biological Chemistry*, **282**, 5207–5216. 91, 94

[13] BILLON, N. (2002). Normal timing of oligodendrocyte development from genetically engineered, lineage-selectable mouse ES cells. *Journal of Cell Science*, **115**, 3657–3665. 8

[14] BJÖRKHEM, I. (2006). Crossing the barrier: oxysterols as cholesterol transporters and metabolic modulators in the brain. *Journal of Internal Medicine*, **260**, 493–508. 101

[15] BOSCH, D.G., BOONSTRA, F.N., GONZAGA-JAUREGUI, C., XU, M., DE LIGT, J., JHANGIANI, S., WISZNIEWSKI, W., MUZNY, D.M., YNTEMA, H.G., PFUNDT, R., VISSERS, L.E., SPRUIJT, L., BLOKLAND, E.A., CHEN, C.A., LEWIS, R.A., TSAI, S.Y., GIBBS, R.A., TSAI, M.J., LUPSKI, J.R., ZOGHBI, H.Y., CREMERS, F.P., DE VRIES, B.B. & SCHAAF, C.P. (2014). NR2f1 mutations cause optic atrophy with intellectual disability. *The American Journal of Human Genetics*, **94**, 303–309. 60

[16] BOUTAUD, O., DOLIS, D. & SCHUBER, F. (1992). Preferential cyclization of 2, 3(s):22(s), 23-dioxidosqualene by mammalian 2, 3-oxidosqualene-lanosterol cyclase. *Biochemical and Biophysical Research Communications*, **188**, 898–904. 18

[17] BOVE, R.M. & GREEN, A.J. (2017). Remyelinating pharmacotherapies in multiple sclerosis. *Neurotherapeutics*, **14**, 894–904. 3, 4, 5, 9, 11, 12

[18] BROWN, A.J. (2009). 24(s), 25-epoxycholesterol: A messenger for cholesterol homeostasis. *The International Journal of Biochemistry & Cell Biology*, **41**, 744–747. 18, 90, 91, 94, 101

[19] BROWN, G.R., HOLLINSHEAD, D.M., STOKES, E.S.E., WATERSON, D., CLARKE, D.S., FOUBISTER, A.J., GLOSSOP, S.C., MCTAGGART, F., MIRRLEES, D.J., SMITH, G.J. & WOOD, R. (2000). A novel series of 4-piperidinopyridine and 4-piperidinopyrimidine inhibitors of 2, 3-oxidosqualene cyclase-lanosterol synthase. *Journal of Medicinal Chemistry*, **43**, 4964–4972. 95

[20] BROWN, G.R., FOUBISTER, A.J., JOHNSON, M.C., NEWCOMBE, N.J., WATERSON, D. & WELLS, S.L. (2001). Novel 4-piperidinopyridine inhibitors of oxidosqualene cyclase-lanosterol synthase derived by consideration of inhibitor pKa. *Bioorganic & Medicinal Chemistry Letters*, **11**, 2213–2216. 95

[21] BRUSTLE, O., JONES, K.N., LEARISH, R.D., KARRAM, K., CHOUDHARY, K., WIESTLER, O.D., DUNCAN, I.D. & MCKAY, R.D. (1999). Embryonic stem cell-derived glial precursors: a source of myelinating transplants. *Science*, **285**, 754–756. 8

[22] BUNGE, R.P. (1968). Glial cells and the central myelin sheath. *Physiological Reviews*, **48**, 197–251. 2, 3

[23] BURGETT, A.W.G., POULSEN, T.B., WANGKANONT, K., ANDERSON, D.R., KIKUCHI, C., SHIMADA, K., OKUBO, S., FORTNER, K.C., MIMAKI, Y., KURODA, M., MURPHY, J.P., SCHWALB, D.J., PETRELLA, E.C., CORNELLA-TARACIDO, I., SCHIRLE, M., TALLARICO, J.A. & SHAIR, M.D. (2011). Natural products reveal cancer cell dependence on oxysterol-binding proteins. *Nature Chemical Biology*, **7**, 639–647. 154

[24] BYSKOV, A.G., ANDERSEN, C.Y. & LEONARDSEN, L. (2002). Role of meiosis activating sterols, MAS, in induced oocyte maturation. *Molecular and Cellular Endocrinology*, **187**, 189–196. 31

[25] CALZÀ, L., FERNANDEZ, M. & GIARDINO, L. (2010). Cellular approaches to central nervous system remyelination stimulation: thyroid hormone to promote myelin repair via endogenous stem and precursor cells. *Journal of Molecular Endocrinology*, **44**, 13 – 23. 12

[26] CAMARGO, N., GOUDRIAAN, A., VAN DEIJK, A.L.F., OTTE, W.M., BROUWERS, J.F., LODDER, H., GUTMANN, D.H., NAVE, K.A., DIJKHUIZEN, R.M., MANSVELDER, H.D., CHRAST, R., SMIT, A.B. & VERHEIJEN, M.H.G. (2017). Oligodendroglial myelination requires astrocyte-derived lipids. *PLOS Biology*, **15**, e1002605. 19

[27] CAMARGO, N., GOUDRIAAN, A., VAN DEIJK, A.L.F., OTTE, W.M., BROUWERS, J.F., LODDER, H., GUTMANN, D.H., NAVE, K.A., DIJKHUIZEN, R.M., MANSVELDER, H.D., CHRAST, R., SMIT, A.B. & VERHEIJEN, M.H.G. (2017). Oligodendroglial myelination requires astrocyte-derived lipids. *PLOS Biology*, **15**, e1002605. 134

[28] CANFRÁN-DUQUE, A., CASADO, M.E., PASTOR, Ó., SÁNCHEZ-WANDELMER, J., DE LA PEÑA, G., LERMA, M., MARISCAL, P., BRACHER, F., LASUNCIÓN, M.A. & BUSTO, R. (2012). Atypical antipsychotics alter cholesterol and fatty acid metabolism in vitro. *Journal of Lipid Research*, **54**, 310–324. 22, 33, 40

[29] CAPELL-HATTAM, I.M., SHARPE, L.J., QIAN, L., HART-SMITH, G., PRABHU, A.V. & BROWN, A.J. (2020). Twin enzymes, divergent control: The cholesterogenic enzymes DHCR14 and LBR are differentially regulated transcriptionally and post-translationally. *Journal of Biological Chemistry*, **295**, 2850–2865. 156

[30] CARDONA, J.G., SMITH, M.D., WANG, J., KIRBY, L., SCHOTT, J.T., DAVIDSON, T., KARNELL, J.L., WHARTENBY, K.A. & CALABRESI, P.A. (2019). Quetiapine has an additive effect to triiodothyronine in inducing differentiation of oligodendrocyte precursor cells through induction of cholesterol biosynthesis. *PLOS ONE*, **14**, e0221747. 124

[31] CARSON, J., NIELSON, M. & BARBARESE, E. (1983). Developmental regulation of myelin basic protein expression in mouse brain. *Developmental Biology*, **96**, 485–492. 131, 132

[32] CHANG, A., NISHIYAMA, A., PETERSON, J., PRINEAS, J. & TRAPP, B.D. (2000). NG2-positive oligodendrocyte progenitor cells in adult human brain and multiple sclerosis lesions. *The Journal of Neuroscience*, **20**, 6404–6412. 4

[33] CHANG, A., TOURTELLOTTE, W.W., RUDICK, R. & TRAPP, B.D. (2002). Premyelinating oligodendrocytes in chronic lesions of multiple sclerosis. *New England Journal of Medicine*, **346**, 165–173. 4, 84, 125, 126

[34] CHUANG, J.C., VALASEK, M.A., LOPEZ, A.M., POSEY, K.S., REPA, J.J. & TURLEY, S.D. (2014). Sustained and selective suppression of intestinal cholesterol synthesis by ro 48-8071, an inhibitor of 2, 3-oxidosqualene:lanosterol cyclase, in the BALB/c mouse. *Biochemical Pharmacology*, **88**, 351–363. 94

[35] CRAWFORD, D.K., MANGIARDI, M., SONG, B., PATEL, R., DU, S., SOFRONIEW, M.V., VOSKUHL, R.R. & TIWARI-WOODRUFF, S.K. (2010). Oestrogen receptor beta ligand: a novel treatment to enhance endogenous functional remyelination. *Brain*, **133**, 2999–3016. 12

[36] DEBIEU, D., BACH, J., HUGON, M., MALOSSE, C. & LEROUX, P. (2001). The hydroxyanilide fenhexamid, a new sterol biosynthesis inhibitor fungicide efficient against the plant pathogenic fungusBotryotinia fuckeliana (botrytis cinerea). *Pest Management Science*, **57**, 1060–1067. 115

[37] DEBRABANDER, J., NIJHAWAN, D., WANG, W., SHAY, J.W. & THEODOROPOULOS, P. (2016). Targeting emopamil binding protein (ebp) with small molecules that induce an abnormal feedback response by lowering endogenous cholesterol biosynthesis. us patent application us 2016/0313302 a1. 29, 44

[38] DESHMUKH, V.A., TARDIF, V., LYSSIOTIS, C.A., GREEN, C.C., KERMAN, B., KIM, H.J., PADMANABHAN, K., SWOBODA, J.G., AHMAD, I., KONDO,

T., GAGE, F.H., THEOFILOPOULOS, A.N., LAWSON, B.R., SCHULTZ, P.G. & LAIRSON, L.L. (2013). A regenerative approach to the treatment of multiple sclerosis. *Nature*, **502**, 327–332. 8, 12, 25, 33, 42, 85, 122

[39] DIETSCHY, J.M. & TURLEY, S.D. (2004). Thematic review series: brain Lipids. Cholesterol metabolism in the central nervous system during early development and in the mature animal. *J. Lipid Res.*, **45**, 1375–1397. 19

[40] DOLLIS, D. & SCHUBER, F. (1994). Effects of a 2, 3-oxidosqualene-lanosterol cyclase inhibitor, 2, 3:22, 23-dioxidosqualene and 24, 25-epoxycholesterol on the regulation of cholesterol biosynthesis in human hepatoma cell line HepG2. *Biochemical Pharmacology*, **48**, 49–57. 91, 94

[41] D'INTINO, G., LORENZINI, L., FERNANDEZ, M., TAGLIONI, A., PERRETTA, G., DEL VECCHIO, G., VILLOSLADA, P., GIARDINO, L. & CALZÀ, L. (2011). Triiodothyronine administration ameliorates the demyelination/remyelination ratio in a non-human primate model of multiple sclerosis by correcting tissue hypothyroidism. *Journal of Neuroendocrinology*, **23**, 778–790. 12

[42] EISELE, B., BUDZINSKI, R., MÜLLER, P., MAIER, R. & MARK, M. (1997). Effects of a novel 2,3-oxidosqualene cyclase inhibitor on cholesterol biosynthesis and lipid metabolism in vivo. *J Lipid Res*, **38**, 564–575. 94

[43] ELITT, M.S., SHICK, H.E., MADHAVAN, M., ALLAN, K.C., CLAYTON, B.L., WENG, C., MILLER, T.E., FACTOR, D.C., BARBAR, L., NAWASH, B.S., NEVIN, Z.S., LAGER, A.M., LI, Y., JIN, F., ADAMS, D.J. & TESAR, P.J. (2018). Chemical screening identifies enhancers of mutant oligodendrocyte survival and unmasks a distinct pathological phase in pelizaeus-merzbacher disease. *Stem Cell Reports*, **11**, 711–726. 8, 142

[44] EMERY, B. & DUGAS, J.C. (2013). Purification of oligodendrocyte lineage cells from mouse cortices by immunopanning. *Cold Spring Harbor Protocols*, **2013**, pdb.prot073973. 7

[45] FANCY, S.P., KOTTER, M.R., HARRINGTON, E.P., HUANG, J.K., ZHAO, C., ROWITCH, D.H. & FRANKLIN, R.J. (2010). Overcoming remyelination failure in multiple sclerosis and other myelin disorders. *Experimental Neurology*, **225**, 18–23. 24, 84

[46] FANCY, S.P., CHAN, J.R., BARANZINI, S.E., FRANKLIN, R.J. & ROWITCH, D.H. (2011). Myelin regeneration: A recapitulation of development? *Annual Review of Neuroscience*, **34**, 21–43. 4

[47] FANCY, S.P.J., HARRINGTON, E.P., YUEN, T.J., SILBEREIS, J.C., ZHAO, C., BARANZINI, S.E., BRUCE, C.C., OTERO, J.J., HUANG, E.J., NUSSE, R., FRANKLIN, R.J.M. & ROWITCH, D.H. (2011). Axin2 as regulatory and therapeutic target in newborn brain injury and remyelination. *Nature Neuroscience*, **14**, 1009–1016. 12

[48] FLASIŃSKI, M., WYDRO, P., BRONIATOWSKI, M., HĄC-WYDRO, K. & FONTAINE, P. (2015). Crucial role of the double bond isomerism in the steroid b-ring on the membrane properties of sterols. grazing incidence x-ray diffraction and brewster angle microscopy studies. *Langmuir*, **31**, 7364–7373. 143

[49] FOLCH, J., LEES, M. & STANLEY, G. (1957). A simple method for the isolation and purification of total lipides from animal tissues. *Journal of Biological Chemistry*, **226**, 497–509. 55

[50] FRANKLIN, R.J.M. & FFRENCH CONSTANT, C. (2008). Remyelination in the CNS: from biology to therapy. *Nature Reviews Neuroscience*, **9**, 839–855. 24

[51] FRANKLIN, R.J.M. & FFRENCH CONSTANT, C. (2008). Remyelination in the CNS: from biology to therapy. *Nature Reviews Neuroscience*, **9**, 839–855. 84

[52] FUKUSHIMA, K., YAMAZAKI, K., MIYAMOTO, N. & SAWADA, K. (2016). Functional characterization of acetylcholine receptors expressed in human neurons differentiated from hippocampal neural stem/progenitor cells. *Journal of Biomolecular Screening*, **21**, 1065–1074. 95

[53] FUNFSCHILLING, U., JOCKUSCH, W.J., SIVAKUMAR, N., MOBIUS, W., CORTHALS, K., LI, S., QUINTES, S., KIM, Y., SCHAAP, I.A., RHEE, J.S., NAVE, K.A. & SAHER, G. (2012). Critical time window of neuronal cholesterol synthesis during neurite outgrowth. *J. Neurosci.*, **32**, 7632–7645. 19

[54] GALLOWAY, D.A., GOWING, E., SETAYESHGAR, S. & KOTHARY, R. (2019). Inhibitory milieu at the multiple sclerosis lesion site and the challenges for remyelination. *Glia*. 126

[55] GATTICCHI, L., CERRA, B., SCARPELLI, P., MACCHIONI, L., SEBASTIANI, B., GIOIELLO, A. & ROBERTI, R. (2017). Selected cholesterol biosynthesis inhibitors produce accumulation of the intermediate FF-MAS that targets nucleus and activates LXRα in HepG2 cells. *Biochimica et Biophysica Acta (BBA) - Molecular and Cell Biology of Lipids*, **1862**, 842–852. 157

[56] GIERA, M., PLÖSSL, F. & BRACHER, F. (2007). Fast and easy in vitro screening assay for cholesterol biosynthesis inhibitors in the post-squalene pathway. *Steroids*, **72**, 633–642. 26

[57] GIERA, M., MÜLLER, C. & BRACHER, F. (2014). Analysis and experimental inhibition of distal cholesterol biosynthesis. *Chromatographia*, **78**, 343–358. 26

[58] GODEFROI, E.F., HEERES, J., CUTSEM, J.V. & JANSSEN, P.A.J. (1969). Preparation and antimycotic properties of derivatives of 1-phenethylimidazole. *Journal of Medicinal Chemistry*, **12**, 784–791. 44

[59] GOLDMAN, S.A., NEDERGAARD, M. & WINDREM, M.S. (2012). Glial progenitor cell-based treatment and modeling of neurological disease. *Science*, **338**, 491–495. 24

[60] GONZALEZ, G.A., HOFER, M.P., SYED, Y.A., AMARAL, A.I., RUNDLE, J., RAHMAN, S., ZHAO, C. & KOTTER, M.R.N. (2016). Tamoxifen accelerates the repair of demyelinated lesions in the central nervous system. *Scientific Reports*, **6**. 4, 11, 12, 25, 33, 39, 85, 122

[61] GREEN, A.J., GELFAND, J.M., CREE, B.A., BEVAN, C., BOSCARDIN, W.J., MEI, F., INMAN, J., ARNOW, S., DEVEREUX, M., ABOUNASR, A., NOBUTA, H., ZHU, A., FRIESSEN, M., GERONA, R., VON BÜDINGEN, H.C., HENRY, R.G., HAUSER, S.L. & CHAN, J.R. (2017). Clemastine fumarate as a remyelinating therapy for multiple sclerosis (ReBUILD): a randomised, controlled, double-blind, crossover trial. *The Lancet*, **390**, 2481–2489. 85

[62] GRØNDAHL, C. (2008). Oocyte maturation. basic and clinical aspects of in vitro maturation (ivm) with special emphasis of the role of ff-mas. *Danish medical bulletin*, **55 1**, 1–16. 31

[63] GYLLING, H., PYRHONEN, S., MANTYLA, E., MAENPAA, H., KANGAS, L. & MIETTINEN, T.A. (1995). Tamoxifen and toremifene lower serum cholesterol by inhibition of delta 8-cholesterol conversion to lathosterol in women with breast cancer. *Journal of Clinical Oncology*, **13**, 2900–2905. 35, 40

[64] HAFLER, D.A. (2004). Multiple sclerosis. *Journal of Clinical Investigation*, **113**, 788–794. 4

[65] HANAKA, S., ABE, T., ITAKURA, H. & MATSUMOTO, A. (2000). Gene expression related to cholesterol metabolism in mouse brain during development. *Brain and Development*, **22**, 321–326. 131

[66] HARTLINE, D. & COLMAN, D. (2007). Rapid conduction and the evolution of giant axons and myelinated fibers. *Current Biology*, **17**, R29–R35. 84

[67] HELLIWELL, S.B., KARKARE, S., BERGDOLL, M., RAHIER, A., LEIGHTON-DAVIS, J.R., FIORETTO, C., AUST, T., FILIPUZZI, I., FREDERIKSEN, M., GOUNARIDES, J., HOEPFNER, D., HOFMANN, A., IMBERT, P.E., JEKER, R., KNOCHENMUSS, R., KRASTEL, P., MARGERIT, A., MEMMERT, K., MIAULT, C.V., MOVVA, N.R., MULLER, A., NAEGELI, H.U., OBERER, L., PRINDLE, V., RIEDL, R., SCHUIERER, S., SEXTON, J.A., TAO, J., WAGNER, T., YIN, H., ZHANG, J., ROGGO, S., REINKER, S. & PARKER, C.N. (2015). FR171456 is a specific inhibitor of mammalian NSDHL and yeast erg26p. *Nature Communications*, **6**. 151

[68] HIRAHARA, Y., MATSUDA, K.I., YAMADA, H., SAITOU, A., MORISAKI, S., TAKANAMI, K., BOGGS, J.M. & KAWATA, M. (2012). G protein-coupled receptor 30 contributes to improved remyelination after cuprizone-induced demyelination. *Glia*, **61**, 420–431. 138

[69] HIRAHARA, Y., MATSUDA, K.I., YAMADA, H., SAITOU, A., MORISAKI, S., TAKANAMI, K., BOGGS, J.M. & KAWATA, M. (2013). G protein-coupled receptor 30 contributes to improved remyelination after cuprizone-induced demyelination. *Glia*, **61**, 420–431. 12

[70] HONDA, A., YAMASHITA, K., HARA, T., IKEGAMI, T., MIYAZAKI, T., SHIRAI, M., XU, G., NUMAZAWA, M. & MATSUZAKI, Y. (2008). Highly sensitive quantification of key regulatory oxysterols in biological samples by LC-ESI-MS/MS. *Journal of Lipid Research*, **50**, 350–357. 51, 107

[71] HUANG, J.K., JARJOUR, A.A., OUMESMAR, B.N., KERNINON, C., WILLIAMS, A., KREZEL, W., KAGECHIKA, H., BAUER, J., ZHAO, C., EVERCOOREN, A.B.V., CHAMBON, P., FFRENCH CONSTANT, C. & FRANKLIN, R.J.M. (2010). Retinoid x receptor gamma signaling accelerates CNS remyelination. *Nature Neuroscience*, **14**, 45–53. 12, 25, 85

[72] HUBLER, Z., ALLIMUTHU, D., BEDERMAN, I., ELITT, M.S., MADHAVAN, M., ALLAN, K.C., SHICK, H.E., GARRISON, E., KARL, M.T., FACTOR, D.C., NEVIN, Z.S., SAX, J.L., THOMPSON, M.A., FEDOROV, Y., JIN, J., WILSON, W.K., GIERA, M., BRACHER, F., MILLER, R.H., TESAR, P.J. & ADAMS, D.J. (2018). Accumulation of 8, 9-unsaturated sterols drives oligodendrocyte formation and remyelination. *Nature*, **560**, 372–376. 25, 85, 86, 87, 95, 100, 102, 104, 115

[73] HUGHES, E.G., KANG, S.H., FUKAYA, M. & BERGLES, D.E. (2013). Oligodendrocyte progenitors balance growth with self-repulsion to achieve homeostasis in the adult brain. *Nature Neuroscience*, **16**, 668–676. 3

[74] HUSSAIN, R., GHOUMARI, A.M., BIELECKI, B., STEIBEL, J., BOEHM, N., LIERE, P., MACKLIN, W.B., KUMAR, N., HABERT, R., MHAOUTY-KODJA, S., TRONCHE, F., SITRUK-WARE, R., SCHUMACHER, M. & GHANDOUR, M.S. (2013). The neural androgen receptor: a therapeutic target for myelin repair in chronic demyelination. *Brain*, **136**, 132–146. 12

[75] JACHAK, G.R., RAMESH, R., SANT, D.G., JORWEKAR, S.U., JADHAV, M.R., TUPE, S.G., DESHPANDE, M.V. & REDDY, D.S. (2015). Silicon incorporated morpholine antifungals: Design, synthesis, and biological evaluation. *ACS Medicinal Chemistry Letters*, **6**, 1111–1116. 27

[76] JIA, Y., WU, T., JELINEK, C.A., BIELEKOVA, B., CHANG, L., NEWSOME, S., GNANAPAVAN, S., GIOVANNONI, G., CHEN, D., CALABRESI, P.A., NATH, A. & COTTER, R.J. (2012). Development of protein biomarkers in cerebrospinal fluid for secondary progressive multiple sclerosis using selected reaction monitoring mass spectrometry (SRM-MS). *Clinical Proteomics*, **9**, 9. 126

[77] JUREVICS, H. & MORELL, P. (1995). Cholesterol for synthesis of myelin is made locally, not imported into brain. *J. Neurochem.*, **64**, 895–901. 19

[78] KASBEKAR, D.P. (2018). A cross-eyed geneticist's view I. Making sense of the lamin B receptor, a chimeric protein. *J. Biosci.*, **43**, 235–237. 122, 144, 156

[79] KEIRSTEAD, H.S. & BLAKEMORE, W.F. (1999). The role of oligodendrocytes and oligodendrocyte progenitors in cns remyelination. In *Advances in Experimental Medicine and Biology*, 183–197, Springer US. 4, 84

[80] KLOPFLEISCH, S., MERKLER, D., SCHMITZ, M., KLOPPNER, S., SCHEDENSACK, M., JESERICH, G., ALTHAUS, H.H. & BRUCK, W. (2008). Negative impact of statins on oligodendrocytes and myelin formation in vitro and in vivo. *Journal of Neuroscience*, **28**, 13609–13614. 40

[81] KORADE, Z., KIM, H.Y.H., TALLMAN, K.A., LIU, W., KOCZOK, K., BALOGH, I., XU, L., MIRNICS, K. & PORTER, N.A. (2016). The effect of small molecules on sterol homeostasis: Measuring 7-dehydrocholesterol in dhcr7-deficient neuro2a cells and human fibroblasts. *Journal of Medicinal Chemistry*, **59**, 1102–1115. 21, 22, 26, 33, 35, 40, 95, 128

[82] KORADE, Ž., LIU, W., WARREN, E.B., ARMSTRONG, K., PORTER, N.A. & KONRADI, C. (2017). Effect of psychotropic drug treatment on sterol metabolism. *Schizophrenia Research*, **187**, 74–81. 13, 15, 21, 22

[83] KREMER, D., GÖTTLE, P., FLORES-RIVERA, J., HARTUNG, H.P. & KÜRY, P. (2019). Remyelination in multiple sclerosis. *Current Opinion in Neurology*, **32**, 378–384. 124, 125

[84] LABARCA, C. & PAIGEN, K. (1980). A simple, rapid, and sensitive DNA assay procedure. *Analytical Biochemistry*, **102**, 344–352. 56

[85] LAGER, A.M., CORRADIN, O.G., CREGG, J.M., ELITT, M.S., SHICK, H.E., CLAYTON, B.L.L., ALLAN, K.C., OLSEN, H.E., MADHAVAN, M. & TESAR, P.J. (2018). Rapid functional genetics of the oligodendrocyte lineage using pluripotent stem cells. *Nature Communications*, **9**. 8, 9, 108, 148

[86] LAI, H.C. & JAN, L.Y. (2006). The distribution and targeting of neuronal voltage-gated ion channels. *Nature Reviews Neuroscience*, **7**, 548–562. 2, 3

[87] LANGE, Y., ECHEVARRIA, F. & STECK, T.L. (1991). Movement of zymosterol, a precursor of cholesterol, among three membranes in human fibroblasts. *J. Biol. Chem.*, **266**, 21439–21443. 130

[88] LARIOSA-WILLINGHAM, K.D., ROSLER, E.S., TUNG, J.S., DUGAS, J.C., COLLINS, T.L. & LEONOUDAKIS, D. (2016). A high throughput drug screening assay to identify compounds that promote oligodendrocyte differentiation using acutely dissociated and purified oligodendrocyte precursor cells. *BMC Research Notes*, **9**. 8, 25, 85

[89] LASSMANN, H. (2001). Classification of demyelinating diseases at the interface between etiology and pathogenesis. *Current Opinion in Neurology*, **14**, 253–258. 84

[90] LECCA, D., RAFFAELE, S., ABBRACCHIO, M.P. & FUMAGALLI, M. (2020). Regulation and signaling of the GPR17 receptor in oligodendroglial cells. *Glia*. 137, 138

[91] LEE, S., LEACH, M.K., REDMOND, S.A., CHONG, S.Y.C., MELLON, S.H., TUCK, S.J., FENG, Z.Q., COREY, J.M. & CHAN, J.R. (2012). A culture system to study oligodendrocyte myelination processes using engineered nanofibers. *Nature Methods*, **9**, 917–922. 37

[92] LEPESHEVA, G.I. & WATERMAN, M.R. (2007). Sterol 14α-demethylase cytochrome p450 (CYP51), a p450 in all biological kingdoms. *Biochimica et Biophysica Acta (BBA) - General Subjects*, **1770**, 467–477. 121

[93] LI, X., ROBERTI, R. & BLOBEL, G. (2014). Structure of an integral membrane sterol reductase from methylomicrobium alcaliphilum. *Nature*, **517**, 104–107. 13

[94] LIANG, Y., BESCH-WILLIFORD, C., AEBI, J.D., MAFUVADZE, B., COOK, M.T., ZOU, X. & HYDER, S.M. (2014). Cholesterol biosynthesis inhibitors as potent novel anti-cancer agents: suppression of hormone-dependent breast cancer by the oxidosqualene cyclase inhibitor RO 48-8071. *Breast Cancer Research and Treatment*, **146**, 51–62. 94

[95] LUSA, S., HEINO, S. & IKONEN, E. (2003). Differential mobilization of newly synthesized cholesterol and biosynthetic sterol precursors from cells. *Journal of Biological Chemistry*, **278**, 19844–19851. 130

[96] MADHAVAN, M., NEVIN, Z.S., SHICK, H.E., GARRISON, E., CLARKSON-PAREDES, C., KARL, M., CLAYTON, B.L.L., FACTOR, D.C., ALLAN, K.C., BARBAR, L., JAIN, T., DOUVARAS, P., FOSSATI, V., MILLER, R.H. & TESAR, P.J. (2018). Induction of myelinating oligodendrocytes in human cortical spheroids. *Nature Methods*, **15**, 700–706. 39

[97] MAGALON, K., ZIMMER, C., CAYRE, M., KHALDI, J., BOURBON, C., ROBLES, I., TARDIF, G., VIOLA, A., PRUSS, R.M., BORDET, T. & DURBEC, P. (2012). Olesoxime accelerates myelination and promotes repair in models of demyelination. *Annals of Neurology*, **71**, 213–226. 12

[98] MAIER, O., JONGE, J.D., NOMDEN, A., HOEKSTRA, D. & BARON, W. (2009). Lovastatin induces the formation of abnormal myelin-like membrane sheets in primary oligodendrocytes. *Glia*, **57**, 402–413. 20, 102

[99] MANOUCHEHRI, N. & STÜVE, O. (2019). Trials and therapies in secondary progressive MS, simplified. *Nature Reviews Neurology*, **15**, 431–432. 126

[100] MARK, M., MULLER, P., MAIER, R. & EISELE, B. (1996). Effects of a novel 2,3-oxidosqualene cyclase inhibitor on the regulation of cholesterol biosynthesis in hepg2 cells. *J Lipid Res*, **37**, 148–158. 91, 94

[101] MATHEWS, E.S., MAWDSLEY, D.J., WALKER, M., HINES, J.H., POZZOLI, M. & APPEL, B. (2014). Mutation of 3-hydroxy-3-methylglutaryl CoA synthase i reveals requirements for isoprenoid and cholesterol synthesis in oligodendrocyte migration arrest, axon wrapping, and myelin gene expression. *Journal of Neuroscience*, **34**, 3402–3412. 20, 102

[102] MAZEIN, A., WATTERSON, S., HSIEH, W.Y., GRIFFITHS, W.J. & GHAZAL, P. (2013). A comprehensive machine-readable view of the mammalian cholesterol biosynthesis pathway. *Biochemical Pharmacology*, **86**, 56–66. 12

[103] MCFARLAND, H.F. & MARTIN, R. (2007). Multiple sclerosis: a complicated picture of autoimmunity. *Nature Immunology*, **8**, 913–919. 4

[104] MEDINA-RODRÍGUEZ, E.M., ARENZANA, F.J., BRIBIÁN, A. & DE CASTRO, F. (2013). Protocol to isolate a large amount of functional oligodendrocyte precursor cells from the cerebral cortex of adult mice and humans. *PLoS ONE*, **8**, e81620. 127

[105] MEFFRE, D., SHACKLEFORD, G., HICHOR, M., GORGIEVSKI, V., TZAVARA, E.T., TROUSSON, A., GHOUMARI, A.M., DEBOUX, C., NAIT OUMESMAR, B., LIERE, P., SCHUMACHER, M., BAULIEU, E.E., CHARBONNIER, F., GRENIER, J. & MASSAAD, C. (2015). Liver x receptors alpha and beta promote myelination and remyelination in the cerebellum. *Proceedings of the National Academy of Sciences*, **112**, 7587–7592. 12

[106] MEI, F., FANCY, S.P.J., SHEN, Y.A.A., NIU, J., ZHAO, C., PRESLEY, B., MIAO, E., LEE, S., MAYORAL, S.R., REDMOND, S.A., ETXEBERRIA, A., XIAO, L., FRANKLIN, R.J.M., GREEN, A., HAUSER, S.L. & CHAN, J.R. (2014). Micropillar arrays as a high-throughput screening platform for therapeutics in multiple sclerosis. *Nature Medicine*, **20**, 954–960. 25, 33, 42

[107] MEI, F., LEHMANN-HORN, K., SHEN, Y.A.A., RANKIN, K.A., STEBBINS, K.J., LORRAIN, D.S., PEKAREK, K., SAGAN, S.A., XIAO, L., TEUSCHER, C., VON BÜDINGEN, H.C., WESS, J., LAWRENCE, J.J., GREEN, A.J., FANCY, S.P., ZAMVIL, S.S. & CHAN, J.R. (2016). Accelerated remyelination during inflammatory demyelination prevents axonal loss and improves functional recovery. *eLife*, **5**. 4, 12, 85, 122, 137

[108] MEI, F., MAYORAL, S.R., NOBUTA, H., WANG, F., DESPONTS, C., LORRAIN, D.S., XIAO, L., GREEN, A.J., ROWITCH, D., WHISTLER, J. & CHAN, J.R. (2016). Identification of the kappa-opioid receptor as a therapeutic target for oligodendrocyte remyelination. *The Journal of Neuroscience*, **36**, 7925–7935. 8, 25, 85

[109] MELJON, A., THEOFILOPOULOS, S., SHACKLETON, C.H.L., WATSON, G.L., JAVITT, N.B., KNÖLKER, H.J., SAINI, R., ARENAS, E., WANG, Y. & GRIFFITHS, W.J. (2012). Analysis of bioactive oxysterols in newborn mouse brain by LC/MS. *Journal of Lipid Research*, **53**, 2469–2483. 132

[110] MERRILL, J.E. (2008). In vitro and in vivo pharmacological models to assess demyelination and remyelination. *Neuropsychopharmacology*, **34**, 55–73. 7, 8

[111] MI, S., MILLER, R.H., TANG, W., LEE, X., HU, B., WU, W., ZHANG, Y., SHIELDS, C.B., ZHANG, Y., MIKLASZ, S., SHEA, D., MASON, J., FRANKLIN, R.J.M., JI, B., SHAO, Z., CHÉDOTAL, A., BERNARD, F., ROULOIS, A., XU, J., JUNG, V. & PEPINSKY, B. (2009). Promotion of central nervous system remyelination by induced differentiation of oligodendrocyte precursor cells. *Annals of Neurology*, **65**, 304–315. 38

[112] MILLER, R.H. (2002). Regulation of oligodendrocyte development in the vertebrate CNS. *Progress in Neurobiology*, **67**, 451–467. 3, 4

[113] MILLER, T.E., LIAU, B.B., WALLACE, L.C., MORTON, A.R., XIE, Q., DIXIT, D., FACTOR, D.C., KIM, L.J.Y., MORROW, J.J., WU, Q., MACK, S.C., HUBERT, C.G., GILLESPIE, S.M., FLAVAHAN, W.A., HOFFMANN, T., THUMMALAPALLI, R., HEMANN, M.T., PADDISON, P.J., HORBINSKI, C.M., ZUBER, J., SCACHERI, P.C., BERNSTEIN, B.E., TESAR, P.J. & RICH, J.N. (2017). Transcription elongation factors represent in vivo cancer dependencies in glioblastoma. *Nature*, **547**, 355–359. 51

[114] MIR, F. & BRETON, G.C.L. (2008). A novel nuclear signaling pathway for thromboxane a2 receptors in oligodendrocytes: Evidence for signaling compartmentalization during differentiation. *Molecular and Cellular Biology*, **28**, 6329–6341. 27

[115] MIRON, V.E., ZEHNTNER, S.P., KUHLMANN, T., LUDWIN, S.K., OWENS, T., KENNEDY, T.E., BEDELL, B.J. & ANTEL, J.P. (2009). Statin therapy inhibits remyelination in the central nervous system. *The American Journal of Pathology*, **174**, 1880–1890. 40

[116] MITSCHE, M.A., MCDONALD, J.G., HOBBS, H.H. & COHEN, J.C. (2015). Flux analysis of cholesterol biosynthesis in vivo reveals multiple tissue and cell-type specific pathways. *eLife*, **4**. 13, 14

[117] MOEBIUS, F.F., REITER, R.J., BERMOSER, K., GLOSSMANN, H., CHO, S.Y. & PAIK, Y.K. (1998). Pharmacological analysis of sterol δ8-δ7 isomerase proteins with [3h]ifenprodil. *Molecular Pharmacology*, **54**, 591–598. 35

[118] MOFFAT, J.G., VINCENT, F., LEE, J.A., EDER, J. & PRUNOTTO, M. (2017). Opportunities and challenges in phenotypic drug discovery: an industry perspective. *Nature Reviews Drug Discovery*, **16**, 531–543. 1, 2

[119] MUTEMBEREZI, V., GUILLEMOT-LEGRIS, O. & MUCCIOLI, G.G. (2016). Oxysterols: From cholesterol metabolites to key mediators. *Progress in Lipid Research*, **64**, 152–169. 18, 99, 122, 146

[120] NAJM, F.J., ZAREMBA, A., CAPRARIELLO, A.V., NAYAK, S., FREUNDT, E.C., SCACHERI, P.C., MILLER, R.H. & TESAR, P.J. (2011). Rapid and robust generation of functional oligodendrocyte progenitor cells from epiblast stem cells. *Nature Methods*, **8**, 957–962. 8, 45

[121] NAJM, F.J., LAGER, A.M., ZAREMBA, A., WYATT, K., CAPRARIELLO, A.V., FACTOR, D.C., KARL, R.T., MAEDA, T., MILLER, R.H. & TESAR, P.J. (2013). Transcription factor-mediated reprogramming of fibroblasts to expandable, myelinogenic oligodendrocyte progenitor cells. *Nat. Biotechnol.*, **31**, 426–433. 9

[122] NAJM, F.J., MADHAVAN, M., ZAREMBA, A., SHICK, E., KARL, R.T., FACTOR, D.C., MILLER, T.E., NEVIN, Z.S., KANTOR, C., SARGENT, A., QUICK, K.L., SCHLATZER, D.M., TANG, H., PAPOIAN, R., BRIMACOMBE, K.R., SHEN, M., BOXER, M.B., JADHAV, A., ROBINSON, A.P., PODOJIL, J.R., MILLER, S.D., MILLER, R.H. & TESAR, P.J. (2015). Drug-based modulation of endogenous stem cells promotes functional remyelination in vivo. *Nature*, **522**, 216–220. 4, 8, 12, 22, 25, 38, 42, 85

[123] NAVE, K.A. (2010). Myelination and the trophic support of long axons. *Nature Reviews Neuroscience*, **11**, 275–283. 84

[124] NELSON, J., STECKBECK, S. & SPENCER, T. (1981). Biosynthesis of 24,25-epoxycholesterol from squalene 2,3;22,23-dioxide. *J Biol Chem*, **256**, 1067–1068. 88

[125] NELSON, J., STECKBECK, S. & SPENCER, T. (1990). Nb-598: a potent competitive inhibitor of squalene epoxidas. *J Biol Chem*, **265**, 18075–18078. 94

[126] NELSON, J.A., STECKBECK, S.R. & SPENCER, T.A. (1981). Biosynthesis of 24,25-epoxycholesterol from squalene 2,3;22,23-dioxide. *J. Biol. Chem.*, **256**, 1067–1068. 18

[127] NIEWEG, K., SCHALLER, H. & PFRIEGER, F.W. (2009). Marked differences in cholesterol synthesis between neurons and glial cells from postnatal rats. *J. Neurochem.*, **109**, 125–134. 19

[128] NIKOLAKAKI, E., MYLONIS, I. & GIANNAKOUROS, T. (2017). Lamin b receptor: Interplay between structure, function and localization. *Cells*, **6**, 28. 122, 144

[129] OLINS, A.L., RHODES, G., WELCH, D.B., ZWERGER, M. & OLINS, D.E. (2010). Lamin B receptor: multi-tasking at the nuclear envelope. *Nucleus*, **1**, 53–70. 145

[130] PEPPARD, J.V., RUGG, C.A., SMICKER, M.A., POWERS, E., HARNISH, E., PRISCO, J., CIROVIC, D., WRIGHT, P.S., AUGUST, P.R. & CHANDROSS, K.J. (2015). High-content phenotypic screening and triaging strategy to identify small molecules driving oligodendrocyte progenitor cell differentiation. *Journal of Biomolecular Screening*, **20**, 382–390, pMID: 25394729. 4, 8, 10, 11

[131] PFEIFFER, S., WARRINGTON, A. & BANSAL, R. (1993). The oligodendrocyte and its many cellular processes. *Trends in Cell Biology*, **3**, 191–197. 3

[132] PINK, J.J., JORDAN, V.C., PUBLICATIONS, C.T.A., LINES, C.C., PINK, J.J. & JORDAN, V.C. (1996). Models of estrogen receptor regulation by estrogens and antiestrogens in breast cancer cell lines. *Cancer Res*. 55

[133] PORTER, T.D. (2015). Electron transfer pathways in cholesterol synthesis. *Lipids*, **50**, 927–936. 14

[134] PUGACH, E.K., FELTES, M., KAUFMAN, R.J., ORY, D.S. & BANG, A.G. (2018). High-content screen for modifiers of niemann-pick type c disease in patient cells. *Human Molecular Genetics*, **27**, 2101–2112. 130

[135] PUTTEN, C.V.D., KUIPERS, H.F., ZUIDERWIJK-SICK, E.A., STRAALEN, L.V., KONDOVA, I., ELSEN, P.J.V.D. & BAJRAMOVIC, J.J. (2011). Statins amplify TLR-induced responses in microglia via inhibition of cholesterol biosynthesis. *Glia*, **60**, 43–52. 19

[136] QUAN, G., XIE, C., DIETSCHY, J.M. & TURLEY, S.D. (2003). Ontogenesis and regulation of cholesterol metabolism in the central nervous system of the mouse. *Developmental Brain Research*, **146**, 87–98. 131, 132

[137] RABELO, V.W.H., ROMEIRO, N.C. & ABREU, P.A. (2017). Design strategies of oxidosqualene cyclase inhibitors: Targeting the sterol biosynthetic pathway. *The Journal of Steroid Biochemistry and Molecular Biology*, **171**, 305–317. 95

[138] RANKIN, K.A., MEI, F., KIM, K., SHEN, Y.A.A., MAYORAL, S.R., DESPONTS, C., LORRAIN, D.S., GREEN, A.J., BARANZINI, S.E., CHAN, J.R. & BOVE, R. (2019). Selective estrogen receptor modulators enhance CNS remyelination independent of estrogen receptors. *The Journal of Neuroscience*, **39**, 2184–2194. 122

[139] ROBINSON, A.P., RODGERS, J.M., GOINGS, G.E. & MILLER, S.D. (2014). Characterization of oligodendroglial populations in mouse demyelinating disease using flow cytometry: Clues for MS pathogenesis. *PLoS ONE*, **9**, e107649. 4

[140] ROWE, A.H., ARGMANN, C.A., EDWARDS, J.Y., SAWYEZ, C.G., MORAND, O.H., HEGELE, R.A. & HUFF, M.W. (2003). Enhanced synthesis of the oxysterol 24(s), 25-epoxycholesterol in macrophages by inhibitors of 2, 3-oxidosqualene:lanosterol cyclase. *Circulation Research*, **93**, 717–725. 18, 91, 94

[141] ROWITCH, D.H. & KRIEGSTEIN, A.R. (2010). Developmental genetics of vertebrate glial–cell specification. *Nature*, **468**, 214–222. 3

[142] SAHER, G. & STUMPF, S.K. (2015). Cholesterol in myelin biogenesis and hypomyelinating disorders. *Biochim. Biophys. Acta*, **1851**, 1083–1094. 19, 21, 128, 129, 130

[143] SAHER, G., BRUGGER, B., LAPPE-SIEFKE, C., MOBIUS, W., TOZAWA, R., WEHR, M.C., WIELAND, F., ISHIBASHI, S. & NAVE, K.A. (2005). High cholesterol level is essential for myelin membrane growth. *Nat. Neurosci.*, **8**, 468–475. 19, 21, 40, 120, 131, 132, 133, 134

[144] SAHER, G., RUDOLPHI, F., CORTHALS, K., RUHWEDEL, T., SCHMIDT, K.F., LÖWEL, S., DIBAJ, P., BARRETTE, B., MÖBIUS, W. & NAVE, K.A. (2012). Therapy of pelizaeus-merzbacher disease in mice by feeding a cholesterol-enriched diet. *Nature Medicine*, **18**, 1130–1135. 30

[145] SÁNCHEZ-WANDELMER, J., DÁVALOS, A., DE LA PEÑA, G., CANO, S., GIERA, M., CANFRÁN-DUQUE, A., BRACHER, F., MARTÍN-HIDALGO, A., FERNÁNDEZ-HERNANDO, C., LASUNCIÓN, M. & BUSTO, R. (2010). Haloperidol disrupts lipid rafts and impairs insulin signaling in SH-SY5y cells. *Neuroscience*, **167**, 143–153. 14

[146] SHARPE, L.J. & BROWN, A.J. (2013). Controlling cholesterol synthesis beyond 3-hydroxy-3-methylglutaryl-CoA reductase (HMGCR). *Journal of Biological Chemistry*, **288**, 18707–18715. 12, 13, 90

[147] SIMON, C., GOTZ, M. & DIMOU, L. (2011). Progenitors in the adult cerebral cortex: Cell cycle properties and regulation by physiological stimuli and injury. *Glia*, **59**, 869–881. 3

[148] SMOLDERS, I., SMETS, I., MAIER, O., VANDEVEN, M., STEELS, P. & AMELOOT, M. (2010). Simvastatin interferes with process outgrowth and branching of oligodendrocytes. *Journal of Neuroscience Research*, **88**, 3361–3375. 20

[149] TALLMAN, K.A., KIM, H.Y.H., KORADE, Z., GENARO-MATTOS, T.C., WAGES, P.A., LIU, W. & PORTER, N.A. (2017). Probes for protein adduction in cholesterol biosynthesis disorders: Alkynyl lanosterol as a viable sterol precursor. *Redox Biology*, **12**, 182–190. 151, 154, 155

[150] TSAI, P.L., ZHAO, C., TURNER, E. & SCHLIEKER, C. (2016). The lamin b receptor is essential for cholesterol synthesis and perturbed by disease-causing mutations. *eLife*, **5**. 156

[151] TSUDA, K. & NISHIO, I. (2005). A selective estrogen receptor modulator, tamoxifen, and membrane fluidity of erythrocytes in normotensive and hypertensive postmenopausal women: An electron paramagnetic resonance investigation. *American Journal of Hypertension*, **18**, 1067–1076. 143

[152] TULENKO, T.N., BOEZE-BATTAGLIA, K., MASON, R.P., TINT, G.S., STEINER, R.D., CONNOR, W.E. & LABELLE, E.F. (2005). A membrane defect in the

pathogenesis of the smith-lemli-opitz syndrome. *Journal of Lipid Research*, **47**, 134–143. 143

[153] WAGES, P.A., KIM, H.Y.H., KORADE, Z. & PORTER, N.A. (2018). Identification and characterization of prescription drugs that change levels of 7-dehydrocholesterol and desmosterol. *Journal of Lipid Research*, **59**, 1916–1926. 22, 128

[154] WARRILOW, A.G., PARKER, J.E., KELLY, D.E. & KELLY, S.L. (2012). Azole affinity of sterol 14α-demethylase (CYP51) enzymes from candida albicans and homo sapiens. *Antimicrobial Agents and Chemotherapy*, **57**, 1352–1360. 51

[155] WASSIF, C.A., BROWNSON, K.E., STERNER, A.L., FORLINO, A., ZERFAS, P.M., WILSON, W.K., STAROST, M.F. & PORTER, F.D. (2007). HEM dysplasia and ichthyosis are likely laminopathies and not due to 3β-hydroxysterol δ14-reductase deficiency. *Human Molecular Genetics*, **16**, 1176–1187. 156

[156] WENDT, K.U., SCHULZ, G.E., COREY, E.J. & LIU, D.R. (2000). Enzyme mechanisms for polycyclic triterpene formation. *Angewandte Chemie International Edition*, **39**, 2812–2833. 13

[157] WERNER, H.B., KRÄMER-ALBERS, E.M., STRENZKE, N., SAHER, G., TENZER, S., OHNO-IWASHITA, Y., MONASTERIO-SCHRADER, P.D., MÖBIUS, W., MOSER, T., GRIFFITHS, I.R. & NAVE, K.A. (2013). A critical role for the cholesterol-associated proteolipids PLP and m6b in myelination of the central nervous system. *Glia*, **61**, 567–586. 138

[158] WILLIS, C.M., NICAISE, A.M., BONGARZONE, E.R., GIVOGRI, M., REITER, C.R., HEINTZ, O., JELLISON, E.R., SUTTER, P.A., TEHENNEPE, G., ANANDA, G., VELLA, A.T. & CROCKER, S.J. (2020). Astrocyte support for oligodendrocyte differentiation can be conveyed via extracellular vesicles but diminishes with age. *Scientific Reports*, **10**. 134

[159] WINDREM, M.S., ROY, N.S., WANG, J., NUNES, M., BENRAISS, A., GOODMAN, R., MCKHANN, G.M. & GOLDMAN, S.A. (2002). Progenitor cells derived from the adult human subcortical white matter disperse and differentiate as oligodendrocytes within demyelinated lesions of the rat brain. *Journal of Neuroscience Research*, **69**, 966–975. 125, 127

[160] WONG, J., QUINN, C.M. & BROWN, A.J. (2004). Statins inhibit synthesis of an oxysterol ligand for the liver x receptor in human macrophages with consequences for cholesterol flux. *Arteriosclerosis, Thrombosis, and Vascular Biology*, **24**, 2365–2371. 91, 94

[161] WONG, J., QUINN, C.M. & BROWN, A.J. (2007). Synthesis of the oxysterol, 24(s), 25-epoxycholesterol, parallels cholesterol production and may protect against cellular accumulation of newly-synthesized cholesterol. *Lipids in Health and Disease*, **6**, 10. 18

[162] WONG, J., QUINN, C.M. & BROWN, A.J. (2007). Synthesis of the oxysterol, 24(s), 25-epoxycholesterol, parallels cholesterol production and may protect against cellular accumulation of newly-synthesized cholesterol. *Lipids in Health and Disease*, **6**, 10. 88, 91, 94

[163] WONG, J., QUINN, C.M., GUILLEMIN, G. & BROWN, A.J. (2007). Primary human astrocytes produce 24(s), 25-epoxycholesterol with implications for brain cholesterol homeostasis. *Journal of Neurochemistry*, **103**, 1764–1773. 134

[164] XING, Y.L., ROTH, P.T., STRATTON, J.A.S., CHUANG, B.H.A., DANNE, J., ELLIS, S.L., NG, S.W., KILPATRICK, T.J. & MERSON, T.D. (2014). Adult neural precursor cells from the subventricular zone contribute significantly to oligodendrocyte regeneration and remyelination. *Journal of Neuroscience*, **34**, 14128–14146. 3

[165] YAMAUCHI, Y. & ROGERS, M.A. (2018). Sterol metabolism and transport in atherosclerosis and cancer. *Frontiers in Endocrinology*, **9**. 135

[166] YAMAUCHI, Y., REID, P.C., SPERRY, J.B., FURUKAWA, K., TAKEYA, M., CHANG, C.C.Y. & CHANG, T.Y. (2007). Plasma membrane rafts complete cholesterol synthesis by participating in retrograde movement of precursor sterols. *Journal of Biological Chemistry*, **282**, 34994–35004. 130

[167] YEUNG, M.S.Y., DJELLOUL, M., STEINER, E., BERNARD, S., SALEHPOUR, M., POSSNERT, G., BRUNDIN, L. & FRISÉN, J. (2019). Dynamics of oligodendrocyte generation in multiple sclerosis. *Nature*, **566**, 538–542. 125

[168] ZERENTURK, E.J., KRISTIANA, I., GILL, S. & BROWN, A.J. (2012). The endogenous regulator 24(s), 25-epoxycholesterol inhibits cholesterol synthesis at DHCR24 (seladin-1). *Biochimica et Biophysica Acta (BBA) - Molecular and Cell Biology of Lipids*, **1821**, 1269–1277. 18

[169] ZHANG, L., THEODOROPOULOS, P.C., ESKIOCAK, U., WANG, W., MOON, Y.A., POSNER, B., WILLIAMS, N.S., WRIGHT, W.E., KIM, S.B., NIJHAWAN, D., BRABANDER, J.K.D. & SHAY, J.W. (2016). Selective targeting of mutant adenomatous polyposis coli (APC) in colorectal cancer. *Science Translational Medicine*, **8**, 361ra140–361ra140. 27, 44

[170] ZHANG, Y., ZHANG, H., WANG, L., JIANG, W., XU, H., XIAO, L., BI, X., WANG, J., ZHU, S., ZHANG, R., HE, J., TAN, Q., ZHANG, D., KONG, J. & LI, X.M. (2012). Quetiapine enhances oligodendrocyte regeneration and myelin repair after cuprizone-induced demyelination. *Schizophrenia Research*, **138**, 8–17. 12

[171] ZHANG, Y., CHEN, K., SLOAN, S.A., BENNETT, M.L., SCHOLZE, A.R., O'KEEFFE, S., PHATNANI, H.P., GUARNIERI, P., CANEDA, C., RUDERISCH, N., DENG, S., LIDDELOW, S.A., ZHANG, C., DANEMAN, R., MANIATIS, T., BARRES, B.A. & WU, J.Q. (2014). An RNA-sequencing transcriptome and

splicing database of glia, neurons, and vascular cells of the cerebral cortex. *Journal of Neuroscience*, **34**, 11929–11947. 12, 137, 146

[172] ZHANG, Y., ZHANG, Y.P., PEPINSKY, B., HUANG, G., SHIELDS, L.B., SHIELDS, C.B. & MI, S. (2015). Inhibition of lingo-1 promotes functional recovery after experimental spinal cord demyelination. *Experimental Neurology*, **266**, 68 – 73. 138